STANFORD UNIVERSITY

CENTER FOR SYSTEMS RESEARCH

Analytical Design of Manned Control Systems

by

Walter George Eppler, Jr.

Guidance and Control Laboratory

ANALYTICAL DESIGN OF MANNED CONTROL SYSTEMS

SUDAAR No. 280
May 1966

Walter George Eppler, Jr.

Department of Aeronautics and Astronautics
Stanford University
Stanford, California

FOREWORD

This report was submitted to Stanford University as a dissertation in partial fulfillment of the requirements for the Ph.D. degree in the Department of Electrical Engineering.

The author gratefully acknowledges the guidance and encouragement given him by the members of his Dissertation Committee. Particular thanks are due to Professor Robert H. Cannon, Jr. who initiated and oriented this work with his prior development of the Rate-Reticle Display. As principal advisor, he gave generously of his time throughout the course of this research and contributed many helpful criticisms and suggestions. Dr. Ronald W. Angel provided the necessary instruction in physiology and neurology, and helped with the measurement and interpretation of the data presented in Chapter 5; working with a person of his enthusiasm and ability was a great pleasure. Many thanks are also due to Professor William K. Linvill for his assistance and interest in this work.

The primary source of funding for this work was the LMSC Independent Research and Development Programs. Additional support, in the form of computer facilities, equipment loan and machine shop support, was provided by a National Aeronautics and Space Administration grant (NsG-133-61) to Stanford University. The work reported in Section 5.2 was performed at the Veterans Administration Hospital in Palo Alto, California.

Finally, the author is pleased to express his appreciation to Lockheed Missiles & Space Company for making it possible to continue his education under the company-sponsored Graduate Study Program.

ABSTRACT

This dissertation treats the problem of designing high-performance, closed-loop control systems which include a human operator. In particular it describes research conducted to answer the following rather general questions:

(1) How should the state of the system be displayed to the operator and how should his responses to the display be processed before they are input to the system?

(2) In what way does the operator's dynamic response limit the performance of the overall system, and how does this limitation depend on which of his several possible outputs is used for controlling the system?

The results presented here are applicable to the design of a wide variety of manned control systems.

An approach, called Control Action Display, is described; essentially it consists of adding a separate feedback loop around the Display, Operator, and Control Devices sections of a conventional system. This feedback is obtained by providing an auxiliary display which presents the instantaneous outputs of the control devices, superimposed upon the conventional display that shows the overall system errors. Control Action Display simplifies the operator's control function by requiring only that he track the system errors with the controller outputs (over which he has instantaneous and exclusive control). Control Action Display also greatly reduces the effects of variability in the operator's response, and thereby makes it possible to design and evaluate manned systems using the straightforward analytical techniques of automatic control system theory.

The Control Action Display principle is demonstrated by designing a system which enables an astronaut to keep his spacecraft aligned to a given visual reference. This system does not require an optical tracker or a rate or position gyroscope, and is therefore potentially more reliable than a completely automatic system or a system using conventional forms of pilot aiding. A fixed-base simulation was performed

in which it was found that an astronaut can easily perform three-axis attitude control maneuvers using either proportional or on-off moment control.

In another example, the Control Action Display approach is applied to the analytical design of a manned system in which the controlled element is inherently unstable. The particular case considered is a variation of the tightrope-walker attitude control system; however, the techniques and results developed here can be used for systems with more practical applications. Experiments showed that Control Action Display made it possible for subjects to maintain their balance on a platform which was free to rotate about a single axis.

Systems using Control Action Display employ the operator in a closed-loop tracking task; the dynamic performance of the overall system depends on the bandwidth of this tracking loop. For this reason, an extensive experimental program was undertaken to determine the various sources of delay in a human's response and to determine how his tracking performance depends on which of his several possible outputs is used as the follow-up variable.

Manual displacement, velocity and acceleration are compared with EMG (electromyograph) and EOG (electro-oculogram) signals under closely controlled conditions during step-function tracking. Results of these experiments showed that variables closer to the central nervous system are subject to less latency than manual displacement and force are. Tracking performance (magnitude, phase and signal-to-noise ratio) was also measured and compared for tests in which operators tracked a random continuous input signal using displacement, force and EMG follow-up signals. Each follow-up variable was tested using the same subjects, target statistics, and display, so that the results can be meaningfully compared. From these tests it is concluded that both the closed-loop bandwidth and the random noise output increase as signals more proximal to the central nervous system are used for the follow-up variable.

TABLE OF CONTENTS

TABLE OF CONTENTS Cont.

TABLE OF CONTENTS Cont.

LIST OF ILLUSTRATIONS

LIST OF ILLUSTRATIONS Cont.

LIST OF ILLUSTRATIONS Cont.

LIST OF ILLUSTRATIONS Cont.

LIST OF TABLES

NOTATION

Symbol	Meaning	Units
	For Chapter 3 and Appendixes A and B.	
l_i	unit vectors along the principal body axes	dimensionless
b	damping constant of dashpot between hand controller and moment-control valve; see Fig. 3-3	ft-lb-sec/rad
D_{1i}	rate display gains for system employing Quickening	sec
D_{2i}	acceleration display gains for system employing Quickening	sec^2
$G_d(s)$	the part of the open-loop transfer function which can be specified by the designer; see Eq. 3.26	sec^2
I_i	moments of inertia about the principal axes	$slug\text{-}ft^2$
K_{ci}	hand controller gains	dimensionless
K_d	open-loop gain specified by the designer; see Eq. 3.25	sec^{-2}
KG(s)	open-loop transfer function of single-axis attitude control systems	dimensionless
K_{ni}	ratio of lead time-constant to the lag time-constant in compensation networks	dimensionless
K_{mi}	gains for the proportional moment-control system relating control moment to valve opening	ft-lb/rad
k_1	spring constant of spring between hand controller and thrust-control valve; see Fig. 3-3	ft-lb/rad
k_2	spring constant of spring across thrust-control valve; see Fig. 3-3	ft-lb/rad
M_i	control moments exerted by reaction control system about the principal axes	ft-lb
M_{oi}	fixed value of control moments exerted by the on-off reaction control system about the principal axes	ft-lb

Symbol	Meaning	Units
s	Laplace transform variable	rad/sec
T	minimum time required to correct initial offset angle in system employing on-off moment control	sec
α	angle between roll axis and projection of line-of-sight onto the vehicle yaw plane; see Figs. 3-1 and 3-2	rad
δ_i	hand controller deflection angles, see Fig. 3-12	rad
ϵ	angle between line-of-sight and its projection onto the vehicle yaw plane; see Figs. 3-1 and 3-2	rad
ζ	damping ratio of second-order system	dimensionless
θ_i	reticle positions referred to body axes; see Fig. 3-1	rad
ρ	angular rotation about the line-of-sight measured with respect to the vehicle yaw axis; see Figs. 3-1 and 3-2	rad
τ_i	time-constant of lead term in compensation networks	sec
ψ_i	input angles to the valves controlling moments about the principal axes	rad
ψ_{oi}	dead zone in valves for the on-off reaction control system about the principal axes	rad
$\vec{\Omega}_{LOS}$	angular velocity of line-of-sight relative to inertial space	rad/sec
$\vec{\Omega}_{LV}$	angular velocity of line-of-sight relative to vehicle	rad/sec
$\vec{\Omega}_V$	angular velocity of vehicle relative to inertial space	rad/sec
ω_c	crossover frequency of the single-axis attitude control system; the frequency at which the Bode diagram crosses the unity-gain line	rad/sec
ω_i	vehicle angular velocities about the principal axes measured with respect to inertial space	rad/sec
ω_n	natural frequency of second-order system	rad/sec

Symbol	Meaning	Units
Convention for subscript i:	1. Roll, 2. Pitch, 3. Yaw	
Convention for subscript j:	1. Star to be brought to origin, 2. Star to be brought into pitch plane above origin	

For Chapter 4 and Appendix C

$\vec{H}_o$	angular momentum of the total system (including tightrope walker and balancing pole) about the rope	slug-ft^2-rad/sec
I_1	moment of inertia of tightrope walker (less arms) about his center of mass	slug-ft^2
I_2	moment of inertia of tightrope walker's arms about their center of mass	slug-ft^2
I_3	moment of inertia of balancing pole about its center of mass	slug-ft^2
K	open-loop gain	rad/sec or dimensionless
K_c	gain of compensation network	ft/rad
K_p	plant gain	rad/ft
ℓ_1	distance between rope and tightrope walker's center of mass	ft
ℓ_2	distance between tightrope walker's shoulders and center of mass of arms	ft
ℓ_3	distance between rope and tightrope walker's shoulders	ft
ℓ_4	length of tightrope walker's arms	ft
$\vec{M}_o$	external moments about rope	ft-lb
m_1	mass of tightrope walker (less arms)	slug
m_2	mass of tightrope walker's arms	slug
m_3	mass of balancing pole	slug
P	open-loop pole	rad/sec
$\vec{r}$	radius vector from rope to center of mass	ft

Symbol	Meaning	Units
s	Laplace variable	rad/sec
x_c	commanded horizontal displacement of the balancing pole	ft
x_p	horizontal distance from rope to point directly below pole center of mass	ft
Z	open-loop zero	rad/sec
α	angle between the tightrope walker and vertical	rad
ζ	damping ratio of second-order system	dimensionless
θ	angle between the tightrope walker's arms and vertical	rad
$\mu(0)$	low-frequency gain of human operator tracking response	dimensionless
ρ	angle between the balancing pole and the horizontal	rad
ω_c	frequency of lead term in compensation network	rad/sec
ω_f	frequency of lag term in compensation network	rad/sec
ω_n	natural frequency of second-order system	rad/sec

Unit vectors:

$\vec{i}$	horizontal (to tightrope walker's left)
$\vec{j}$	vertical (upward)
$\vec{k}$	along rope (in direction faced by tightrope walker)

For Chapter 5 and Appendixes D and E

A_{m1}	absolute magnitude of maximum acceleration	$in./sec^2$
A_{m2}	absolute magnitude of maximum deceleration	$in./sec^2$
C	instantaneous capacitance of variable capacitor in velocity measuring circuit	farad
C_1	bias contained in correlation function computed by CAT 400/CORR 256 computer	$in.^2$
C_2	constant required to normalize autocorrelation function	dimensionless

Symbol	Meaning	Units
C_{max}	maximum capacitance of variable capacitor in velocity measuring circuit	farad
C_o	initial capacitance of variable capacitor in velocity measuring circuit	farad
$\dot{C}$	rate of change of capacitance of variable capacitor in velocity measuring circuit	farad/sec
D_1	duration of acceleration	sec
D_2	duration of deceleration	sec
E	supply voltage for velocity measuring circuit	V
EMG	electromyographic (muscle action) voltage detected at surface of muscle	V
$e_{\dot{x}}$	output voltage of velocity measuring circuit	V
F	force exerted by muscle	lb
$H(\omega)$	transfer function of closed-loop tracking system	dimensionless
$\lvert H(\omega) \rvert$	magnitude of closed-loop transfer function	db
$\measuredangle H(\omega)$	phase angle of closed-loop transfer function	deg
$h(\sigma)$	impulse response of closed-loop transfer function	sec^{-1}
I	input signal, referred to display	in.
Im	imaginary part of the power spectral densities	$in.^2$ sec
IS	muscle action potential of Infraspinatus muscle	V
K_a	amplifier gain	dimensionless
L	length of pole used in Hand Monitor	in.
L_1	latency between step target displacement and the onset of action potential in the agonist muscle (or for cases in which it was more sharply defined, cessation of the antagonist activity was used)	sec
L_2	latency between step target displacement and beginning of saccadic eye movement	sec
L_3	latency between step target displacement and beginning of acceleration	sec
M	number of frequencies for which power spectral densities are evaluated	dimensionless
N	number of different values of the time-shift argument for which correlation functions are evaluated	dimensionless

Symbol	Meaning	Units
N'	number of sample intervals (of duration T'_s) required for correlation function to reach zero	dimensionless
O	operator output, referred to display	in.
P	muscle action potential of Pectoralis muscle	V
$P_{1\&2}$	poles of the approximation to the operator's closed-loop transfer function	rad/sec
q	charge on variable capacitor in velocity measuring circuit	coulomb
R	resistance of load resistor in velocity measuring circuit	ohm
Re	real part of the power spectral densities	$in.^2$ sec
s	Laplace variable	rad/sec
$\frac{S}{N}(\omega)$	ratio of signal component to noise component in the output of a closed-loop tracking system	dimensionless
T	time constant of filter	sec
T_a	analysis interval of time function used in computing correlation functions	sec
T_s	sample interval of time function used in computing correlation functions; also sample interval of time-shift argument of correlation functions	sec
T'_s	sample interval of correlation function used in computing power spectral densities	sec
T_1	delay between onset of agonist EMG activity and the beginning of hand acceleration in the model for practiced rapid moves	sec
T_2	duration of acceleration and deceleration in the model for practiced rapid moves	sec
T_3	time constant of first-order lag in dynamics between muscle action potential and muscle force	sec
t	time	sec
V_m	absolute magnitude of maximum velocity	in./sec
X_e	instantaneous (horizontal) position of eye fixation	in.
X_h	instantaneous position of the hand	in.
$\dot{X}_h$	instantaneous velocity of the hand	in./sec

Symbol	Meaning	Units
$\ddot{X}_h$	instantaneous acceleration of the hand	in./sec^2
X_t	instantaneous position of the input target	in.
Z_1	zero of the approximation to the operator's closed-loop transfer function	rad/sec
$\Delta\omega$	frequency increment for power spectral density computations	rad/sec
ϵ	instantaneous tracking error; i.e., the distance between the input and follow-up variables	in.
ζ	damping ratio of second-order system	dimensionless
$\mu(0)$	magnitude of closed-loop transfer function at low frequencies	dimensionless
$\rho(\tau)$	correlation coefficient	dimensionless
ρ_{max}	maximum value of correlation coefficient	dimensionless
σ	dummy variable	sec
τ	time-shift argument of correlation function	sec
τ_{max}	time shift for which crosscorrelation between input and output is a maximum	sec
τ_o	transport lag of Wilde-Westcott/Crossover Model	sec
Φ	auto or cross-power spectral density	in.^{2} sec
φ	auto or crosscorrelation function	in.^{2}
$\hat{\varphi}$	auto or crosscorrelation function before bias removal and normalization	in.^{2}
ω	frequency	rad/sec
ω_{co}	crossover frequency of Wilde-Westcott/Crossover Model	rad/sec
ω_n	natural frequency of second-order system	rad/sec

Subscript Convention

d	operator's displacement output
e	operator's eye-position output
f	operator's force output
i	input signal
m	operator's muscle action potentials

Symbol	Meaning	Units
m'	operator's muscle action potentials after processing	
n	output noise; that component of the operator output which is uncorrelated with the input signal	
o	output signal	
t	input target	

Chapter 1

INTRODUCTION

1.1 Background

Over the past twenty years automatic control system theory has developed to the extent that very sophisticated analytical techniques now exist for designing linear and nonlinear systems to meet almost any desired criteria. In contrast, the design of manned control systems has, with only few exceptions, tended to develop on a more empirical, cut-and-try basis in which each system was considered a new and special case. This dissertation submits a new approach to the problems of how to use man in control systems, how to design control systems which include man and how man limits the performance which can be obtained from such systems.

1.2 Role of Man in Manned Control Systems

Before discussing design procedures in detail it is appropriate to consider why man should be included in control systems at all. The reason is simply that in many cases, using a human operator reduces the resulting complexity and increases the reliability of the overall system.

One role in which man is frequently employed is that of a visual data transducer. The alternative is to use some form of television to convert the visual data into electrical signals for subsequent processing. It should be noted, however, that a very-high-performance system is required to match the resolution, sensitivity, and data rate inherent in man's visual capability. In order to use a television system the designer must also provide the commands necessary to aim the camera at all times, while a human is able to search, acquire and track objects of interest with a minimum of instruction.

In some cases the system is implemented in such a way that the input data is acquired in the form of a video signal; two such cases are:

1) The television signal transmitted to earth from an unmanned lunar landing vehicle.

2) The output of a fire-control radar in an interceptor aircraft.

Even in these two cases it has proved to be advantageous to convert the signal into pictorial form so that the human operator can be used as a pattern recognition device. In the first example a man viewing the television monitor on earth can select an appropriate landing site for the lunar vehicle. The completely unmanned system would require (for example) some type of correlation guidance computer (Ref. 1) which could be preloaded with a picture of the desired landing site; the latter approach appears to be considerably more complicated than the one which uses man's pattern recognition capabilities. Similarly, the operator observing a radar scope can interpret and filter the video data and input only the information component to the rest of the fire control system.

The spacecraft attitude control system described in Chapter 3 is a good example of the way in which man's visual and pattern recognition capabilities simplify the system design. By identifying and tracking two specified stars the astronaut performs the function which would otherwise require automatic star-tracking equipment and a complex* celestial map-matching system.

Another important function performed by the human operator in a control system is that of a decision-maker in unexpected situations; this capability, demonstrated by astronauts in several orbital flights, increases the overall system reliability. A very considerable increase in complexity would be required to provide this capability in a completely automatic system by preprogramming appropriate instructions for all possible combinations of events.

Manned control systems should be designed to simplify the mechanics of the operator's task so that he can devote most of his attention

*According to Ref. 2, "Once a star map has been established, it is necessary to identify the constellation or group of stars. It is interesting to note that a human can handle this problem with ease whereas it is a relatively difficult problem to instrument. Hence, a person can readily identify Ursa Major (Big Dipper) from any orientation but it is not correspondingly as simple to mechanize this identification."

to his primary functions of visual data transducer, pattern recognition device and decision-maker. However, this principle must be applied with the realization that simplifying the operator's tasks usually requires additional instrumentation and hardware. Systems in which man's only function is to set his observations and decisions into an otherwise automatic controller usually require considerable hardware for their mechanization. For this reason the systems to be considered here are ones in which the operator is in the loop at all times when control is being exerted.

1.3 Organization of Presentation

The material which follows is divided into six chapters and five appendixes. Chapter 2 describes the general approach recommended for the analytical design of manned control systems. In Chapter 3 and Appendixes A and B this approach is explained with reference to a manned spacecraft attitude control system. Chapter 4 and Appendix C demonstrate that the recommended approach is applicable to intrinsically unstable dynamic systems; the particular application considered is a variation of the tightrope walker attitude control system. Chapter 5 and Appendixes D and E describe experiments conducted to determine how man's dynamic response limitations depend on which of his several possible output variables is used as input to the other parts of the system. A summary of the results and recommendations for further study are given in Chapter 6.

1.4 Contributions

It is considered that this dissertation makes the following contributions to the field of understanding and designing manned control systems:

(1) A general approach is presented which makes it possible to design manned control systems and evaluate their performance using the straightforward, conventional analytical techniques of automatic control system theory.

(2) To demonstrate the effectiveness of this approach, it is used to design a control system with which an astronaut can keep his spacecraft aligned to a given visual reference. The resulting system performs well with a minimum of pilot concentration and effort with either on-off or proportional moment control. Further, the system does not require a star tracker or rate or position gyros, and is therefore more reliable than a completely automatic system or systems using conventional forms of pilot aiding. A fixed-base simulation study was conducted to demonstrate the performance of the recommended system and to compare it with systems designed using other approaches.

(3) It is shown that the recommended approach is applicable to manned systems in which the controlled element is inherently unstable. For demonstration, the method is explained with reference to the tightrope walker attitude control problem; however, the techniques developed can be used to design a wide variety of systems having more practical application. Experiments in which subjects balanced themselves on a bearing-mounted platform (i.e., one free to rotate about a single axis) were used to verify the correctness of the approach.

(4) Results are presented of comprehensive experimental measurements of human dynamic response in certain tracking tasks. Manual displacement, velocity and acceleration during step-function pursuit tracking are compared with EMG (electromyograph) and EOG (electro-oculogram) signals under closely controlled conditions. These data are used to quantify the behavior of the neuromuscular and oculomotor systems during tracking. It is shown that muscles used for manual tracking receive commands before the beginning of eye movement; this indicates that the neuromuscular system is not cascaded with the oculomotor system.

(5) Experimental measurements and conclusions are presented regarding the suitability of employing muscle force or EMG, instead of hand displacement, as the feedback signal in a tracking control loop. Tracking performance (magnitude, phase, and signal-to-noise ratio) was measured and compared for tests in which several operators tracked a random continuous input signal using (in separate tests) displacement, force, and EMG as the follow-up variable. Each follow-up variable was

tested using the same subjects, target statistics and display, so that the results may be meaningfully compared. From the data presented, it is concluded that both the closed-loop bandwidth and the random noise output increase as signals more proximal to the central nervous system are used for the follow-up variable, so that the net improvement in performance is small. These data can be used to establish an upper limit on the performance achievable by manned control systems.

(6) A model is presented which is shown to represent accurately the closed-loop tracking performance of typical operators over the frequency range of interest in manual control. Although the model is simple enough to be useful in synthesizing manned control systems, it is in good agreement with measurements made using either displacement or force as the follow-up variable. With this model, the synthesis may be carried out using root-locus techniques.

Chapter 2

GENERAL APPROACH FOR DESIGNING MANNED CONTROL SYSTEMS

2.1 Introduction

The object of this section is to describe a general approach to the design of manned control systems. Use of this approach makes it possible to design systems and evaluate their performance using the straightforward analytical techniques of control system theory. Equally important is the fact that systems designed using this approach simplify the operator's control tasks and permit him to devote most of his attention to other functions.

2.2 Conventional System Design

Figure 2-1 is a block diagram of the configuration ordinarily used in manned control systems. The system inputs are compared with the measured plant output to derive the system errors. Very often these system errors are processed by a compensation filter network before they are presented on the operator's display. The operator responds to the display (typically dials, oscilloscopes, etc.) by manipulating control devices (such as levels, pedals, etc.). The operator's response is usually processed by a second compensation filter network (which may be mechanized within the control devices) and input to the rest of the system. The plant responds to both the processed controller signals and to external disturbances.

In the configuration shown in Fig. 2-1 the system designer must specify:

(1) The form and parameters of the predisplay compensation network (when used)

(2) The type of display

(3) The scale-factor at which the information should be displayed

(4) The type of control device

(5) The form and parameters of the response compensation network (when used).

The difficulties which the system designer experiences in attempting to make these specifications result directly from the fact that there is really no unique open-loop response from display input to controller output. In fact, the operator is so loosely coupled to the display that (to the author's knowledge) this open-loop response cannot be measured except during closed-loop tests.* For this reason, display gain and other static gains are usually established with the aid of simulation (Ref. 3) rather than analytically. Similarly, the specification of the required compensation networks shown in Fig. 2-1 is complicated by the fact that the open-loop transfer function used to represent the human operator is a function of several variables. In addition to varying among different operators, and with time for a particular operator, the transfer function depends on the dynamics of the rest of the system and on the spectrum of inputs to the system (Refs. 4, 5 and 6). The designer must also devote considerable attention to the selection of the proper control devices, because the operator often uses kinesthetic feedback to estimate the instantaneous value (or one of its derivatives) of his control action.

From the operator's point of view, the system shown in Fig. 2-1 has several important disadvantages. When the plant and compensation networks consists of one or more integrations (as is the case for most systems of interest) there is a delay between the operator's actions and the response of the plant. This delay makes it difficult for the operator to determine the appropriate control action to apply for any given state of the system as presented on his display. Another difficulty

*A strictly open-loop test would be one in which the operator responds to a display without receiving any feedback (other than proprioceptive) from his actions. It is clear that the results of such a test would be quite variable; for example, the operator would have no criterion for selecting an amplitude of response so that the static gain would be arbitrary.

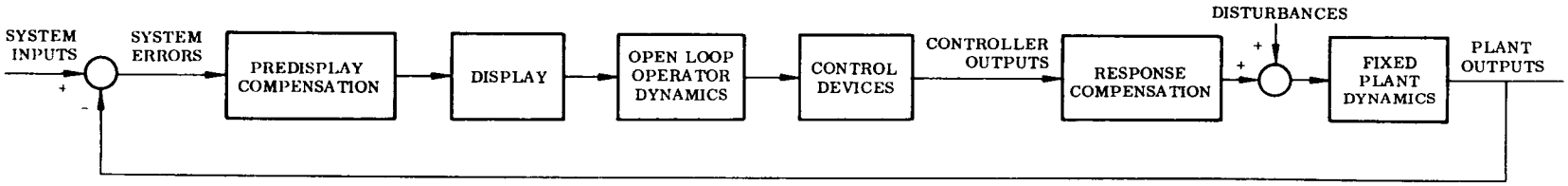

Fig. 2-1 Conventional Manually-Controlled Closed-Loop System

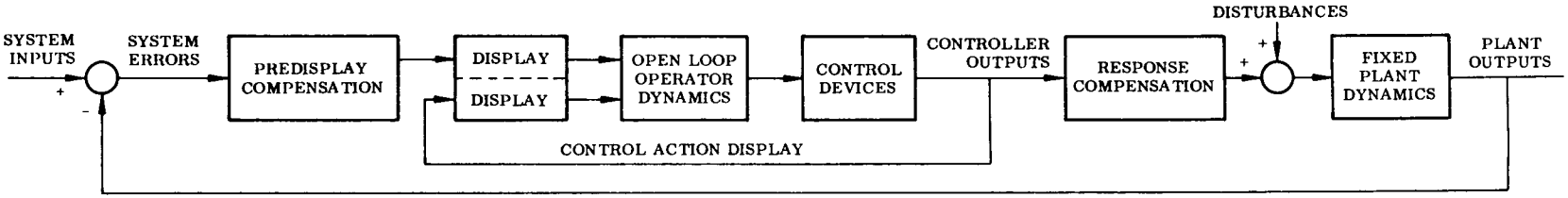

Fig. 2-2 Manually-Controlled Closed-Loop System Incorporating Control Action Display

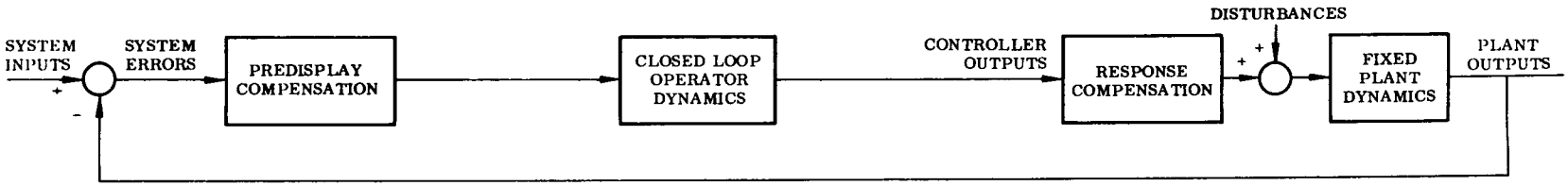

Fig. 2-3 System Representation Used for Analytical Design and Evaluation

is that the operator does not have an accurate knowledge of the instantaneous control action he is exerting; his only knowledge of it comes from inexact, proprioceptive feedback and from delayed feedback through the plant and compensation networks. Figure 2-1 shows that the operator cannot distinguish between the effect of his control action and the effect of inputs or disturbances to the system; this makes it difficult for him to learn the dynamics between his actions and display.

To summarize, the configuration shown in Fig. 2-1 is not well suited for either design or operation. Because the open-loop response of the human operator is subject to wide variations, the analytical specification of compensation networks and static gains can be only approximate at best. In operation, the system does not provide the information necessary for the operator to determine unambiguously:

(1) What control action should be applied?

(2) What control action is being applied?

(3) What was the effect of past control action?

2.3 Introduction to Control Action Display

Figure 2-2 shows the configuration recommended for use in manned control systems. It is identical to the one given in Fig. 2-1 except that an additional feedback loop has been added in the form of an auxiliary display which presents the instantaneous outputs of the control devices superimposed on the display showing the processed system errors. In systems incorporating this Control Action Display, the operator's task is simply to track the processed system errors with the controller outputs. Specifically, he uses his hand controller to place a control display over an error display. The compensation sections are chosen in such a way that this action on the part of the operator will result in the desired performance for the overall system. It will be shown that this approach provides important advantages in both the design and operation of manned control systems.

From the designer's point of view, Control Action Display is a tight feedback loop around the display, operator, and control devices

sections which previous discussion indicated to be the principal sources of uncertainty. The effect of this feedback is to make the closed-loop response of these elements less variable than their open-loop response is for the conventional system shown in Fig. 2-1. For this reason, systems employing Control Action Display are more amenable to analytical design.

Further study of Fig. 2-2 shows that, by equating the displayed controller outputs to the displayed system errors (i.e., by perfect tracking), the operator acts as a transducer which converts complex visual information into a form which can be used by the rest of the system. In performing this function he can often replace a battery of complex tracking and pattern recognition devices which would be required by an unmanned system. The designer should therefore incorporate the closed inner loop (consisting of the display, operator and control devices sections) at any place in the system where such functions are required.

Note also that, because kinesthetic feedback is not necessary in systems employing Control Action Display, a wide variety of operator responses can be considered for input to the rest of the system. This is the justification for studying, in Chapter 5, the tracking performance which can be attained using such operator outputs as direction of eye fixation and filtered electromyographic (i.e., muscle action potential) signals.

From the operator's point of view, systems incorporating Control Action Display are preferable to systems of the type shown in Fig. 2-1 simply because they are easier to control. In particular, Control Action Display eliminates all of the operator's difficulties described in the preceding section.

At all times, and for any state of the system, the operator knows exactly what control action to apply; i.e., he needs only to superimpose the displayed controller outputs on the displayed (processed) system errors. The compensation networks are chosen in such a way that this action causes the desired system response.

Control Action Display informs the operator exactly what control actions he is applying to the system at all times. Because

these quantities are presented directly on the display, without delay or other processing, it is unnecessary to provide kinesthetic feedback to the operator; this simplifies the design of the control devices in that detents, dashpots, etc. are not required.

The fact that the displayed system errors respond to inputs and disturbances, as well as to control actions, does not cause the confusion referred to in the preceding section. In systems using Control Action Display, the operator's function is to track the (processed) system errors with the control device output, and not specifically to null the system errors. For this reason it is unnecessary for him to learn the dynamic response between his control actions and the displayed system errors.

2.4 General Analytical Design Procedure

Elements of the Control Action Display principle introduced in the preceding section have been used in manned control systems in the past (Refs. 7, 8 and 9). In these cases, however, its use was described only with reference to a specific hardware implementation and without any indication of its general applicability. The purpose of this section is to describe a general design procedure which applies the Control Action Display principle and the analytical techniques of automatic control system theory to the design of manually controlled closed-loop systems. Use of this approach makes it possible to establish by theoretical means the effect of various parameters on system performance, and to specify nearly optimal parameter values without recourse to extensive simulation and subjective evaluation (Ref. 10).

The recommended design procedure is composed of the following four steps:

(1) Select the display and control variables. Usually this selection is strongly influenced by the function of the system and the hardware available to implement it. The closed inner loop, consisting of the display, operator and control devices sections (see Fig. 2-2), should be placed in the outer loop at a point which results in the minimum system complexity.

(2) Perform a preliminary system design in which the inner loop is represented as a constant gain equal to the reciprocal of the display gain. The design is carried out analytically using conventional automatic control system synthesis techniques. Specifically the compensation networks and static gains are selected to satisfy the following criteria:

   (a) The resulting system must have the necessary stability.
   (b) The system response to input commands, initial conditions, and disturbances must meet the given specifications.
   (c) The closed-loop frequency response or the dominant closed-loop poles of the system should not exceed approximately 2 rad/sec.

(3) Refine the design by including the closed-loop dynamics of the inner loop (see Fig. 2-3). In particular, recompute the static gains and compensation network parameters, taking into account the operator's closed-loop frequency response or pole-zero representation given in Chapter 5.

(4) Simulate the system with the operator in the loop.

2.5 Summary

This chapter has described how displaying the operator's instantaneous control actions results in systems which can be designed by straightforward analytical techniques and which can be operated with a minimum of concentration and effort. A design procedure was tabulated which is applicable to a wide variety of manned control systems. This procedure will be explained further and compared with other approaches in Chapters 3 and 4.

Chapter 3

DESIGN OF A SPACECRAFT ATTITUDE CONTROL SYSTEM

3.1 Introduction

The object of this chapter* is to demonstrate the design procedures outlined in Chapter 2, using a spacecraft attitude control system as an example. This system is typical of applications in which the system errors are displayed directly, without an opportunity for predisplay processing (see Fig. 2-2). This chapter demonstrates that the conventional analytical techniques of frequency-domain synthesis (see Chapter 22 of Ref. 12) and phase-plane synthesis (see Chapter 11 of Ref. 13) can be used to derive nearly optimal parameter values.

Section 3.3 describes the operation of the overall system and (together with Appendix A) presents all of the relationships necessary to describe its behavior. An analysis of a single-axis system is presented in Section 3.4 in order to derive the various system parameters and to estimate the closed-loop performance which can be expected of such systems. Section 3.5 outlines several other techniques which have been used or proposed to aid an operator in controlling a dynamical plant; the differences between these approaches and the Control Action Display technique are delineated. Section 3.6 and Appendix B describe a fixed-base simulation study performed to determine the effectiveness of the Control Action Display technique and to compare it with the other approaches.

3.2 Background

Attitude control is usually not required continuously throughout the entire duration of earth orbital or space missions. In fact,

*Portions of the material presented here were previously published in Ref. 11.

attitude control fuel can be conserved by allowing long periods of drifting flight, and experience has shown that astronauts are not adversely affected by this type of operation. However, attitude control is essential for certain phases of typical missions including:

(1) Making visual observations
(2) Retrofire from earth or lunar orbit
(3) Rendezvousing and docking with another vehicle
(4) Lunar landing.

The fact that attitude control is required only infrequently makes it possible to consider using a human operator to implement this function. It will be shown in this chapter that including man in the spacecraft attitude control system reduces the overall complexity (compared with a fully automatic system) and thereby increases the reliability.

The attitude control system used for Project Mercury (Ref. 14) had two modes of operation in which the pilot exercised manual control over the moment about each of the three axes. In one mode the three-axes hand controller was connected directly to valves which provided proportional moment control about the three axes; in the other mode, called the "fly-by-wire" mode, the hand controller actuated solenoid valves which resulted in on-off moment control. However, according to Bailey (Ref. 15), "Mercury experience to date has indicated that direct manual control over the reaction control thrust nozzles is apt to be quite wasteful of fuel." This inefficient fuel utilization is apparently caused by overshoot and hunting which result when a human operator tries to control a multidimensional, high-order dynamical plant.

This difficulty is due to the fact that conventional attitude control systems are arranged according to Fig. 2-1 where there are two integrations between the pilot's corrective actions (control moments) and his display variables (line-of-sight angles). It is shown in Section 3.6 that the use of Control Action Display simplifies the operator's task and makes efficient fuel utilization possible.

3.3 Description of the Overall System

Figure 3-1 shows the pilot's view as he looks out of the spacecraft through either the window or periscope. The pilot focuses his attention on two prescribed stars out of the entire star field; in doing this he takes the place of the star-tracker and pattern-recognition device which would be required in a fully automatic attitude control system. Thoughout this description it is assumed that the pilot wishes to orient the spacecraft in such a way that Star 1 is on the roll axis and Star 2 is directly above it in the pitch plane.

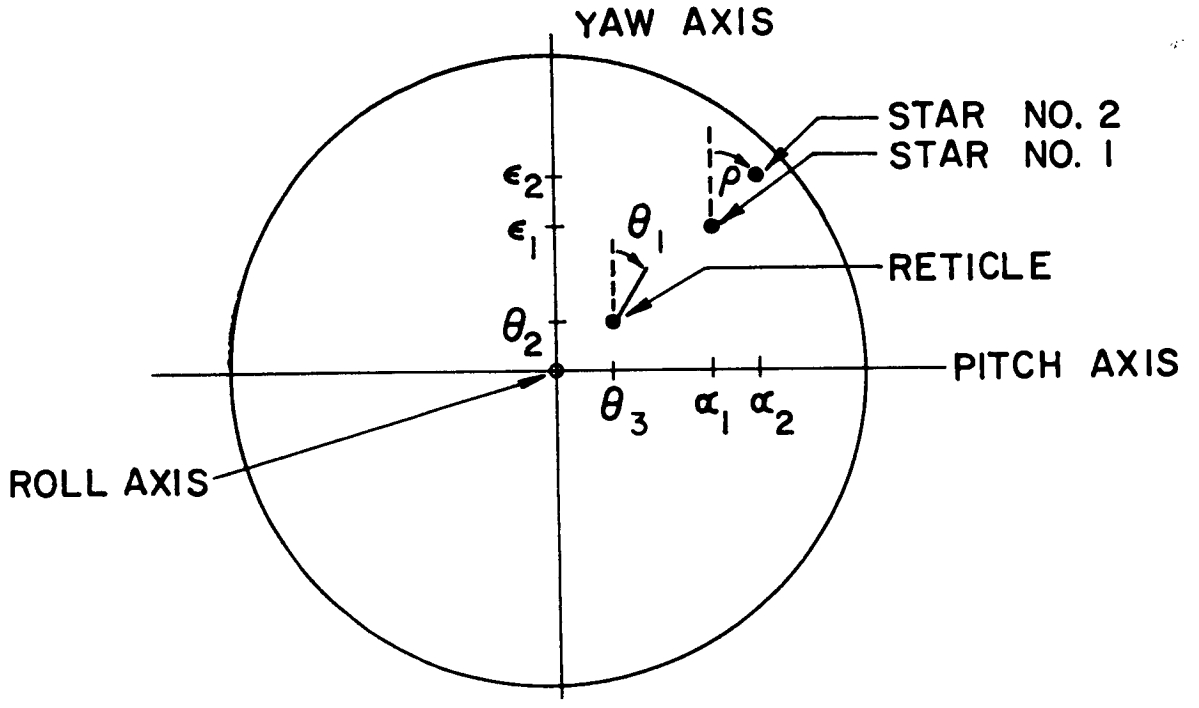

Fig.3-1 View from Spacecraft Window Showing Two Stars and Vector Reticle.

The pilot observes the positions of the stars with respect to the vehicle-fixed coordinate system shown in Figs. 3-1 and 3-2. Equations 3.1, 3.2 and 3.3, derived in Appendix A, relate the body rates to the angular rate of the line of sight.

$$\omega_1 = - \dot{\rho} \cos \alpha \cos \epsilon + \dot{\epsilon} \sin \alpha \qquad (3.1)$$

$$\omega_2 = - \dot{\epsilon} \cos \alpha - \dot{\rho} \sin \alpha \cos \epsilon \qquad (3.2)$$

$$\omega_3 = - \dot{\alpha} + \dot{\rho} \sin \epsilon \qquad (3.3)$$

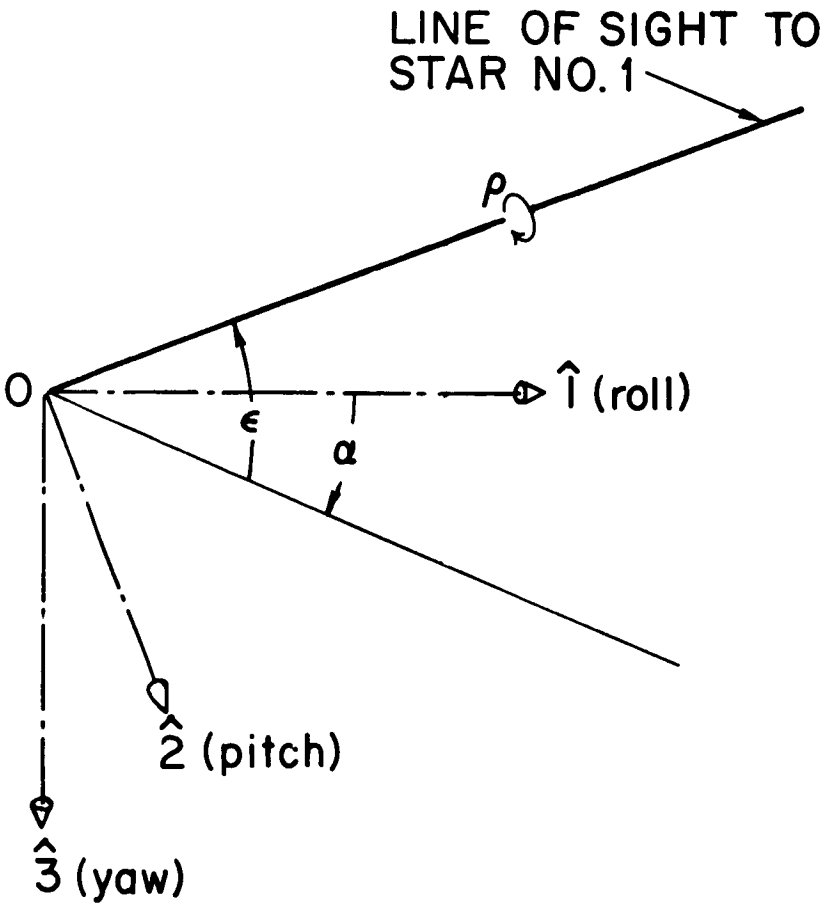

Fig. 3-2 Vehicle-Fixed Coordinates and Error Angles

For small values of α and ϵ, Eqs. 3.1, 3.2 and 3.3 can be approximated according to the following expressions

$$\omega_1 \approx - \dot{\rho} \qquad (3.4)$$

$$\omega_2 \approx - \dot{\epsilon} \qquad (3.5)$$

$$\omega_3 \approx - \dot{\alpha} \qquad (3.6)$$

From these equations it can be seen that the angles ρ, ϵ, and α are approximate measures of the attitude errors in roll, pitch, and yaw, respectively.

To aid the pilot in maintaining attitude control of his spacecraft, an auxiliary display is provided in the form of a vector reticle shown in Fig. 3-1. This reticle is connected to the three-axis hand controller and caused to move over the window through the apparent (to a pilot seated at a specified distance from the window) angles θ_1, θ_2 and θ_3 in response to controller deflections in the roll, pitch, and yaw directions, respectively; see Fig. 3-12. Equation 3.7 describes the behavior of the vector reticle for Control Action Display.

$$\theta_i = K_{ci}\delta_i \qquad i = 1,2,3 \tag{3.7}$$

The pilot is instructed to manipulate the hand controller as necessary in order to point the reticle at Star 2 while keeping its origin over Star 1. He can do this quite easily (provided that a condition to be discussed in the next section is met) because he has instantaneous and exclusive control over the reticle position; this is what is meant by Control Action Display.

In addition to positioning the reticle, the hand controller deflections are also connected to the moment control valves through a lead-lag compensation network. Equation 3.8 gives the input angles to the valves in terms of the hand controller deflections.

$$\frac{\Psi_i(s)}{\delta_i(s)} = \frac{(\tau_i s + 1)}{K_{ni}\left(\frac{\tau_i}{K_{ni}} s + 1\right)} \qquad i = 1,2,3 \tag{3.8}$$

Figure 3-3 shows that the required compensation can be obtained mechanically by coupling the hand controller to the spring-loaded valve through a parallel spring/dashpot combination;* such an implementation should result in a highly reliable system. The control moments exerted about

*It is emphasized that the purpose of the dashpot and springs is to process the pilot's response and not to provide any kinesthetic feedback to him.

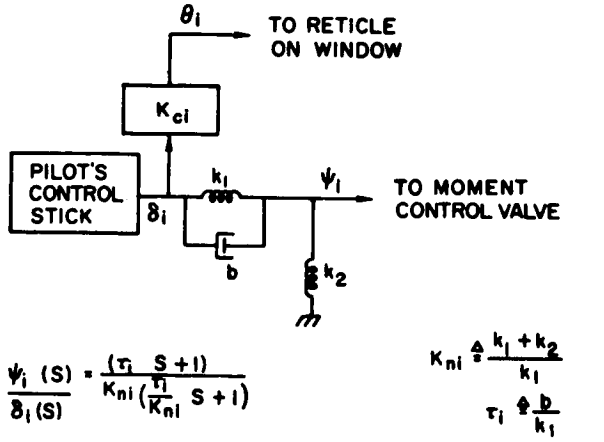

(a) Schematic

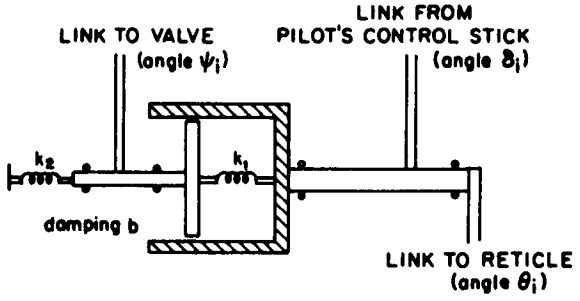

(b) Possible mechanical arrangement

Fig. 3-3 Mechanical Implementation of Lead-Lag Network

the principal axes of the vehicle in response to jet control-valve opening are expressed by Eqs. 3.9 and 3.10 for the case of proportional and on-off moment control, respectively.

$$M_i = K_{mi}\Psi_i \qquad i = 1,2,3 \tag{3.9}$$

$$M_i = \begin{cases} 0 & \text{for } |\Psi_i| < \Psi_{oi} \\ M_{oi}\ \text{sgn}(\Psi_i) & \text{for } |\Psi_i| > \Psi_{oi} \end{cases} \qquad i = 1,2,3 \tag{3.10}$$

These control moments* cause angular accelerations about the principal axes which are given by

$$\dot{\omega}_1 = \frac{M_1}{I_1} + \frac{I_2 - I_3}{I_1}\omega_2\omega_3 \tag{3.11}$$

$$\dot{\omega}_2 = \frac{M_2}{I_2} + \frac{I_3 - I_1}{I_2}\omega_3\omega_1 \tag{3.12}$$

$$\dot{\omega}_3 = \frac{M_3}{I_3} + \frac{I_1 - I_2}{I_3}\omega_1\omega_2 \tag{3.13}$$

The control moments applied through the compensation network by the pilot, when he positions the reticle, reduce the attitude error and cause the stars to rotate and move toward the center of the window. Provided only that the pilot continues to track the moving star pattern with the reticle, the vehicle will assume a steady-state orientation in which Star 1 is located at the center of the window and Star 2 is directly above it, as desired.

3.4 Single-Axis Analysis of Control Action Display

The Control Action Display principle is most easily explained by considering the case in which the motion is restricted to the pitch plane. This case is defined by the following relations

$$\alpha(0) = \rho(0) = \omega_1(0) = \omega_3(0) = M_1 = M_3 = 0 \tag{3.14}$$

Equations 3.15 through 3.20, describing the single-axis case, are obtained by substituting Eq. 3.14 into the equations developed in the

*In these equations, moments due to gravity-gradient, magnetic field, etc., are neglected because they do not contribute significantly to the vehicle motion during the time interval (typically 15 sec) required for an attitude control maneuver.

preceding section. These relationships are shown in block diagram form in Figs. 3-4 and 3-5 which will serve as the basis for discussion throughout the rest of this section.

$$\dot{\epsilon} = - \omega_2 \tag{3.15}$$

$$\theta_2 = K_{c2}\delta_2 \tag{3.16}$$

$$\Psi_2(s) = \frac{(\tau_2 s + 1)}{K_{n2}\left(\frac{\tau_2}{K_{n2}} s + 1\right)} \delta_2(s) \tag{3.17}$$

$$M_2 = K_{m2}\Psi_2 \tag{3.18}$$

$$M_2 = \begin{cases} 0 & \text{for } |\Psi_2| < \Psi_{o2} \\ M_{o2}\,\mathrm{sgn}(\Psi_2) & \text{for } |\Psi_2| > \Psi_{o2} \end{cases} \tag{3.19}$$

$$\dot{\omega}_2 = \frac{M_2}{I_2} \tag{3.20}$$

From Figs. 3-4 and 3-5 it is seen that attitude control systems incorporating Control Action Display consist of two loops which will be referred to as the "inner loop" and "outer loop". The inner loop contains the pilot, hand controller, and display; its input is ϵ and its output is δ_2. The outer loop contains the inner loop in addition to the compensation network, the moment control system (either proportional, as in Fig. 3-4, or on-off as in Fig. 3-5), and the vehicle dynamics.

The inner loop employs a pursuit display in which the inner-loop input ϵ and output δ_2 are presented separately on the same display. It is generally held (Ref. 16) that tracking performance obtained using a pursuit display is superior to that obtained using a compensatory display (i.e., one in which only the difference between system input and output is displayed).

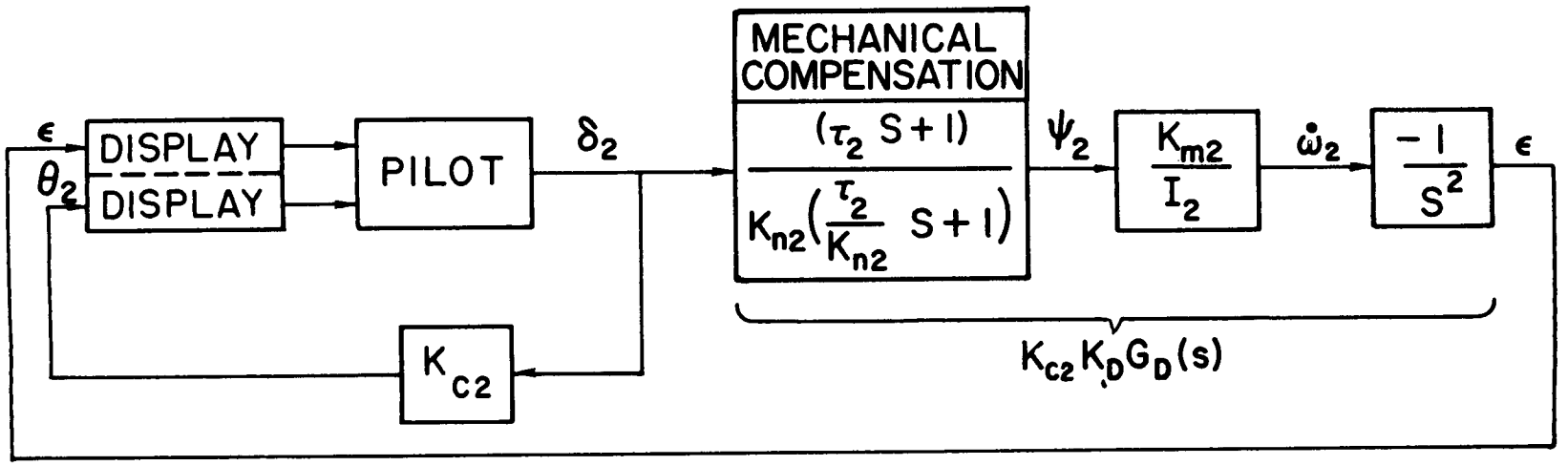

Fig. 3-4 Block Diagram of Pitch Control System Using Control Action Display with Proportional Moment Control

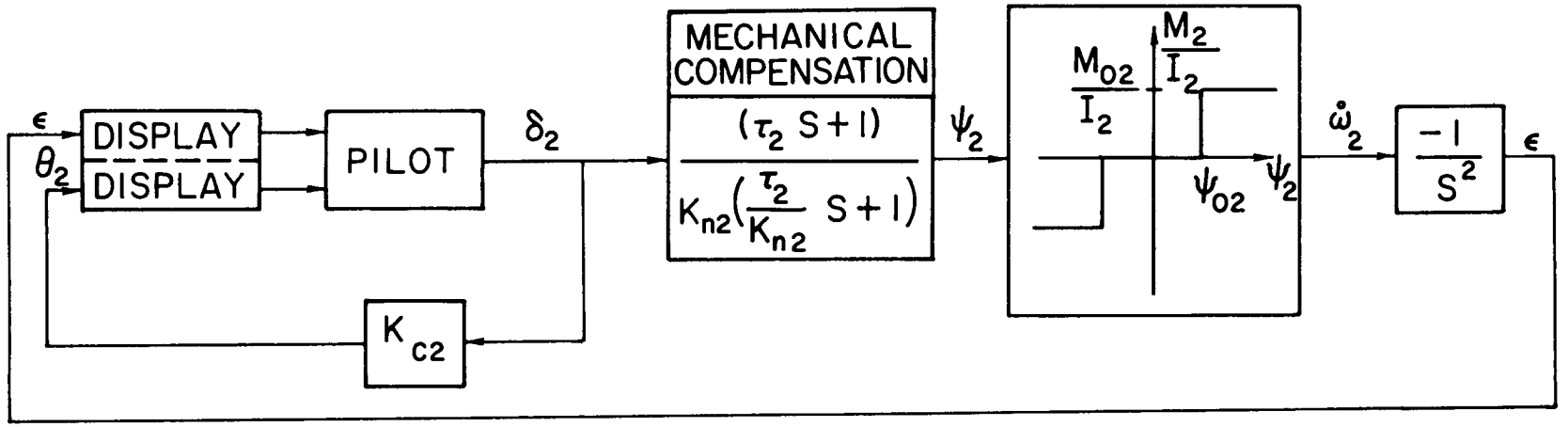

Fig. 3-5 Block Diagram of Pitch Control System Using Control Action Display with On-Off Moment Control

The pilot's task is to manipulate the hand controller in such a way that the reticle is always positioned over the star; that is, he provides the "equal sign" in the equation

$$\theta_2 = \epsilon \tag{3.21}$$

Under this condition the transfer function of the entire inner loop containing the pilot, display, and hand controller reduces to a constant gain given by

$$\frac{\delta_2}{\epsilon} = \frac{1}{K_{c2}} \tag{3.22}$$

The consequence of providing feedback around the inner loop by displaying the pilot's control action is to make the response of the overall system less dependent on the elements contained within the inner loop. Then the design of a manually operated attitude control system is reduced to the problem of specifying appropriate compensation for a known plant in order to obtain a suitable response.

To insure that the inner loop approximates a constant gain, it is necessary to choose a compensation network which causes the vehicle to react slowly enough to allow the pilot to act as a competent "follow-up device" (i.e., to satisfy Eq. 3.21). The transients which the pilot must follow are identically those which would occur in a completely automatic system in which the attitude error (derived from a star tracker, for example) is fed into the compensation network through a gain of $(K_{c2})^{-1}$.

The appropriate compensation can be specified equivalently in the frequency domain by requiring that the crossover frequency of the overall system (i.e., the frequency for which the Bode plot of the outer loop crosses unity gain) be much lower than the bandwidth of the inner loop. The approximate closed-loop frequency response of the inner loop given in Table 3.1 was derived from Fig. 3-6, in which the pilot is represented by one of the transfer functions derived in Chapter 5 (see Table 5.2). Table 3.1 and Fig. 3-7 show that the closed loop containing

the display, pilot, and hand controller contributes negligibly (i.e., less than 23 degrees of phase shift) to the dynamics of the overall system, for frequencies lower than 2.0 rad/sec.

Table 3.1

Typical Frequency Response of Closed Inner Loop

ω (rad/sec)	0.5	1.0	1.5	2.0	3.0	4.0	5.0	6.0	7.0	8.0
$\left\lvert\frac{\theta_2(\omega)}{\epsilon(\omega)}\right\rvert$ (db)	-1.0	-1.0	-0.9	-0.9	-0.8	-0.6	-0.5	-0.4	-0.5	-0.8
$\measuredangle \frac{\theta_2(\omega)}{\epsilon(\omega)}$ (deg)	-5.6	-11.3	-17.0	-22.8	-34.7	-47.2	-60.6	-74.8	-89.8	-105.2

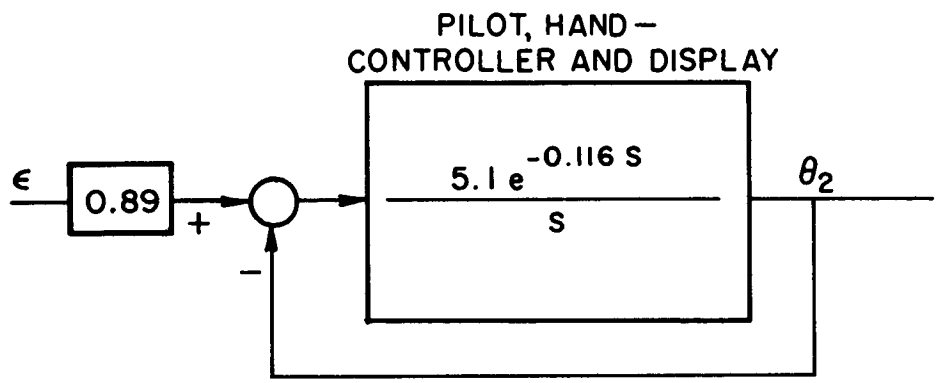

Fig. 3-6 Block Diagram of Closed Inner Loop in which Pilot Is Represented as Linear Transfer Function

Reference to the block diagram of the system employing proportional moment control (Fig. 3-4) shows that the open-loop transfer function of the outer loop is given by

$$KG(s) = \left[\frac{1}{K_{c2}} \quad \frac{\theta_2(s)}{\epsilon(s)}\right] \cdot \left[\frac{\epsilon(s)}{\delta_2(s)}\right] \tag{3.23}$$

Transfer function of inner loop

Transfer function of compensation and vehicle dynamics

Equation 3.23 is rewritten in a form which separates the parameters under control of the designer from the response determined by the pilot. The result is given by the following three equations

$$KG(s) = \left[\frac{K_{m2}}{K_{c2}K_{n2}I_2} \cdot \frac{(\tau_2 s + 1)}{s^2\left(\frac{\tau_2}{K_{n2}} s + 1\right)}\right] \cdot \frac{\theta_2(s)}{\epsilon(s)} = K_d G_d(s) \frac{\theta_2(s)}{\epsilon(s)} \tag{3.24}$$

Specified by designer

Determined by pilot

$$K_d = \frac{K_{m2}}{K_{c2}K_{n2}I_2} \tag{3.25}$$

$$G_d(s) = \frac{(\tau_2 s + 1)}{s^2\left(\frac{\tau_2}{K_{n2}} s + 1\right)} \tag{3.26}$$

Provided that a crossover frequency much lower than 2 rad/sec is chosen, the appropriate time constant and gain are given by

$$\tau_2 = \frac{\sqrt{K_{n2}}}{\omega_c} \tag{3.27}$$

$$K_d = \frac{\omega_c^2}{\sqrt{K_{n2}}} \tag{3.28}$$

Figure 3-7 is a Bode diagram for a typical system in which the time constant and gain were chosen to give a crossover frequency of 0.5 rad/sec.* This figure shows that the inner loop contributes negligibly to the dynamics near the crossover frequency, and therefore the closed-loop response of the single-axis attitude control system is determined primarily by the compensation network and vehicle dynamics.

The use of Control Action Display in a system employing on-off moment control is illustrated by Fig. 3-5. The pilot's control stick (in addition to moving the reticle on the window) is coupled through a spring and dashpot (Fig. 3-3) to on-off attitude jet control valves. The closed-loop response of this system is determined primarily by the values of M_{o2}/I_2 and τ_2 because (as in the case of proportional thrust control) the inner loop acts as a constant gain. The proper choice of M_{o2}/I_2 and τ_2 can be explained by referring to the phase-plane diagram in Fig. 3-8. The optimum (i.e., minimum response time) switching line is given by

$$\dot{\epsilon} + \left(2 \frac{M_{o2}}{I_2} |\epsilon|\right)^{1/2} \text{sgn}(\epsilon) = 0 \qquad (3.29)$$

Although this equation could be implemented using a nonlinear spring and/or dashpot, perfectly adequate performance can be obtained using the linear approximation given by

$$\tau_2 \dot{\epsilon} + \epsilon = 0 \qquad (3.30)$$

The value of τ_2 is chosen such that the approximate switching line intercepts the optimum switching line on the trajectory starting from a nominal offset angle. The rate gain and angular acceleration can be expressed in terms of the nomial offset angle and the minimum transient time, according to Eqs. 3.31 and 3.32, respectively.

*This implies that this system will be most effective for those applications in which the frequency of the inputs and disturbances is not significantly greater than 0.5 rad/sec.

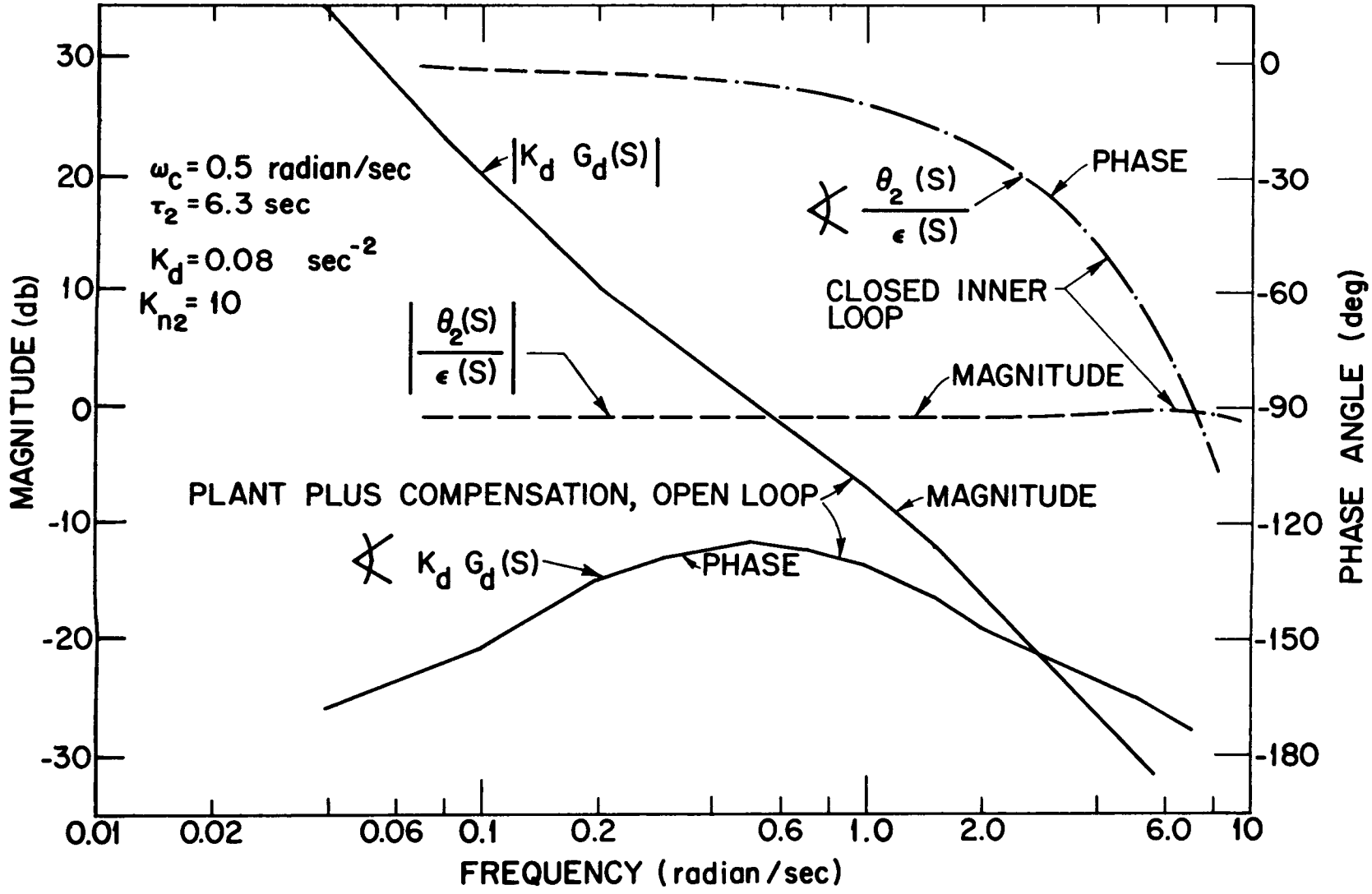

Fig. 3-7 Bode Diagram of Typical System

$$\tau_2 = \frac{1}{4} T \tag{3.31}$$

$$\frac{M_{o2}}{I_2} = \frac{4\epsilon(0)}{T^2} \tag{3.32}$$

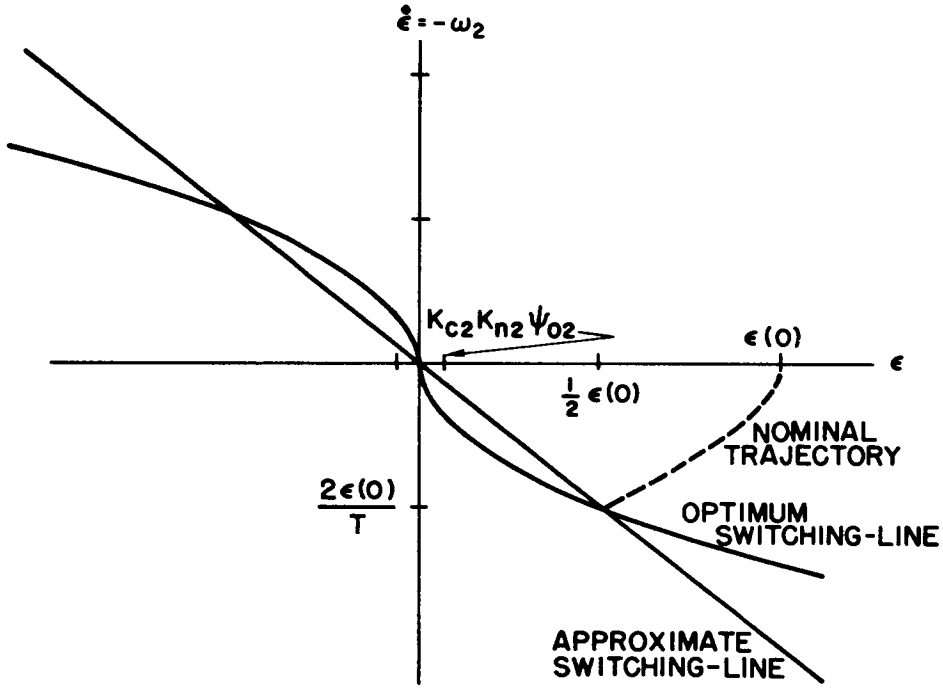

Fig. 3-8 Phase-Plane Analysis of On-Off Control System

Trajectories starting at greater (less) than the nominal offset angle intersect the approximate switching line too late (early) and require more than one thrust reversal and slightly greater than the minimum time to reach null. The presence of a lag term in the compensation network and the thrust dead zone also degrade the performance slightly.

At the end of the acquisition phase (the time during which a large initial offset is brought within the thrust control valve dead zone), a small residual angular velocity may be present. During the

subsequent station keeping phase the pilot can reverse this velocity by applying very short (on the order of 0.1 sec) bursts of thrust whenever the vehicle attitude drifts beyond some prescribed tolerance. In this way he causes the vehicle to follow a stable limit cycle of the type described by Gaylord and Keller (Ref. 17).

To summarize the results of this action: The single-axis analysis shows that displaying instantaneously the pilot's response has the effect of providing a tight feedback loop around the pilot, hand controller, and display. This feedback causes that section of the system to act as a constant gain despite variations in pilot response. The response of the system is determined primarily by the dynamics of the vehicle and compensation network. The designer selects a compensation network to obtain a satisfactory system response, subject to the constraint that the system must react slowly enough to allow the pilot to track the stars with the reticle. Compensation networks suitable for systems employing both proportional and on-off thrust control were derived.

3.5 Other Techniques Used for Manned Control Systems

Of the various techniques for manual control described in the literature, the one proposed by Campbell (Ref. 7) for the control of an interceptor airplane is the most closely related to Control Action Display. In this system the pilot's control stick is connected to a reticle and to the autopilot which commands yaw and pitch rates.

Quickening (Refs. 18, 19 and 20) is a technique which has been applied with considerable success in a wide variety of manual control applications. This technique is most easily explained by referring to Figs. 3-9 and 3-10, which illustrate the use of Quickening in single-axis attitude control systems employing proportional and on-off moment controls. The reticle is driven by a weighted sum of angular acceleration and angular rate about the principal axes as given by

$$\theta_2 = D_{12}\omega_2 + D_{22}\dot{\omega}_2 \qquad (3.33)$$

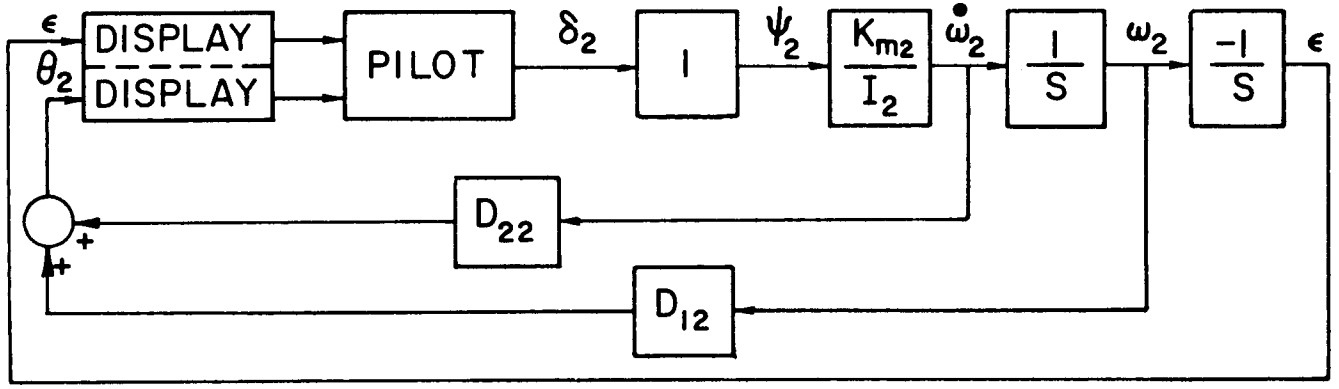

Fig. 3-9 Block Diagram of Pitch Control System Using Quickening or Rate-Reticle Display With Proportional Moment Control

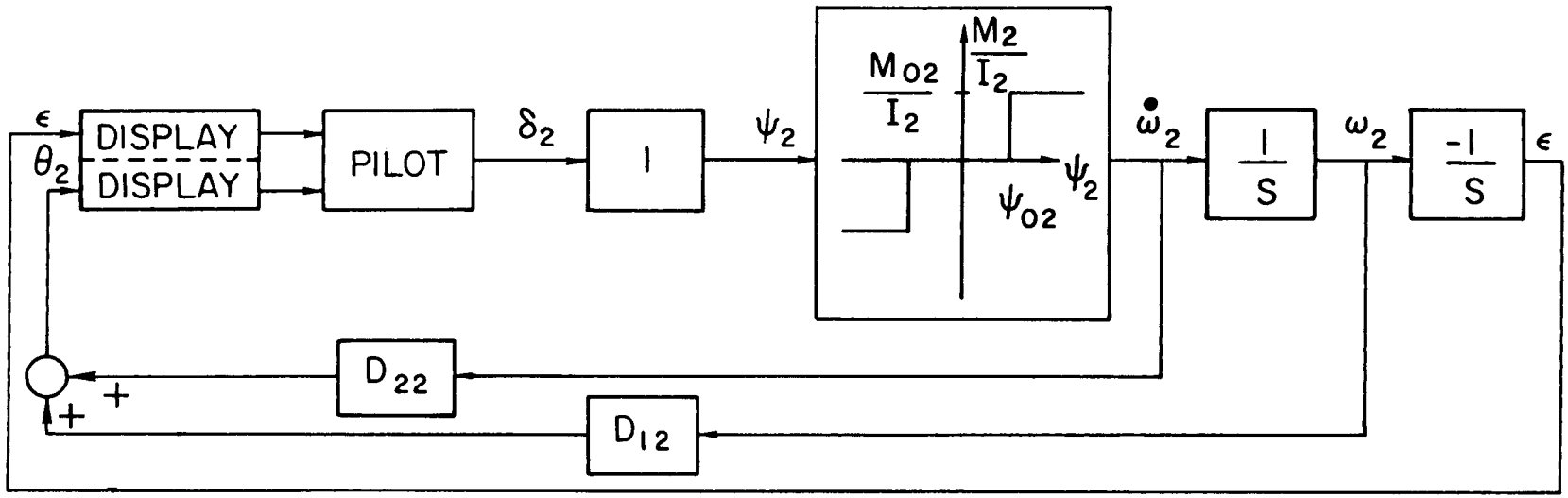

Fig. 3-10 Block Diagram of Pitch Control System Using Quickening or Rate-Reticle Display With On-Off Moment Control

The pilot manipulates the hand controller in an effort to keep the reticle superimposed over the star, i.e., he supplies the "equal sign" in Eq. 3.34*

$$\theta_2 = \epsilon \tag{3.34}$$

Provided that Eq. 3.34 is always satisfied, the transfer function between attitude error and vehicle angular acceleration is given by Eq. 3.35, and the open-loop transfer function of the single axis system is given by Eq. 3.36

$$\frac{\dot{\omega}_2(s)}{\epsilon(s)} = \frac{s}{D_{12}\left(\frac{D_{22}}{D_{12}} s + 1\right)} \tag{3.35}$$

$$KG(s) = \frac{1}{D_{12}\left(\frac{D_{22}}{D_{12}} s + 1\right) s} \tag{3.36}$$

If the display gains D_{12} and D_{22} are chosen according to Eqs. 3.37 and 3.38 the closed-loop system will respond as a second-order system having a natural frequency ω_n and a damping ratio ζ ; the numerical values apply to a typical case in which the natural frequency is 0.5 rad/sec and the damping ratio is 0.5.

---

*Some of the earlier work on Quickening explained this approach with reference to a compensatory display in which the pilot attempted to null the weighted sum of acceleration, rate, and error according to Eq. 3.34a

$$D_{12}\omega_2 + D_{22}\dot{\omega}_2 - \epsilon = 0 \tag{3.34a}$$

This has the same effect as attempting to satisfy Eq. 3.34 where θ_2 is given by Eq. 3.33. In fact, the quantity $(D_{12}\omega_2 + D_{22}\dot{\omega}_2 - \epsilon)$ is the distance between the reticle and star, and nulling this quantity corresponds exactly to tracking the star with the reticle.

$$D_{12} = \frac{2\zeta}{\omega_n} = 2 \text{ sec} \tag{3.37}$$

$$D_{22} = \frac{1}{\omega_n^2} = 4 \text{ sec}^2 \tag{3.38}$$

Equation 3.37 shows that setting D_{12} equal to zero results in an unstable system. From the open-loop transfer function given by Eq. 3.36, it can be seen that setting D_{22} equal to zero results in a system which exhibits a first-order response with a time constant equal to D_{12}; this is the case of the Rate-Reticle Display considered by Cannon (Ref. 21).

Comparison of Figs. 3-4 and 3-9 (or Figs. 3-5 and 3-10) indicates that Quickening differs from Control Action Display in two important respects:

(1) With Quickening, no compensation is used between the pilot and the jet control valves. Equation 3.35 shows that the compensation (specifically the filtered derivative) required to stabilize the system is obtained in the inner loop by operation of the display.

(2) Comparison of Eqs. 3.16 and 3.39 indicates that the open-loop dynamics of the inner loop are more complex in the case of Quickening and Rate Reticle ($D_{22} = 0$) then for Control Action Display.*

$$\theta_2(s) = D_{12}\,\omega_2(s) + D_{22}\,\dot{\omega}_2(s) = \frac{K_{m2}}{I_2}\left(D_{22} + \frac{D_{12}}{s}\right)\delta_2(s) \tag{3.39}$$

The reticle position is determined not only by the pilot's instantaneous response, but must** also contain a component which is proportional to the integral of his past responses. The types of

*Equation 3.39 suggests the possibility of mechanizing the quickened system according to Fig. 3-11 and thereby avoiding the necessity of providing velocity and acceleration sensors on each of the three axes.

**As mentioned previously, the requirement for a nonzero D_{12} follows from Eq. 3.37.

tracking employed within the inner loop are known as "direct," "aided," and "velocity" tracking in the case of Control Action Display, Quickening, and Rate Reticle, respectively. Lincoln and Smith (Ref. 22) have shown that direct pursuit tracking is consistently more accurate than aided tracking, and that velocity tracking is very poor in comparison with direct and aided tracking. In the case of a system using on-off thrust control (Fig. 3-10), the on-off characteristic is also contained within the inner loop. The introduction of this gross nonlinearity in the display loop makes it nearly impossible for the pilot to track the designated stars with the reticle.

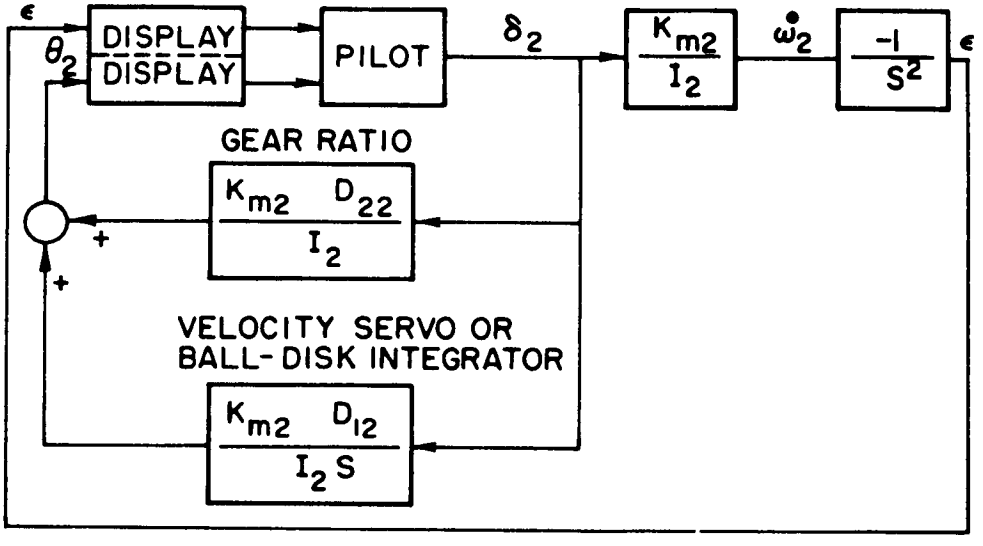

Fig. 3-11 Alternative Implementation of Quickened System

Still another technique used in the design of manually-controlled systems is Kelly's Predictor Instrument (Refs.23 and 24). This approach displays the predicted time history of the system errors computed by an analog computer model of the plant operating many times faster than real-time; the prediction is usually made under the assumption that the controller is returned to zero at that instant of time.

This approach differs from Control Action Display in two respects: (1) The display does not indicate what corrective action the pilot should take but instead displays the transient which will result if no corrections are applied; coding the information is required in order to present multidimensional transients on a two-dimensional display. (2) The attitude errors and body rates must be available as electrical signals for input to the fast-time analog computer; a star tracker would be required to convert a visual reference into attitude-error signals, and of course substantial computer equipment is required.

3.6 Simulation of Three-Axis Attitude Control Systems

An analog computer study was performed to determine the effectiveness of Control Action Display, Quickening, and Rate Reticle in a three-axis attitude control system. In this fixed-base simulation, the pilot's view of the star field and reticle (Fig. 3-1) was presented on an oscilloscope. The coordinates of Stars 1 and 2 were generated using Eqs. 3.40 and 3.41 which approximate Eqs. A.7 and A.8 of Appendix A for small α and ϵ.

$$\dot{\alpha}_j = - \omega_3 - \epsilon_j \omega_1 \qquad j = 1,2 \tag{3.40}$$

$$\dot{\epsilon}_j = \alpha_j \omega_1 - \omega_2 \qquad j = 1,2 \tag{3.41}$$

For this case the angular rate at which Star 2 moves around Star 1 on the display is given by

$$\dot{\rho} = \frac{d}{dt}\left[\tan^{-1}\frac{\alpha_2 - \alpha_1}{\epsilon_2 - \epsilon_1}\right] = - \omega_1 \tag{3.42}$$

Although this expression was not used explicitly in generating the display, it was used to compute the line-of-sight angle shown in Figs. 3-13 to 3-16 and Fig. 3-22. The cross coupling due to differences in principal moments of inertia (see Eqs. 3.11 to 3.13) was neglected in the derivation of the body rates about the three axes. The reticle was

positioned according to Eqs. 3.43 and 3.44 for Control Action Display and Quickening/Rate Reticle, respectively; Rate Reticle is a special case of Quickening in which $D_{2i} = 0$.

$$\theta_i = K_{ci}\,\delta_i \qquad i = 1,2,3 \tag{3.43}$$

$$\theta_i = D_{1i}\,\omega_i + D_{2i}\dot{\omega}_i \qquad i = 1,2,3 \tag{3.44}$$

The variables used in the oscilloscope display were sampled by an electromechanical commutator at a rate of 20 samples/sec, which resulted in a flicker-free presentation. The pilot controlled the spacecraft using a spring-restrained, three-axis controller illustrated in Fig. 3-12; notice the one-to-one correspondence between the directions of controller and display of deflections.

Figures 3-13 through 3-21 show typical results of an attitude control maneuver defined by the initial conditions given in Eq. 3.45 and the parameters listed in Table 3.2.

$$\alpha_1(0) = \epsilon_1(0) = 0.4 \text{ rad} \qquad \alpha_2(0) = \epsilon_2(0) = 0.5 \text{ rad}$$

$$\omega_1(0) = \omega_2(0) = \omega_3(0) = 0 \tag{3.45}$$

Figures 3-13 through 3-16 show the line-of-sight angles as functions of time for the maneuver defined by Eq. 3.45. These particular runs were selected from among several trial runs for each of the four systems because they closely approximate the transient performance which would have resulted if the pilot had kept the reticle perfectly aligned over the star pattern throughout the entire maneuver. The transient responses for the so-called "perfect pilot", given by the dashed curves in Figs. 3-13 through 3-16, were obtained by connecting the appropriate error signals directly to the control jet inputs in place of the control stick outputs δ_i, so that Eqs. 3.43 and 3.44 were satisfied for Control Action Display and Quickening/Rate-Reticle, respectively.

Table 3.2

Parameters Used in Simulation of Three-Axis Attitude Control System

Figs. 3-13, 3-17 and 3-18: Maneuver Using Control Action Display with Proportional Moment Control

$K_{c1} = 3.0$	$K_{c2} = 1.25$	$K_{c3} = 1.25$
$K_{m1}/I_1 = 1.5\ \text{sec}^{-2}$	$K_{m2}/I_2 = 1.0\ \text{sec}^{-2}$	$K_{m3}/I_3 = 1.0\ \text{sec}^{-2}$
$\tau_1 = 7.9$ sec	$\tau_2 = 6.3$ sec	$\tau_3 = 6.3$ sec
$K_{n1} = 10$	$K_{n2} = 10$	$K_{n3} = 10$

Figs. 3-14, 3-17 and 3-19: Maneuver Using Control Action Display with On-Off Moment Control

$K_{c1} = 3.0$	$K_{c2} = 1.25$	$K_{c3} = 1.25$
$M_{o1}/I_1 = 0.12\ \text{rad/sec}^2$	$M_{o2}/I_2 = 0.08\ \text{rad/sec}^2$	$M_{o3}/I_3 = 0.08\ \text{rad/sec}^2$
$\psi_{o1} = 4 \times 10^{-3}$ rad	$\psi_{o2} = 4 \times 10^{-3}$ rad	$\psi_{o3} = 4 \times 10^{-3}$ rad
$\tau_1 = 1.25$ sec	$\tau_2 = 1.25$ sec	$\tau_3 = 1.25$ sec
$K_{n1} = 10$	$K_{n2} = 10$	$K_{n3} = 10$

Figs. 3-15, 3-17 and 3-20: Maneuver Using Quickening with Proportional Moment Control

$D_{11} = 2.5$ sec	$D_{12} = 2.0$ sec	$D_{13} = 2.0$ sec
$D_{21} = 3.5\ \text{sec}^2$	$D_{22} = 2.8\ \text{sec}^2$	$D_{23} = 2.8\ \text{sec}^2$
$K_{m1}/I_1 = 0.4\ \text{sec}^{-2}$	$K_{m2}/I_2 = 0.4\ \text{sec}^{-2}$	$K_{m3}/I_3 = 0.4\ \text{sec}^{-2}$

Figs. 3-16, 3-17 and 3-21: Maneuver Using Rate-Reticle Display with Proportional Moment Control

$D_{11} = 3.5$ sec	$D_{12} = 2.5$ sec	$D_{13} = 2.5$ sec
$D_{21} = 0\ \text{sec}^2$	$D_{22} = 0\ \text{sec}^2$	$D_{23} = 0\ \text{sec}^2$
$K_{m1}/I_1 = 0.2\ \text{sec}^{-2}$	$K_{m2}/I_2 = 0.2\ \text{sec}^{-2}$	$K_{m3}/I_3 = 0.2\ \text{sec}^{-2}$

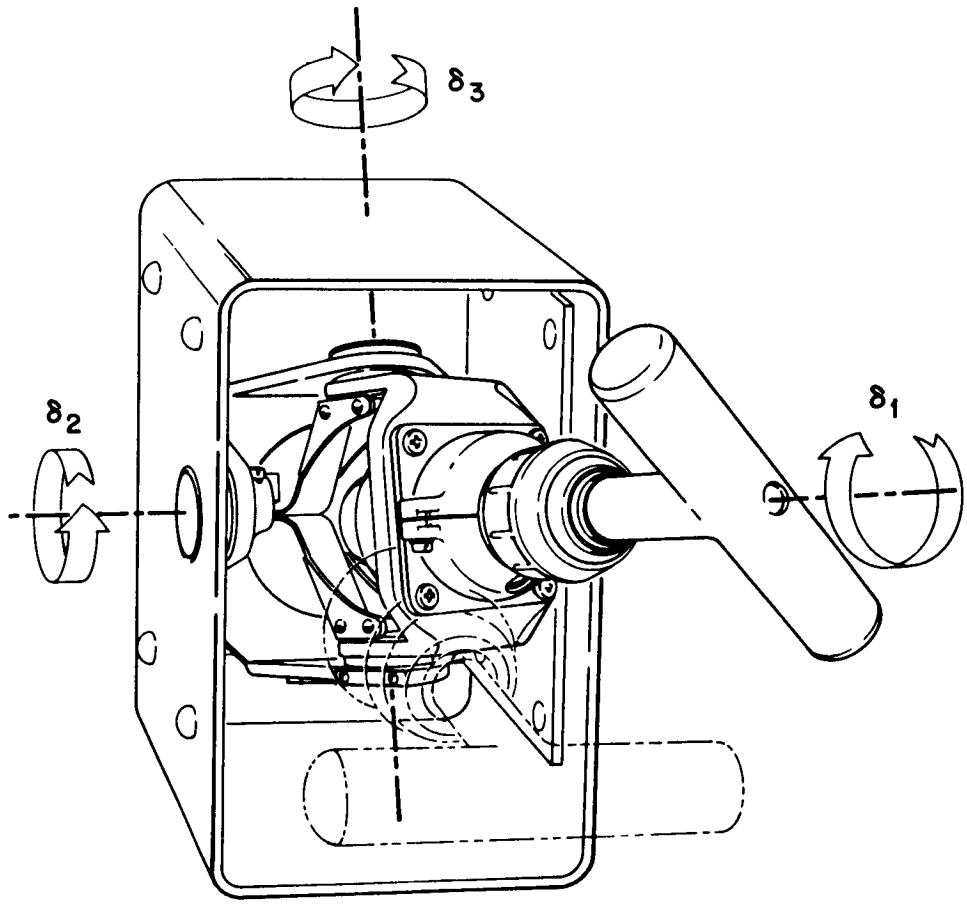

Fig. 3-12 Diagram of Hand Controller Used in Simulator Studies

It should be noted that, because corrections were applied in roll, pitch and yaw simultaneously, the transient response in each axis is considerably different from that which is derived on the basis of the single-axis analysis given in Sections 3.4 and 3.5. For example, in this particular maneuver, roll motion is strongly coupled into yaw with the result that errors in α are reduced much more rapidly than errors in ϵ.

Transient Response Comparison

Figures 3-13 and 3-15 show that (for the prefect pilot) systems using Control Action Display and Quickening, with proportional moment control, exhibit similar transient behavior: both are typical second-order responses with moderate overshoot and approximately equal duration.

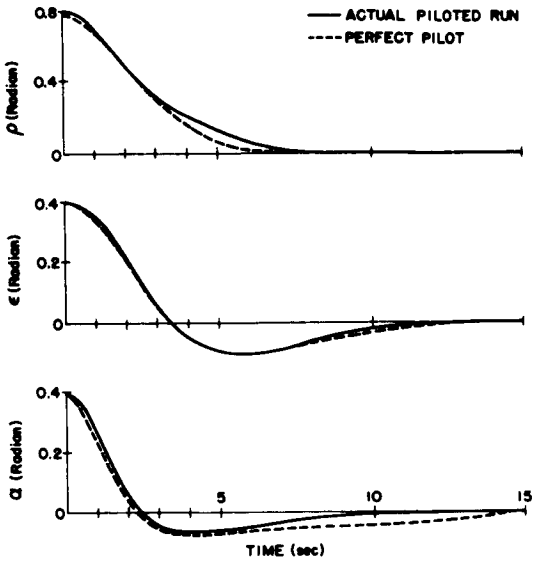

Fig. 3-13 Transient Response of System Using Control Action Display with Proportional Moment Control

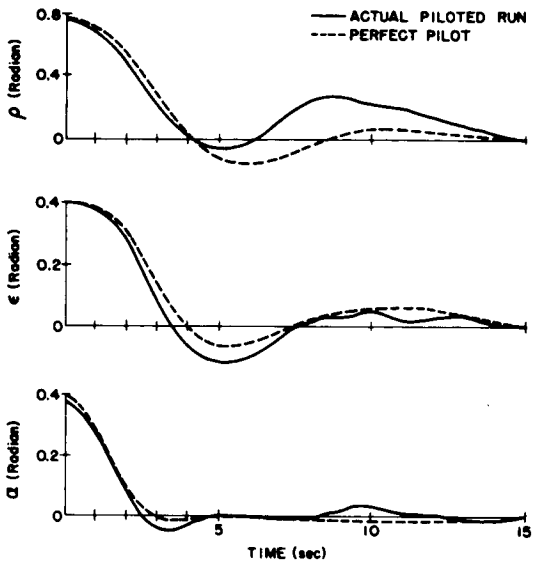

Fig. 3-14 Transient Response of System Using Control Action Display with On-Off Moment Control

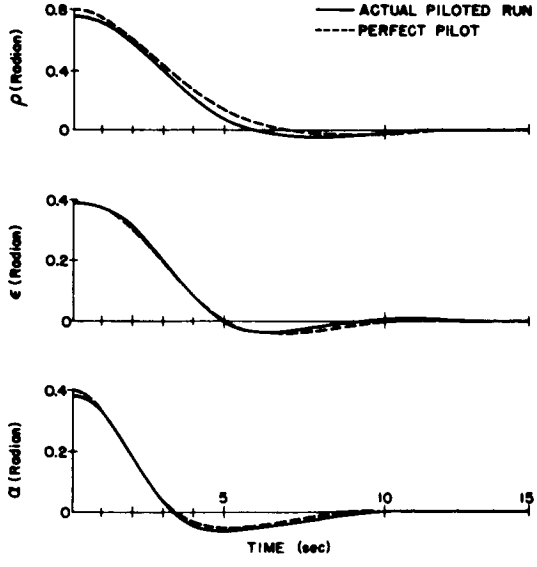

Fig. 3-15 Transient Response of System Using Quickening with Proportional Moment Control

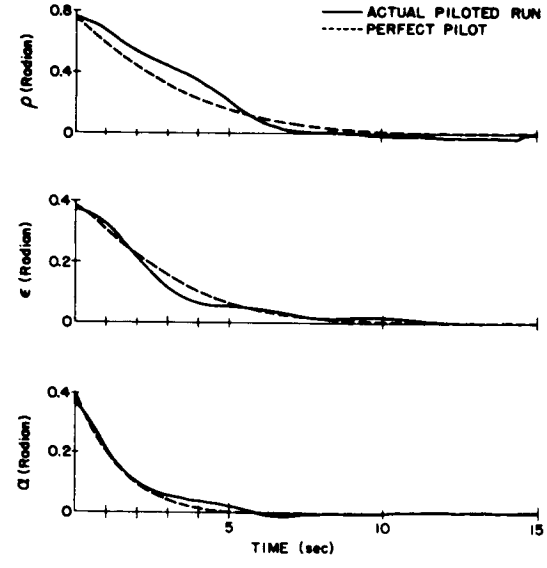

Fig. 3-16 Transient Response of System Using Rate Reticle with Proportional Moment Control

The overshoot is somewhat greater in the case of Control Action Display using on-off moment control; this effect, shown in Fig. 3-14, is due to the fact that the approximate switching-line (see Fig. 3-8) was derived for initial conditions slightly different from those which were actually used. For the case of the perfect pilot, the system using Rate-Reticle with proportional moment control exhibits the typical first-order response shown in Fig. 3-16.

Ease-of-Tracking Comparison

Figure 3-17 shows the pilot's display* at designated instants of time during the specific runs shown in Figs. 3-13 through 3-16. It can be seen that the tracking for these selected runs was moderately accurate in all cases. It should be emphasized, however, that, on the basis of the limited number of experiments performed to date, it appears that Control Action Display is preferable to Quickening, and substantially superior to Rate-Reticle Display for the manual control of spacecraft using proportional moment control.** This superiority derives from the ease and reduced concentration with which the pilots tested can perform various attitude control maneuvers. The advantage of Control Action Display over the other two techniques is outstanding in the case of systems employing on-off moment control.

Fuel Consumption Comparison.

Figures 3-18 through 3-21 show the angular accelerations as functions of time about each of the three principal axes for selected runs (although not the same runs as in Figs. 3-13 through 3-17) using each of the four systems. The fuel used in each case, estimated as the

* The grid markings in the oscilloscope presentation would not be a part of the pilot's display in the actual system. They are presented in these photographs to permit a quantitative evaluation of the data.

** Note that this ranking is in agreement with the results of Lincoln and Smith (Ref. 22) who found that the performance obtained using direct pursuit tracking was somewhat better than aided tracking, which was in turn better than velocity tracking.

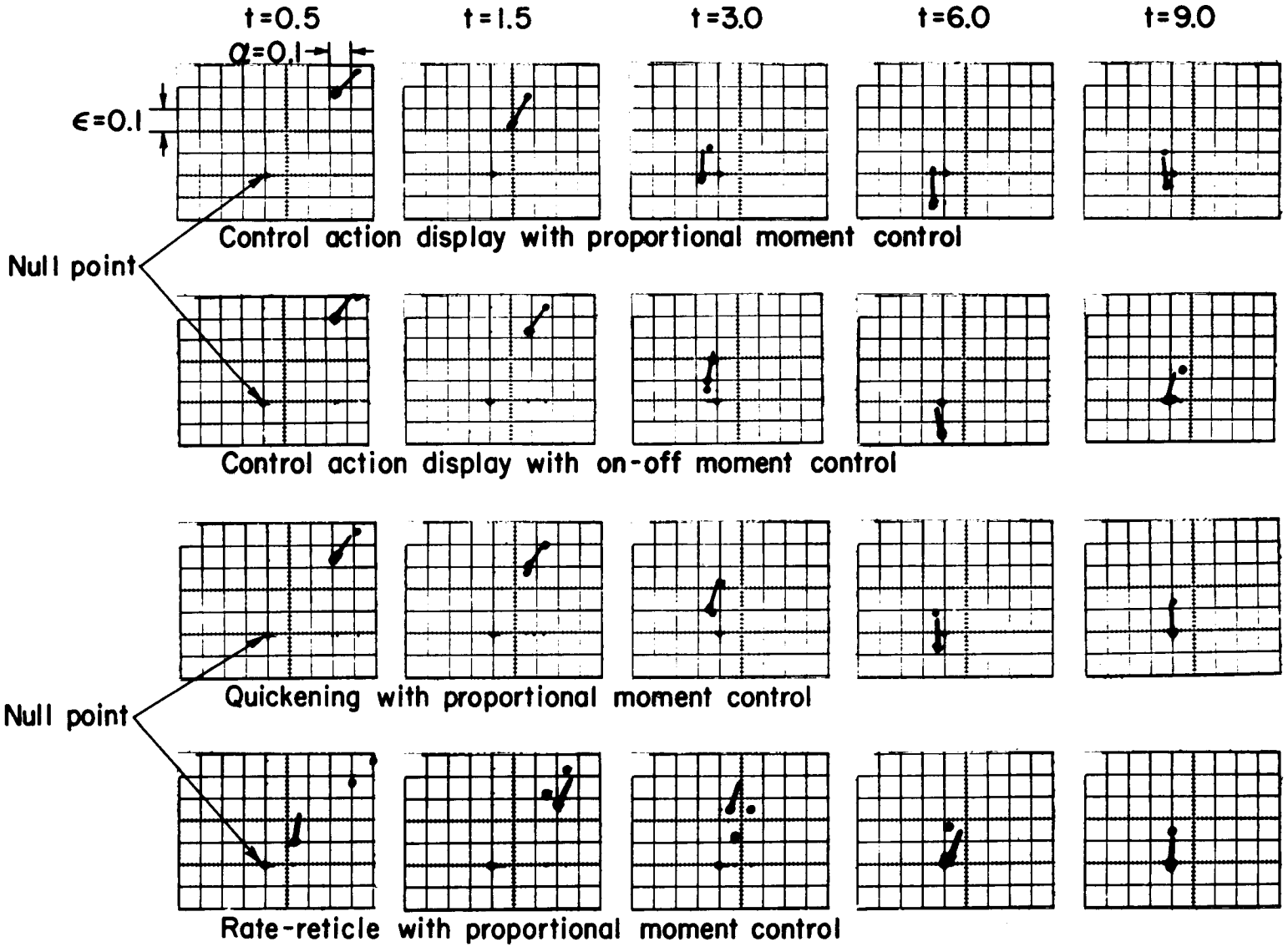

Fig. 3-17 Pilot's Display at Selected Times During Attitude Control Maneuver

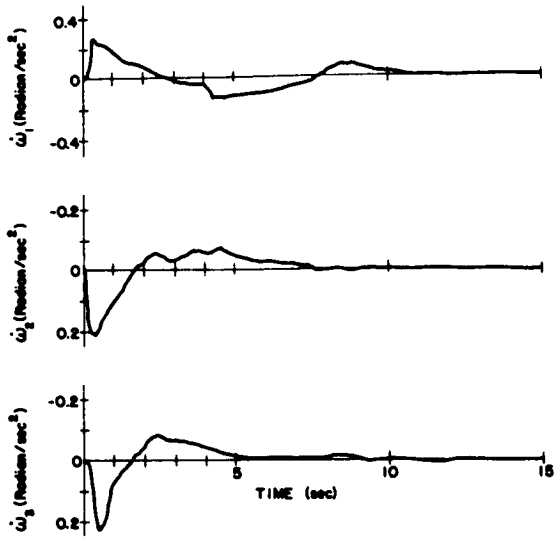

Fig. 3-18 Angular Accelerations for System Using Control Action Display with Proportional Moment Control

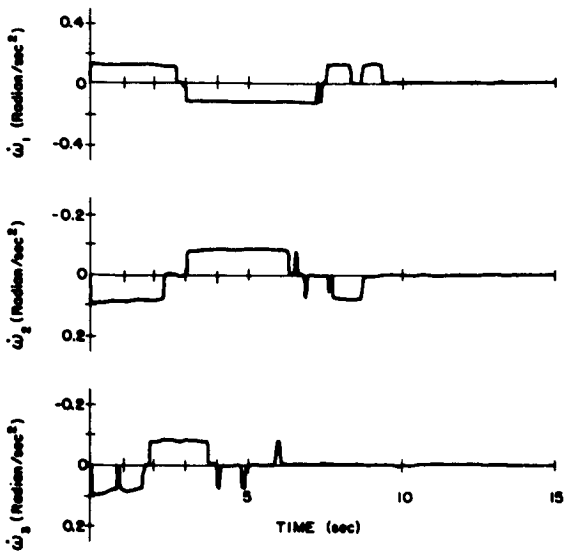

Fig. 3-19 Angular Accelerations for System Using Control Action Display with On-Off Moment Control

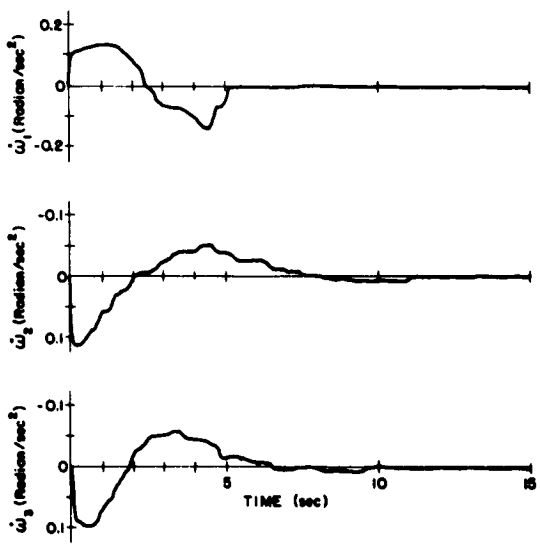

Fig. 3-20 Angular Accelerations for System Using Quickening with Proportional Moment Control

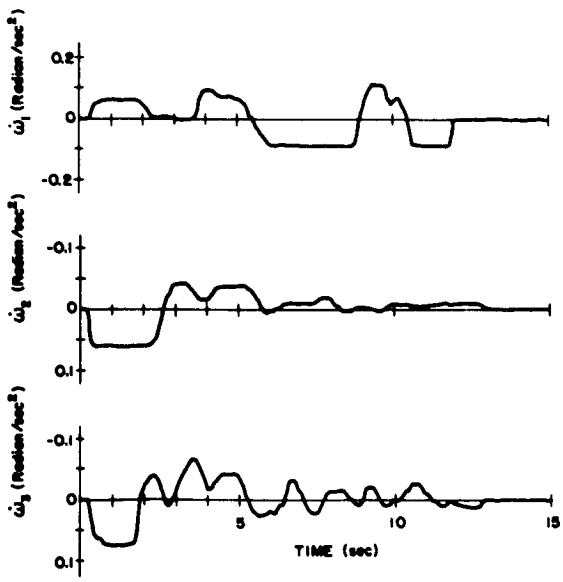

Fig. 3-21 Angular Accelerations for System Using Rate Reticle with Proportional Moment Control

absolute value of the area under these curves, appears to be approximately the same for all cases except Rate-Reticle, which required somewhat more fuel. In practice the time allowed for the maneuver is more important in determining the fuel requirement than the detailed response characteristics in the case of systems using Control Action Display or Quickening; the fuel required varies inversely with the time allowed for the maneuver.

Station-keeping Mode

Figure 3-22 shows the line-of-sight angles during a typical station-keeping operation. In this case the attitude angles are allowed to drift within prescribed limits (e.g., $\pm$ 1/4 rad in roll and $\pm$ 1/8 rad in pitch and yaw) before the pilot actuates the appropriate thrust jet. For the case shown in Fig. 3-22 the pilot simply placed the Control Action Display reticle over the star pattern and pressed a pushbutton on the hand controller which caused a 100 millisecond torque impulse (12×10^{-3} rad/sec in roll and 8×10^{-3} rad/sec in pitch and yaw) about whichever axis was out of tolerance. From Fig. 3-22 it can be seen that the system exhibits a stable limit-cycle response about all three axes which the pilot can control with very little effort.

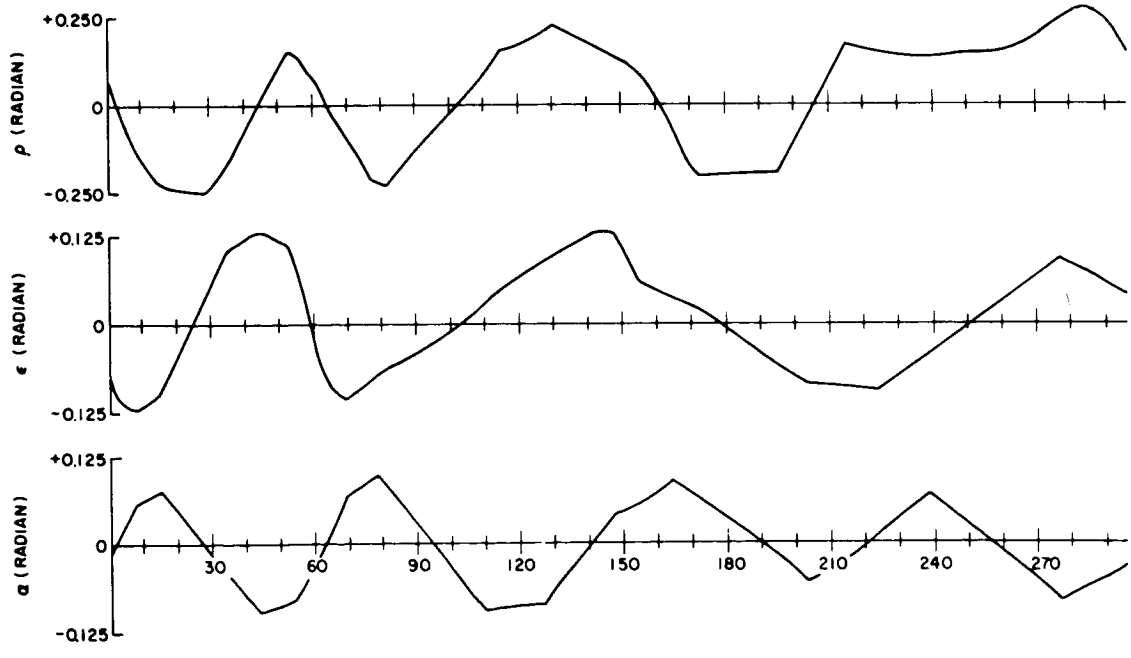

Fig. 3-22 Line-of-Sight Angles for Typical Station-Keeping Operation

3.7 Summary

The design approach outlined in Chapter 2 has been applied to a spacecraft attitude control problem. The use of Control Action Display made it possible to employ conventional analytical techniques to specify system parameters and to predict system performance; the particular methods used were frequency domain and phase-plane synthesis. The resulting system did not require a star tracker or a position or rate gyroscope and should therefore be more reliable than a completely automatic system or a system which employs Quickening or Rate Reticle aiding.

Simulation results indicated that the best runs for systems using Control Action Display, Quickening and Rate-Reticle with proportional moment control exhibit comparable transient responses and require approximately the same amount of fuel for a given maneuver. However, more consistent results are obtained with substantially less effort when using Control Action Display. Simulation results also show that Control Action Display makes it possible to control spacecraft employing on-off moment control (probably the case of greatest interest) almost as well and as easily as spacecraft employing proportional moment control.

Chapter 4

DESIGN OF A TIGHTROPE WALKER ATTITUDE CONTROL SYSTEM

4.1 Introduction

The design of a tightrope walker attitude control system is pertinent to this study for the following reasons:

1) It demonstrates the application of Control Action Display to systems in which the display variable can be processed but the control variable is given.
2) It illustrates the use of the root-locus technique for synthesizing manned control systems.
3) It is an example of an application in which a human operator is employed in an intrinscially unstable system.

According to Fig. 2-2, the closed-loop tracking system consisting of the operator and his Control Action Display theoretically can be placed anywhere in the overall control loop. In practice, however, the variable tracked by the operator and the way his output affects the system should both be selected so that the resulting complexity of the overall system is minimized. Chapter 3 described a system in which the display was given (i.e., the star field presentation was not amenable to any sort of processing) but the operator's response could be processed in a compensation network (e.g., see Fig. 3-3) before it is input to the given plant. In this chapter the Control Action Display principle is applied to a system in which the designer is free to select and process the display variable, but can not change the way the operator's output affects the given plant.

In the past, the synthesis of most manned control systems has been carried out using frequency-response techniques; that is the approach used in Chapter 3 (see Fig. 3-7) for designing the spacecraft attitude control system. Such frequency-response methods were popular because the

system transfer function was usually well-behaved along the jω-axis, and because most measurements of human operator dynamics were expressed in terms of a frequency response. The synthesis of the tightrope-walker attitude control system is more conveniently carried out by root-locus methods, because (as shown in Appendix C) the transfer function of the open-loop plant has two zeros on the jω-axis and a pole in the right-half of the s-plane. The root-locus design procedure described in this chapter also illustrates the application of the pole-zero model of the human operator developed in Chapter 5.

Whereas the plant considered in Chapter 3 had two poles at the origin, the open-loop transfer function of the tightrope walker attitude control system has one pole in each the right and left half of the s-plane. It therefore provides an interesting example of the way in which a human operator can be employed in intrinsically unstable dynamic systems. The techniques and results described in this chapter may be pertinent to the design of similar systems (for what may be more practical applications) such as attitude control of the thrust supported platform for lunar transportation described in Ref. 25.

4.2 Description of Overall System

Figure 4-1 is a schematic representation of the tightrope walker attitude control problem. Because the man is constrained to keep one foot directly in line with the other, he cannot exert the torques ordinarily used to maintain balance. The open-loop dynamics of this system are essentially those of the inverted pendulum studied by Higdon and Cannon (Ref. 26). However, by translating and rotating the long balancing pole, the tightrope walker can control the moments caused by inertial forces and the external moments due to gravitational forces about the rope, and can thereby stabilize the overall system. The important variables, designated α, θ, ρ, and x_p, are defined in this figure.

In Appendix C, a model of the overall system is developed using information provided by a professional tightrope walker. According to

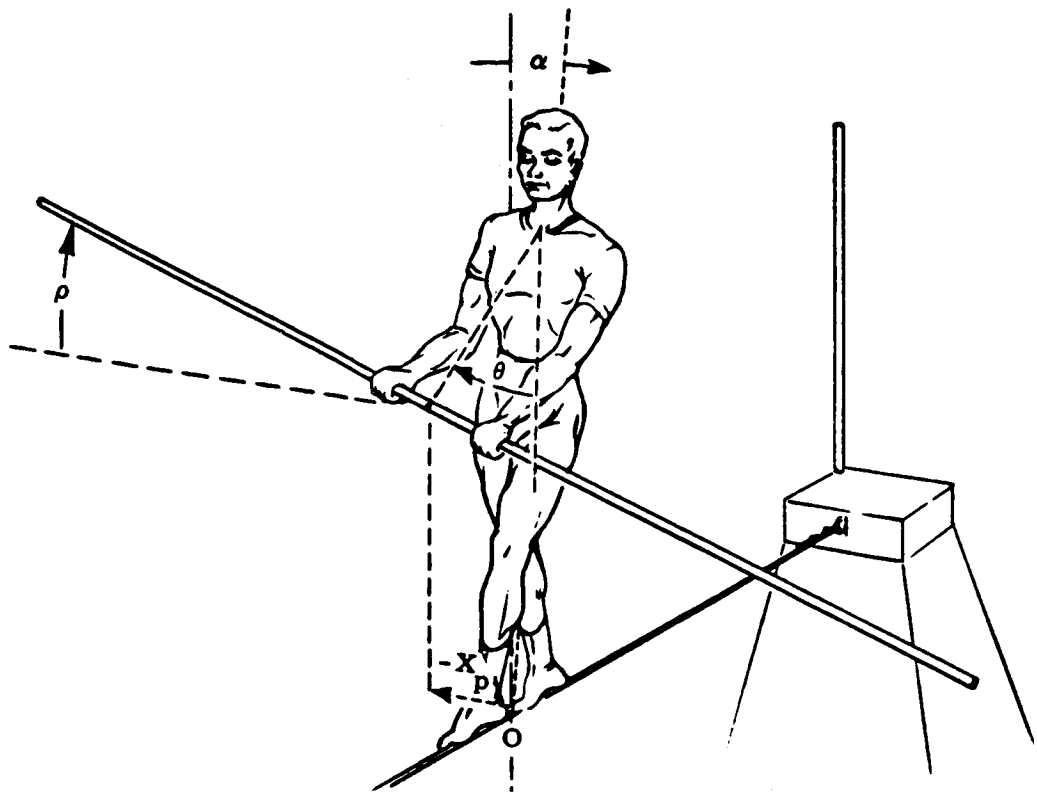

Fig. 4-1 Tightrope Walker Attitude Control Problem

this model, the man perceives his attitude error and its time derivatives from visual feedback and from the vestibular semicircular canals of the inner ear, respectively. He tries to maintain his body (except for his arms) as rigid as possible while rotating and translating the balancing pole according to the relations

$$\rho = \theta \tag{4.1}$$

$$\frac{X_p(s)}{\alpha(s)} = - \frac{K_c \omega_f (s + \omega_c)}{\omega_c (s + \omega_f)} \tag{4.2}$$

where typically

K_c = 27 ft/rad = 5.6 in./deg; ω_c = 1.74 rad/sec; ω_f = 10.0 rad/sec

The response of the open-loop plant is given by

$$\frac{\alpha(s)}{X_p(s)} = \frac{K_p(s + jZ_2)(s - jZ_2)}{(s + P_3)(s - P_3)} \tag{4.3}$$

where typically

$K_p = 3.54 \times 10^{-2}$ rad/ft; Z_2 = 2.88 rad/sec; P_3 = 2.28 rad/sec

Appendix C shows that these equations result in a stable system (see Fig. C-3) and are consistent with the tightrope walker's estimate of the control motion he actually uses.

Considerable aptitude, practice, and expert coaching are required to learn the complex motor skill of tightrope walking. However, according to the theory developed in Chapter 2, the application of Control Action Display should enable a person with no previous training to maintain his balance on a tightrope after only a few trials. In an attempt to test this conjecture such a system was devised and experiments were conducted using a taut cable elevated several inches from the floor.

Figure 4-2 shows how the Control Action Display principle was applied to the tightrope walker attitude control problem. A rate gyro attached to the subject's waist measured the attitude error rate in a plane normal to the cable; thus the gyroscope provided the information ordinarily derived from visual feedback and from the vestibular semicircular canals of the inner ear. A small analog computer processed the gyroscope output to give the one-dimensional command x_c which was displayed as the horizontal displacement of an X-Y plotter. This plotter was placed on a table in front of the subject* at approximately the height of the balancing pole center of mass. The plotter reference

*It was not intended that the subject walk along the cable but instead that he maintain his balance while standing in one place.

position (i.e., $x_c = 0$) was directly above the cable. The subject observed his instantaneous control action as the horizontal displacement of a mark drawn on the balancing pole at its center of mass. His task was simply to translate the pole (and rotate it as required by Eq. 4.1) to keep the mark aligned with the indicator on the X-Y plotter; i.e., he acted to equate x_p with x_c. This control motion affected his attitude angle according to the open-loop plant dynamics given by Eq. 4.3.

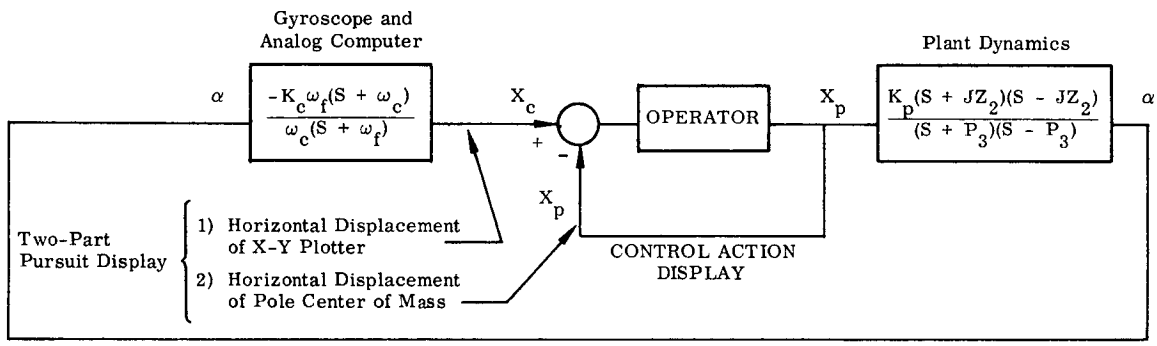

Fig. 4-2 Control Action Display Applied to Tightrope Walker Attitude Control Problem

As in Chapter 3, this system uses a pursuit display which presents (separately but on the same display) a command variable and the operator's instantaneous output; this is the basis of the Control Action Display principle. For the tightrope walker attitude control system shown in Fig. 4-2, the command variable can be selected and processed, but the dynamics between operator output and the system output cannot be altered. This is in contrast with the spacecraft attitude control system in which the command variable is given (see Fig. 3-1), but the operator output can be processed (see Fig. 3-3) before it is input to the rest of the system.

Two difficulties developed when untrained subjects attempted to maintain their balance on a taut wire using commands derived from the output of a rate gyro connected to their waist:

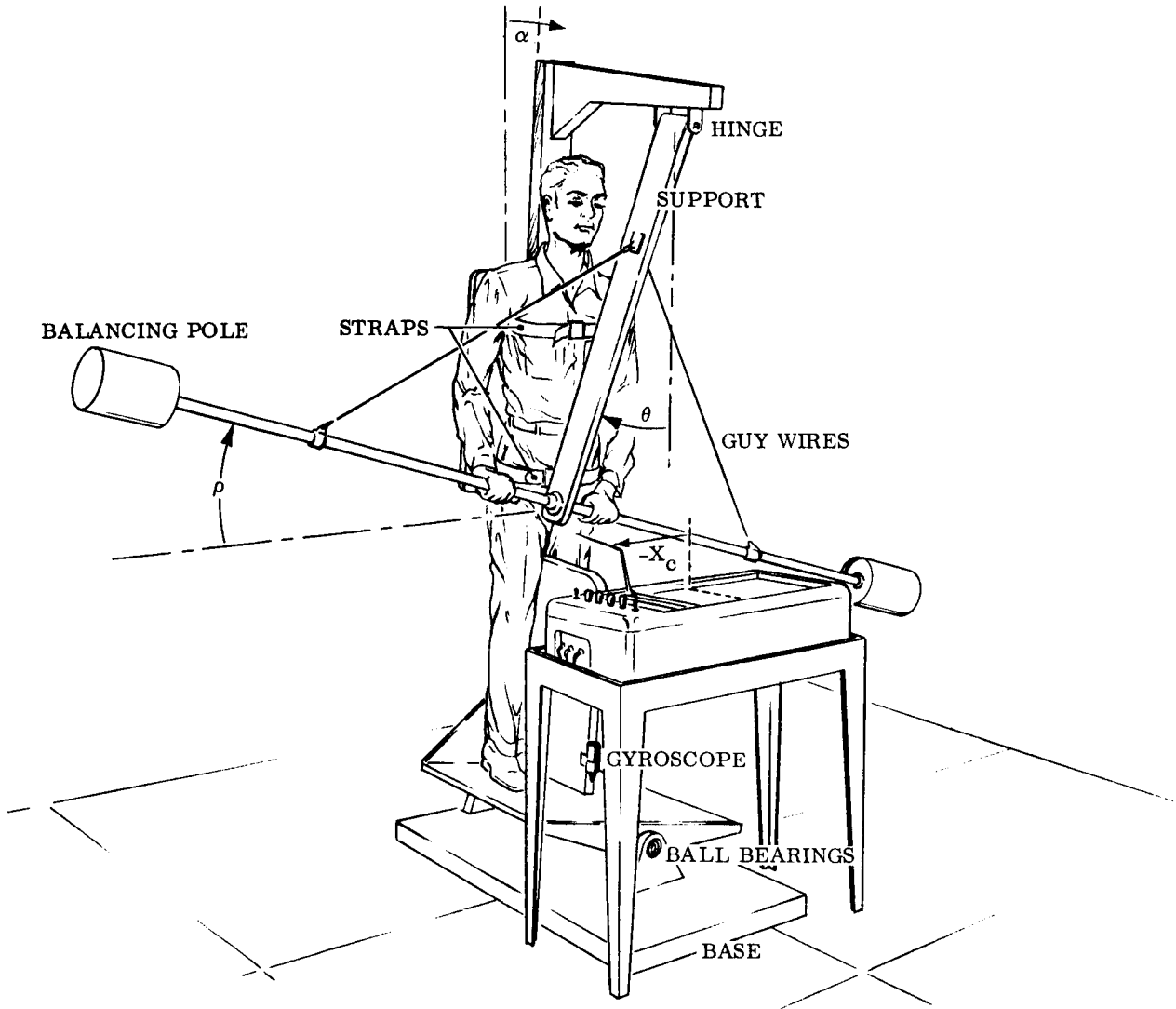

Fig. 4-3 Diagram of Experiment Used to Test the Application of Control Action Display to the Tightrope Walker Attitude Control Problem

1) They could not overcome the instinctive habit of bending their body to correct for unbalance. This body bending has two effects:
   a) It caused center of gravity shifts and inertia forces which are not accounted for by the plant dynamics of Eq. 4.3.
   b) It caused erroneous commands to be displayed, because the gyroscope measured localized bending instead of rigid body

attitude error rate. These commands were fast, large-amplitude displacements of the X-Y plotter which the subjects could not possibly follow with a 30 lb balancing pole.

2) The subjects tended to translate the pole only, and did not rotate it to satisfy Eq. 4.1.

Because they failed to emulate the tightrope walker's actions in these two important respects, none of the subjects was able to maintain his balance either with or without Control Action Display.

To make it easier for the subjects to keep their body rigid and to rotate the balancing pole according to Eq. 4.1 (i.e., to avoid the difficulties described in the previous paragraph) the apparatus shown in Fig. 4-3 was constructed. The subject stood on a platform which was mounted on ball bearings and free to rotate in a plane. The subject (facing the $-\dot{\alpha}$ direction) was strapped to the platform in such a way that body bending was limited as much as possible. The platform also carried the balancing pole; guy wires between the support and the balancing pole supplied the constraint (given by Eq. 4.1) which eliminates one degree of freedom and makes it possible to use only a one-dimensional control variable. This quantity, x_c (derived from the output of a rate gyro mounted on the platform), was displayed as the horizontal displacement of the X-Y plotter arm. The subject's task was simply to apply the force and torque required to track the plotter arm with a mark* on the balancing pole; this is analogous to tracking the star field with the reticle in Chapter 3.

4.3 Analytical Design of System

The block diagram describing the overall system is given in Fig. 4-4. The plant parameters (computed from Eq. C-18) for the system

*Here the difference between Control Action Display and Quickening is particularly apparent. Systems employing Quickening would derive a quantity equal to the weighted sum of angular position and rate but would present it on a display (for example a meter or oscilloscope) which is unrelated to the mark on the balancing pole.

including the platform are not significantly different from those (see Eq. 4.3) which apply to the tightrope walker alone. Also included in the block diagram is a transfer function representing the closed-loop tracking performance of a typical operator using a pursuit display. This transfer function, taken from Table 5.2, was derived from empirical tracking data by methods described in Chapter 5.

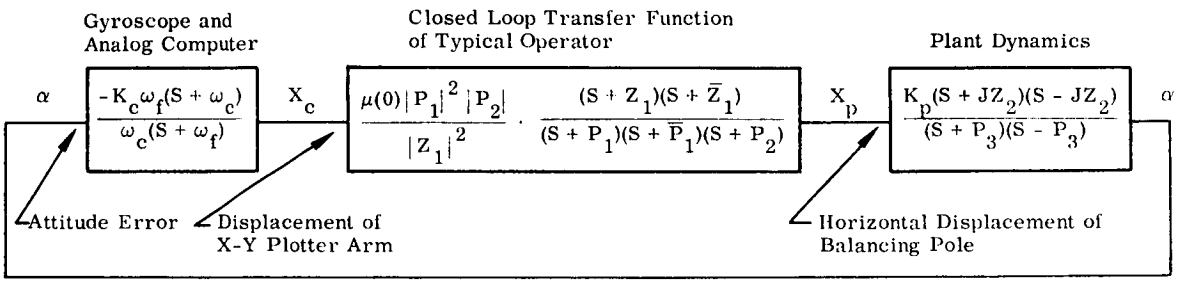

COMPENSATION	OPERATOR	PLANT
$K_c = 24 \frac{ft}{radian} \approx 5 \frac{in.}{deg}$	$\mu(0) = 0.86$	$K_p = 2.3 \times 10^{-2} \frac{radian}{ft}$
$\omega_c = 1.90 \frac{radian}{sec}$	$P_1 = 4.21 + J\,6.22 \frac{radian}{sec}$	$P_3 = 2.36 \frac{radian}{sec}$
$\omega_f = 10.0 \frac{radian}{sec}$	$P_2 = 33.7 \frac{radian}{sec}$	Z_2 3.60 $\frac{radian}{sec}$
	$Z_1 = -19.1 + J\,11.0 \frac{radian}{sec}$	

Fig. 4-4 Block Diagram of Attitude Control System for Balancing Platform

The dynamics of both the plant and the operator are considered fixed, and cannot be specified by the designer. Because the plant has two zeros on the imaginary axis and a pole in the right half of the s-plane, the design is more conveniently carried out using root-locus techniques than the frequency-response methods described in Chapter 3. The form of the compensation network (i.e., control law) shown in Fig. 4-4 is derived in Appendix C by using the root-locus approach. As a result, the only parameters which need to be specified are K_c, ω_c, and ω_f.

Figure 4-5* shows the root-locus diagram (for increasing values of K_c) for the entire system including the plant, operator and compensation network. From Fig. 4-5a it is clear that the overall system is stable for the parameter values listed; the numerical values of all six closed-loop poles are given for the case K_c = 24 ft/rad. Figure 4-5b is an expanded view showing the root-locus of the dominant poles. The closed-loop operating poles are designated for gain variation of $\pm$ 5% from the nominal value of 24 ft/rad. This figure indicates that acceptable system performance can be obtained for only a very narrow range of gain settings.

4.4 Experimental Results

The system shown in Fig. 4-3 was used to demonstrate the applicability of Control Action Display to intrinsically unstable systems by experimentally verifying the correctness of results derived in the preceding section. The subject, strapped to the platform, moved the balancing pole as required to track the horizontal motion of an X-Y plotter; this plotter was driven by the processed output signal from a rate gyro connected to the platform. An experimenter held the platform/subject combination at the attitude angle for which it was (as nearly as possible) neutrally stable and had zero angular velocity. He then activated the analog computer and released the platform. In this way the attitude angle used in the computation (derived by integrating the rate gyro output) was referenced to the angle of neutral stability, and the subject took control with (almost) zero attitude error and error rate.

Figure 4-6** shows the results of a typical experiment. The system is stable and exhibits a natural frequency of approximately

---

* The solid line sections of the root-locus diagrams shown in this chapter and Appendix C were plotted from data computed using Program No. 9.4.038, General Program Library for the IBM 1620 computer. This program, described in Ref. 27, computes the closed-loop roots with an estimated accuracy of four decimal digits.

** In Figs. 4-6, 4-7 and 4-8 the channel showing $\dot{\alpha}$ has been filtered by a first-order filter having a time constant of 0.1 second.

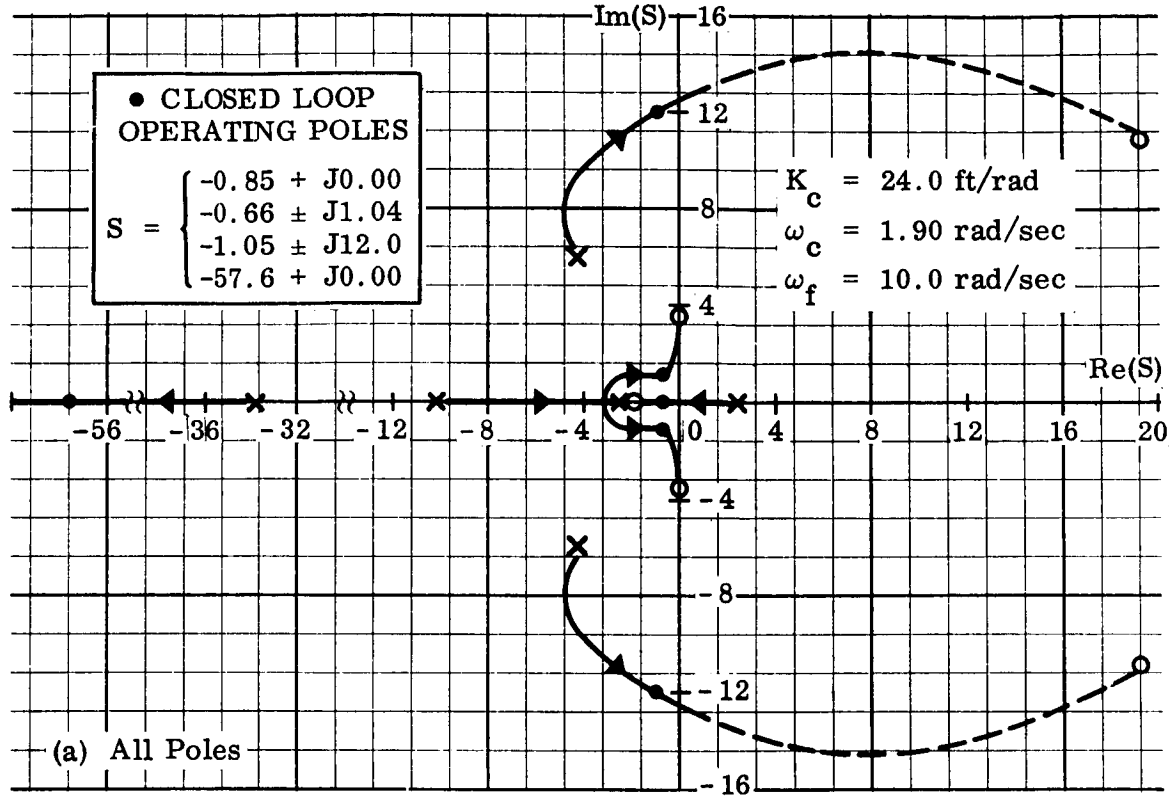

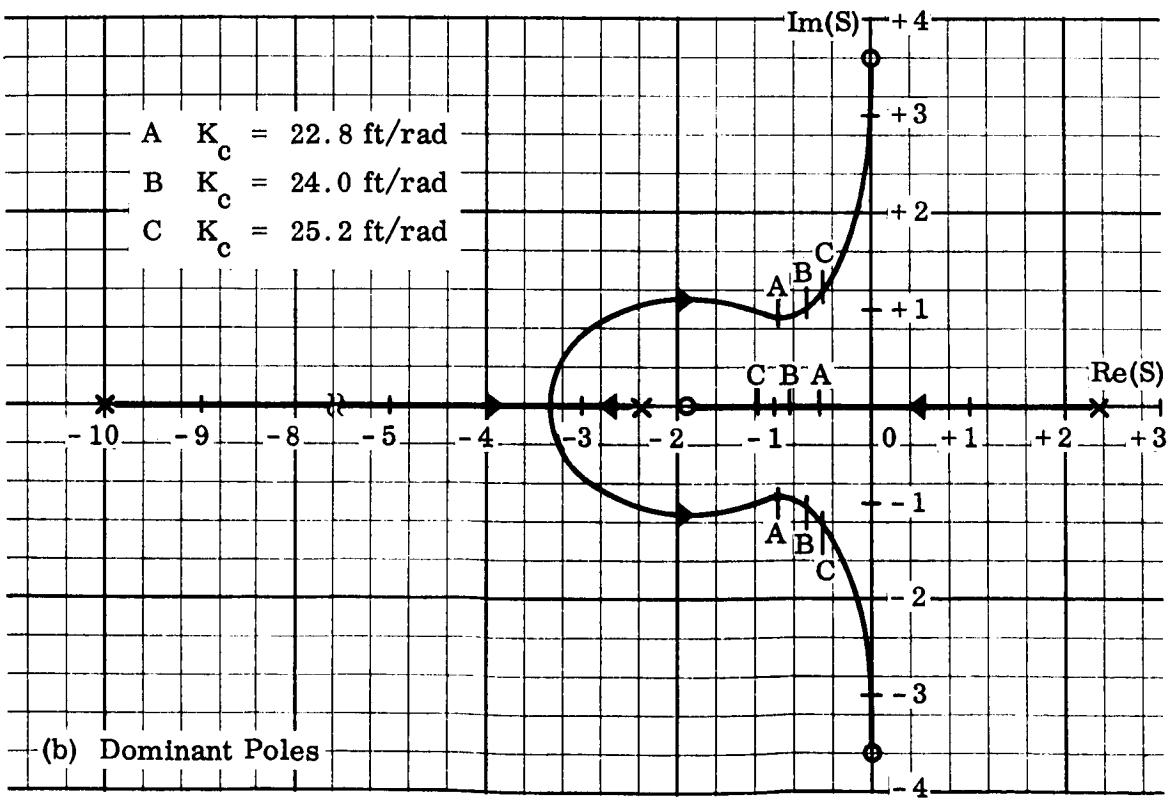

Fig. 4-5 Root-Locus Synthesis of Balancing Platform Attitude Control System

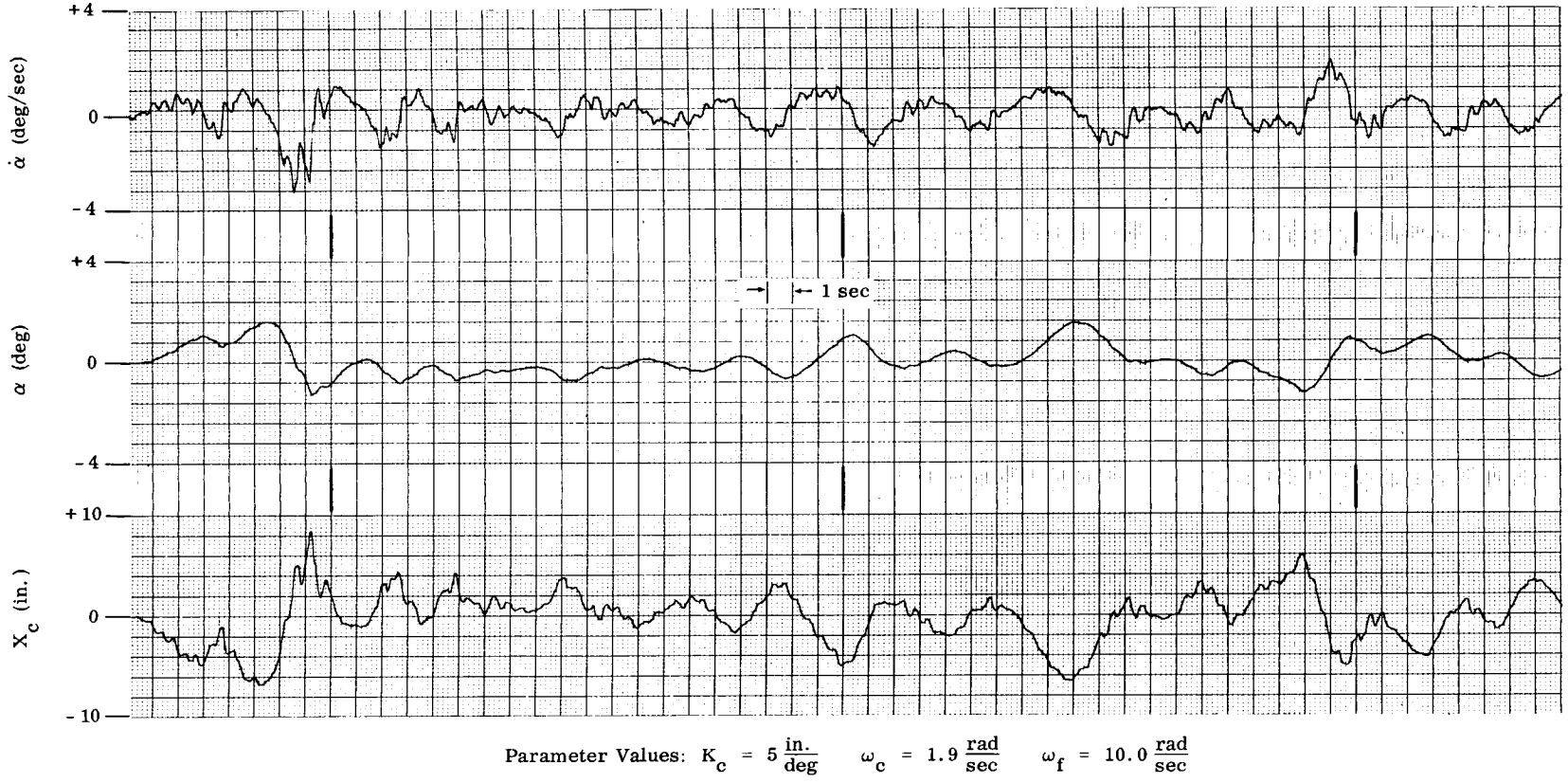

Fig. 4-6 Results of a Typical Experiment Using the Balancing Platform with Control Action Display

1.4 rad/sec, which agrees closely with the value of the dominant closed-loop poles given in Fig. 4-5b. Superimposed on this low-frequency hunting is a lightly damped oscillation of approximately 2 cycles/sec. This oscillation is believed to result from the operator-contributed poles (at $s = -1.05 \pm j12.0$) shown in Fig. 4-5a; another possibility is that it is due to structural vibration of the platform-subject combination. From a series of tests using various values of display gain, it was determined that the operators usually selected a gain very nearly equal to the one derived from the root-locus analysis of Fig. 4-5. This confirms the fact (evident from Fig. 4.5b) that the system performance is a very sensitive function of display gain.

According to Fig. 4-6, the normal excursions of attitude error and error rate are quite small; they were usually less than 4 deg and 4 deg/sec for successful runs. For this reason the small-angle approximations used in Appendix C (for deriving the equations of motion) appear to be justified. It is also interesting to note that the vestibular semicircular canals (used by the tightrope walker instead of a gyroscope) must be quite sensitive to permit such tight attitude control.

The system shown in Fig. 4-3 was tested by six male subjects between 25 and 35 years of age; none had any previous acrobatic experience but all had normal reflexes. Three of the six subjects were unable to stabilize the platform because they could not overcome the natural tendency to bend their body instead of moving the balancing pole to regain equilibrium. After a few attempts (during which a preferred value for K_c was selected) the other three subjects were able to maintain control for periods exceeding 30 seconds; runs of approximately 90 second duration were achieved in several cases. The successful runs terminated when the subject was distracted or when errors accumulated in the derived attitude angle due to gyro drift or movement of the subject on the platform. No subject was able to stabilize the platform without the aid of Control Action Display; Fig. 4-7 clearly demonstrates that for a typical attempt the system was not under control at any time.

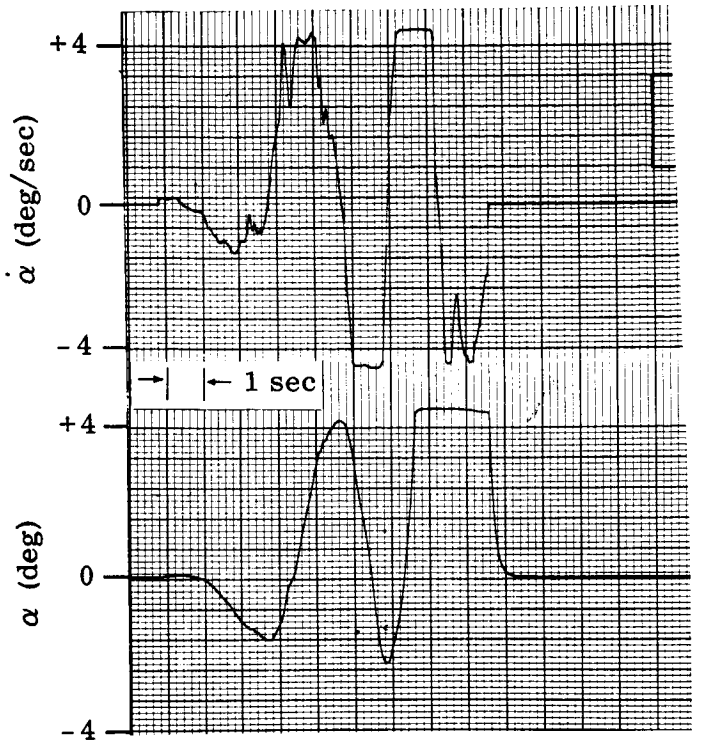

Fig. 4-7 Results of a Typical Experiment Using the Balancing Platform without Control Action Display

In another series of experiments the dynamics of the plant and compensation network (see Fig. 4-4) were simulated using an analog computer. The command variable x_c was displayed on an X-Y plotter as before. The simulated displacement of the balancing pole x_p was input to the computer from the Hand Monitor shown in Figs. 5-2 and D-2 and described in Appendix D. As before, the subject observed the command variable and his instantaneous response to it. His task was simply to keep the tracking pole of the Hand Monitor aligned with the arm of the X-Y plotter.

Figure 4-8 shows the results of a typical experiment using the simulated tightrope walker attitude control system. It is similar to Fig. 4-6 in both the amplitude of the excursions and the frequency

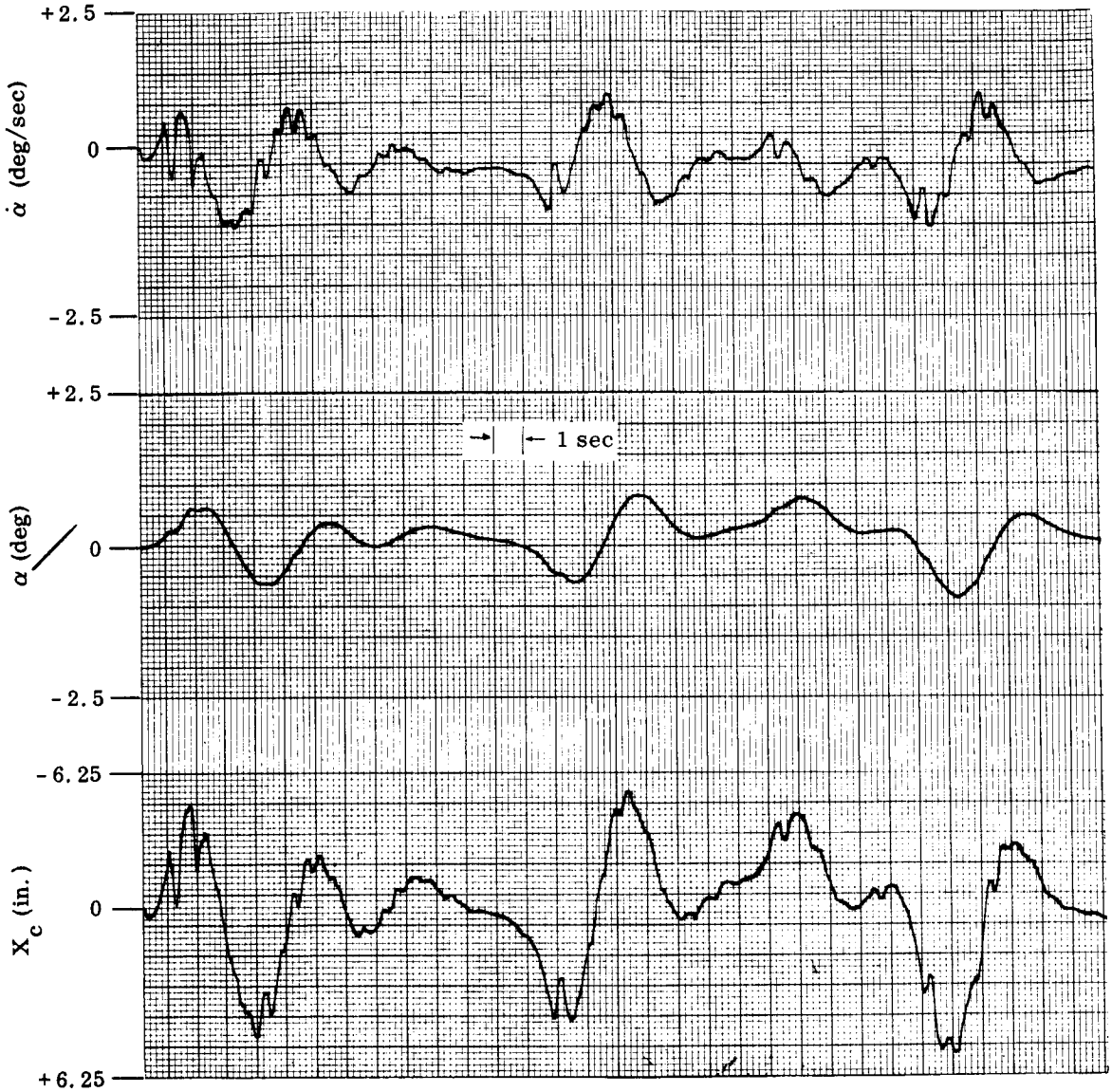

$K_c = 24 \frac{ft}{rad} \approx 5 \frac{in.}{deg}$ $\quad K_p = 2.3 \times 10^{-2} \frac{rad}{ft}$

$\omega_c = 1.90 \frac{rad}{sec}$ $\quad P_3 = 2.36 \frac{rad}{sec}$

$\omega_f = 10.0 \frac{rad}{sec}$ $\quad Z_2 = 3.60 \frac{rad}{sec}$

Fig. 4-8 Results of a Typical Experiment Using the Simulated Balancing Platform with Control Action Display

components of the response. The presence of the lightly damped, 2 cycle/sec oscillation in the simulated system response argues that the high-frequency oscillation observed in the platform experiments was due to operator contributed poles (at $s = -1.05 \pm j12.0$ in Fig. 4-5a) rather than to structural vibrations. The argeement between Figs. 4-6 and 4-8 indicates that Eq. 4.3 is an accurate description of the plant dynamics for those cases in which the subject did not move with respect to the platform.

It was found that all four subjects tested could easily stabilize the simulated tightrope walker attitude control system after only a few trials. This is interpreted to mean that the difficulty experienced by three subjects in controlling the actual platform was caused by some effect not included in the mathematical model of the system as they operated it. The ease with which the simulated system can be controlled demonstrates that considerable benefit can be realized when Control Action Display is applied to intrinsically unstable systems.

4.5 Summary

This chapter has described the application of the Control Action Display principle to intrinsically unstable dynamic systems. A root-locus synthesis procedure was used to specify the display processing required to control the fixed plant. It was experimentally demonstrated that the analysis provided an accurate description of the actual system, and that the use of Control Action Display made it possible for operators to stabilize a system which they could not control otherwise.

Chapter 5

INNER-LOOP PERFORMANCE OBTAINED EXPERIMENTALLY USING VARIOUS OPERATOR OUTPUTS FOR CONTROL ACTION DISPLAY

5.1 Background

5.1.1 Object of the Study

A procedure for designing the display and compensation sections of manually controlled, closed-loop systems has been described in Chapters 2, 3 and 4. From the preceding description of Control Action Display it is evident that the compensation network and plant dynamics must be specified within constraints imposed by the performance of the closed inner loop containing the Display, Operator and Control Devices sections. Chapter 3 shows that the crossover frequency of the compensation network and plant should occur at a frequency for which the closed inner loop (see Fig. 2-2) contributes very little phase shift. Similarly, in Chapter 4 it was shown that the dominant closed-loop poles of the overall system should be well inside the closed-loop poles of the inner loop. For this reason the performance of the closed inner loop often dictates the upper limit on overall system bandwidth and is, therefore, of primary importance.

Another important measure of inner-loop performance is the amount of random noise that is transmitted to the rest of the system; random noise is that part of the controller output which is uncorrelated with the system error. Applications, such as spacecraft attitude control, which attach a penalty to excessive control action, require a minimization of this random noise. The object of the study described in this chapter is to determine which of the several possible outputs of a human operator should be used in order to increase the bandwidth of the closed inner-loop while maintaining the component of random noise at an acceptable level.

Figure 2-2 shows that the configuration of the inner-loop dictates the nature of the tracking task in which the operator is employed, as follows:

(1) The controlled element is a unity (or constant) gain; this is the basis of Control Action Display.

(2) The operator is engaged in pursuit tracking; the (processed) system error and the controller output are presented separately on the same display.

Because kinesthetic feedback is not necessary in systems employing Control Action Display, a wide variety of operator responses can be considered for input to the rest of the system. The suitability of the operator's performance is measured by the transfer function and the random-noise output of the closed inner-loop. The measurement of the operator's open-loop transfer function and its variation are not important to this study.

Four different types of operator outputs will be considered in this chapter. The first two are the commonly used manual displacement and manual force, as measured by a three-axis hand controller and a pressure stick, respectively. In an effort to reduce delays in the response of the inner loop, the feasibility of using two different signals closer to the operator's central nervous system will be investigated. These are muscle action potentials (EMG) and angular displacement of the eye (EOG), both of which can be detected using surface electrodes.

To summarize, the object of this study is to determine which of several possible operator outputs should be used for Control Action Display to close the inner loop. The outputs investigated are:

(1) Manual displacement

(2) Manual force

(3) Muscle action potentials

(4) Angular displacement of the eye

The tracking task is limited to (1) unity (or constant) gain controlled element and (2) pursuit tracking. Results are evaluated on the basis of the closed-loop response. The desired result is to increase the bandwidth while maintaining the random noise at an acceptable level.

5.1.2 Organization of the Chapter

The material presented in Section 5.2 deals with tracking of step inputs. The purpose of the experiments described there is to identify and measure the various components of delay in a human operator's tracking response. The use of step inputs results in a well-defined response which simplifies the task of isolating and measuring latencies. Performance is measured during single step-moves and used to derive a model which describes the dynamics between muscle action potentials and manual displacement. Results obtained by tracking a series of random step inputs show the relationships between hand and eye movements in manual tracking and indicate ways in which delays in the operator's response can be reduced. These results are also used to derive a closed-loop transfer function of the operator and to test various operator models proposed in the literature.

Analysis of the step-function responses indicated that certain operator outputs were subject to less delay than the normally used manual displacement. Section 5.3 describes tracking experiments conducted to determine whether the performance of the inner loop (see Fig. 2-2) can be improved by using these outputs for Control Action Display. The particular outputs investigated experimentally were manual displacement, manual force, and muscle action potential. In addition, Young's eye-tracking results (Refs. 28 and 29) were analyzed to determine the feasibility of using angular displacement of the eye to close the inner loop. The experiments in Section 5.3 differ from those in Section 5.2 in that the subjects tracked a random continuous signal, which is more typical of the system errors in the overall control system shown in Figs. 2-1 and 2-2. The results of these experiments are presented as closed-loop magnitude, phase, and signal-to-noise ratio for each of three subjects, using each of three operator outputs. The magnitude and phase data were analyzed to derive a pole-zero representation of the operator's closed-loop response which can be used for root-locus design of the overall manned control system.

Section 5.4 presents conclusions which follow from the experimental work reported in Sections 5.2 and 5.3. Appendixes D and E describe in some detail the equipment and procedures used to perform the experiments of Sections 5.2 and 5.3 respectively.

5.2 Tracking of Step Inputs

5.2.1 Introduction

The purpose of this section is to identify and measure the various components of delay in a human operator's motor-control response. Step-function inputs were used in order to simplify the task of isolating and measuring these various latencies. The first part of this section describes tests using single step-moves; the purpose of these tests is to derive a model of the human motor-control system from muscle action potentials to displacement of the hand. In the second part of this section, tracking tests, using a series of many random step inputs, are analyzed to show the relationship between hand and eye movements in manual tracking and to indicate ways in which delays in the operator's response can be reduced. Results of these tests are also used to derive a closed-loop transfer function for comparison with measured transfer functions described in Section 5.3.

5.2.2 Model of the Human Motor-Control System for Practiced Rapid Moves

The model of the human motor-control system to be derived here has muscle action potentials as its input and displacement of the hand as its output. Muscle action potentials are electrical signals which may be detected between two electrodes placed over the muscle. These potential differences are caused by the propagation of a wave of depolarization along the muscle. This depolarization is believed* to cause a chemical change within the muscle which results in the generation of a force.

Figure 5-1 summarizes the physiological significance of electromyographic signals detected at the surface of the muscle. Commands are transmitted to the muscle through the efferent motor nerve, which is typically composed of 1290** large nerve fibers. Approximately 774

---

* The events between the depolarization of the muscle membrane and the contraction of the myofibrils are referred to as "excitation-contraction coupling." According to Woodbury and Ruch (Ref. 30) these events are not yet completely defined.

** The values quoted here are from Ref. 31.

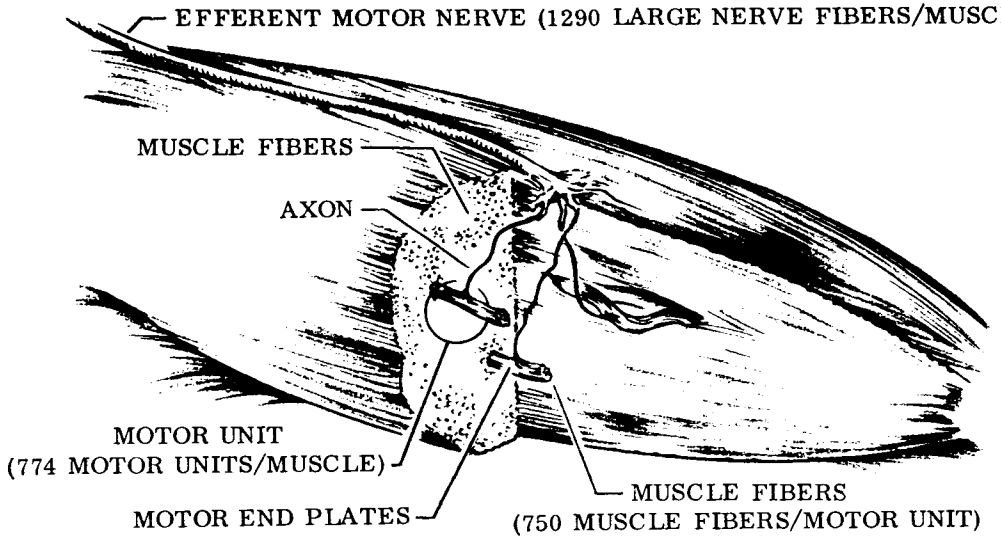

(a) Structure of Typical Muscle

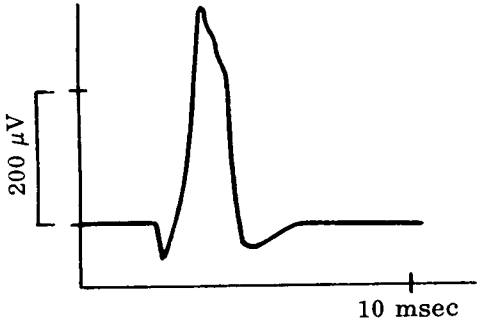

(b) Response of One Muscle Fiber

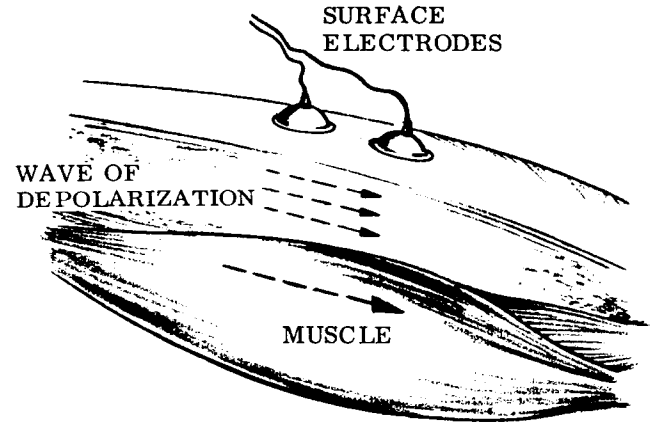

(c) Electrode Placement

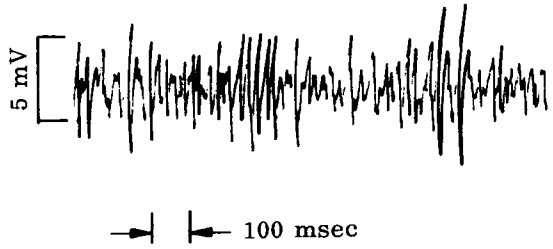

(d) Typical EMG Signal During Voluntary Contraction

Fig. 5-1 Physiological Significance of Muscle Action Potentials

of these axons connect to motor units each of which is typically composed of 750 muscle fibers. When excited by a command, a muscle fiber fires (i.e., discharges) causing a bipolar voltage pulse (measured with respect to a neutral reference) of approximately 5 msec duration. The voltage measured between two electrodes on the surface over the muscle is a summation of asynchronous pulses from hundreds of muscle fibers, and is indicative of the general level of muscle activity.

Muscle action potentials were chosen as the starting point for the present model because they are the most proximal signals (i.e., the closest in space and time to events within the central nervous system) which can be used as a controller (i.e., operator) output in the tracking system shown in Fig. 2-2. It is believed that use of more proximal signals, such as electroencephalograph (EEG) is not practical because of the great difficulty which would be encountered in detecting and processing them. Notice particularly that no attempt is made here to model that part of the motor-control system which issues the "commands" that result in the generation of muscle action potentials; it is not pertinent to this study because its output cannot be detected directly for use as an operator output in a tracking system. Displacement of the hand was chosen as the model output because it contains all components of delay in an operator's response and because it is often used as the controller output in conventional tracking systems.

All of the tracking studies described in this section were made using the configuration shown in Fig. 5-2. The subject grasped the end of the suspended tracking pole which supported his arm, and monitored the left-right component of hand motion. His task was to position the pole over a moving spot of light projected from the rear onto a translucent strip approximately 18 in. in front of him. Appendix D gives a detailed description of the Hand Monitor and the equipment used to project the moving spot of light. In addition to the mechanical variables, muscle action potentials were recorded from the right Pectoralis major and from the Infraspinatus. These voltages were detected using pairs of surface electrodes placed on the subject's chest and back.

The tracking motion employed required internal and external rotation of the upper arm with the elbow held approximately fixed.

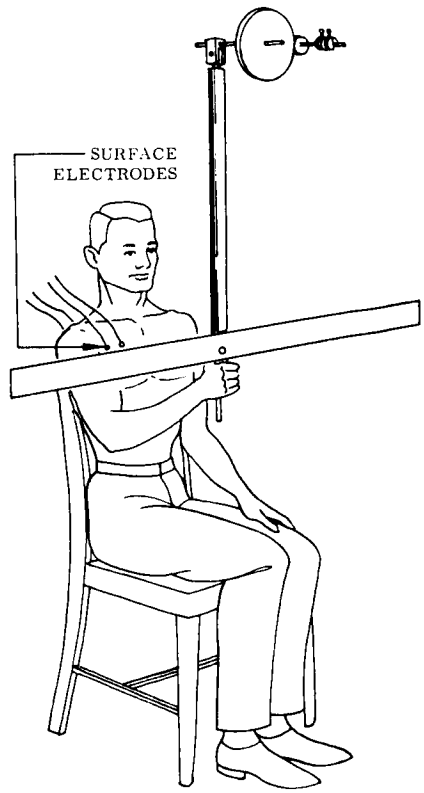

Fig. 5-2 Configuration Used for Step-Function Tracking Studies

Figure 5-3 shows schematically* how such moves are accomplished. For internal rotation (i.e., moving the right hand to the left) the Pectoralis muscle provides the accelerating force and is known as the agonist. Because muscles can exert force only in tension, the decelerating force must be provided by an opposing muscle called the antagonist; for internal rotation the Infraspinatus muscle is considered to be the antagonist. In the case of external rotation the roles of the two muscle groups are reversed.

*It is recognized that Fig. 5-3 is a simplification of the actual situation, and that several groups of muscles participate in these moves. However, these muscles are assumed to act synergistically, and it is convenient to consider them as only two distinct groups.

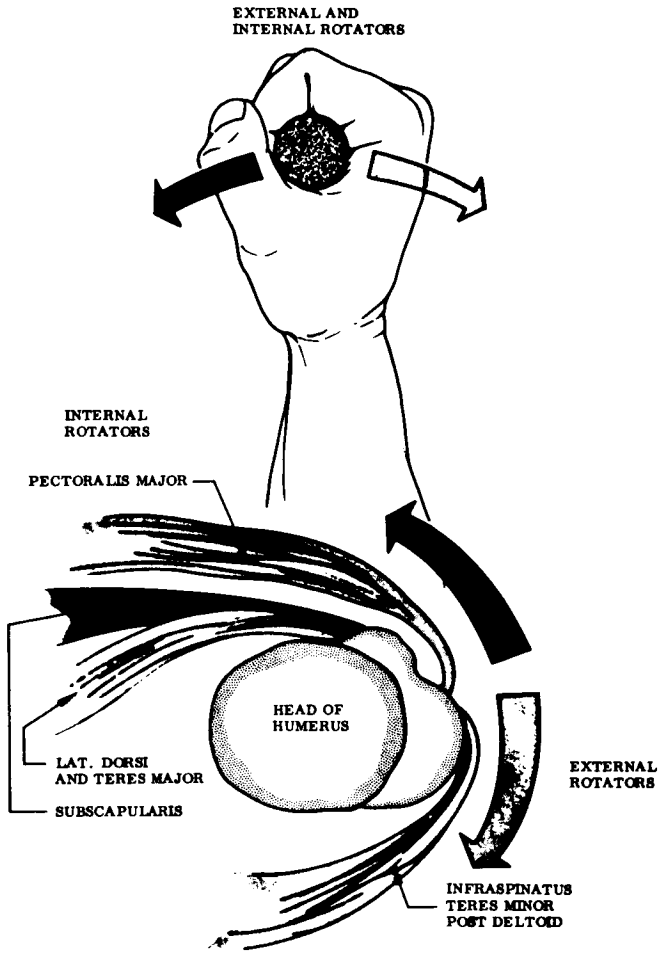

Fig. 5-3 Role of Muscles in Tracking Movements

Figure 5-4 shows the velocity and EMG patterns for a typical, practiced, rapid hand movement of 6 in. to the left. The move is completed in approximately 140 msec, with the hand attaining a maximum velocity of 85 in./sec and a maximum acceleration (derived by a graphical differentiation of the velocity waveform) of 1.75×10^3 in./sec^2. The velocity waveform is nearly triangular, which agrees with the results described in Refs. 32 and 33. Figures 5-5 and 5-6 present the same information in the form of phase plane trajectories. As a first approximation, it is assumed that the arm in its rotation within the shoulder

Subject: No. 3

Task: Rapid move of 6 in. to the left
Trace 1: EMG from Pectoralis muscle 2×10^{-3} volt/cm
Trace 2: Hand velocity 35 $\frac{\text{in./sec}}{\text{cm}}$
Trace 3: EMG from Infraspinatus muscle 1×10^{-3} volt/cm
Time Base: 50×10^{-3} sec/cm

Fig. 5-4 Velocity and EMG Patterns for a Rapid Hand Movement

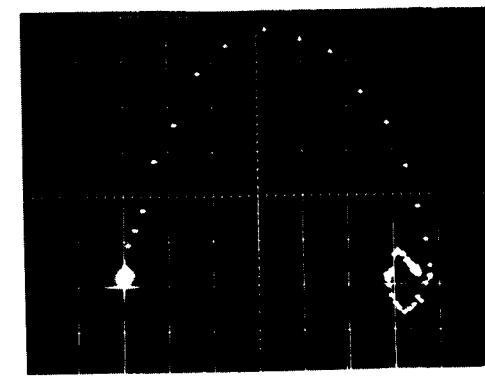

Subject: No. 7

Task: Rapid move of 6 in. to the right
Horizontal: Hand displacement 1 in./cm
Vertical: Hand velocity 14 $\frac{\text{in./sec}}{\text{cm}}$
Time Marks: Every 10 msec

Fig. 5-5 Phase-Plane Trajectory for a Single Rapid Hand Movement

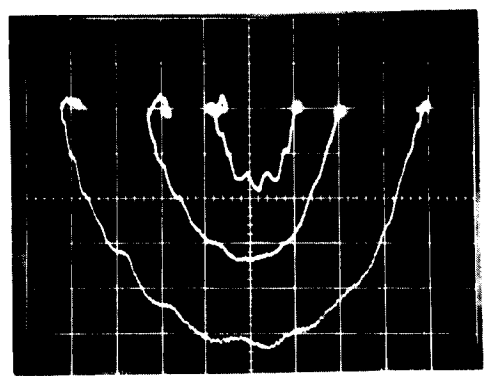

Subject: No. 2

Task: Rapid moves of 2, 4, and 8 in. to the left
Horizontal: Hand displacement 1 in./cm
Vertical: Hand velocity 14 $\frac{\text{in./sec}}{\text{cm}}$

Fig. 5-6 Phase-Plane Trajectories for Rapid Hand Movements of Varying Distances

Subject: No. 3

Task: Rapid move of 6 in. to the left
Trace 1: EMG from Pectoralis muscle 2×10^{-3} volt/cm
Trace 2: Hand acceleration 1×10^{3} $\frac{\text{in./sec}^2}{\text{cm}}$
Trace 3: EMG from Infraspinatus muscle 1×10^{-3} volt/cm
Time Base: 50×10^{-3} sec/cm

Fig. 5-7 Acceleration and EMG Patterns for a Rapid Hand Movement

joint can be represented as a pure inertia, and that the nearly triangular velocity waveform implies that the muscles exert an on-off force program.

In this connection it is important to note the alternating (i.e., on-off) bursts of activity in the EMG signals. The interpretation proposed here is that each burst of EMG activity coincides, after some delay, with the generation of a force by that particular muscle. This interpretation seems to be valid for at least two reasons: (1) The muscle action potentials result from depolarization across the muscle; according to physiologists this same depolarization causes the muscle to exert force. (2) Several investigators (Refs. 34 and 35) have found that for isometric contraction at constant force, the filtered EMG signal is proportional to muscle force.

Figure 5-4 shows that the acceleration of the hand to the left follows the EMG volley in the Pectoralis muscle (i.e., the agonist) by approximately 70 msec; the 75-msec duration of this first burst agrees very closely with the duration of acceleration to the left. The Infraspinatus muscle (i.e., the antagonist) becomes active at almost exactly the same time that activity in the agonist ceases. The onset of antagonist activity precedes the measured deceleration of the hand by 70-msec. The 80-msec duration of the antagonist volley agrees very closely with the duration of the deceleration.

To ensure that the time delay between EMG and measured velocity was not due to mechanical slippage in the Hand Monitor (see Appendix D), the EMG pattern was compared with the output of an accelerometer mounted on the tracking pole next to the subject's hand. Figure 5-7 shows the acceleration and EMG pattern for a rapid 6-in. move to the left by the same subject used for Fig. 5-4; note the similarity in EMG patterns for these two moves. Figure 5-7 confirms the conclusions derived from Fig. 5-4 in the following particulars:

(1) The onset of EMG activity in the Pectoralis muscle precedes the beginning of acceleration by approximately 65 msec.

(2) The duration of Pectoralis EMG activity (approximately 80 msec) agrees very closely with the duration of the acceleration to the left

(3) The maximum acceleration was approximately 1.5×10^3 in./sec^2

In addition to providing an independent check on the operation of the Hand Monitor, Fig. 5-7 accurately displays the first phase* of the acceleration pattern. Note that the acceleration waveform is not exactly rectangular; this can also be seen from the tracking results to be presented later in this section.

The relationship between muscle action potential and the muscle force which it produces was also studied in the case of isometric contraction. Figure 5-8 shows the force and EMG patterns which result when a subject voluntarily makes a rapid change in the force he is applying to a stationary force transducer (see Appendix D). Initially the subject is exerting a constant force of 6 lb to the left and the Pectoralis muscle exhibits a steady level of EMG activity. The cessation of this activity coincides almost exactly with the onset of activity in the Infraspinatus muscle, and precedes the beginning of force change by approximately 60 msec.** After another 100 msec, the force reaches a value of 6 lb toward the right, which is maintained by a steady level of muscle activity in the Infraspinatus. Figure 5-9 shows the force and EMG patterns which result from voluntary alternation of muscle force at 5 cycles/sec in isometric contraction. The duration of EMG bursts in the Pectoralis and Infraspinatus muscles are equal; this duration is also equal to the intervals of positive and negative forces. In the case of alternating contractions, the force lags the EMG volleys by approximately 80 msec. This lag includes the effect of force rise-time in addition to transport delay.

---

* The accelerometer used for this test was of the piezoelectric type (i.e., effectively ac coupled), and therefore could not measure accelerations having durations longer than 70 msec. For this reason it was useful in defining only the onset and first phase of acceleration but not for accurately reproducing the complete waveform. Accelerations for the tracking runs, to be presented later in this section, had to be measured by differentiating the velocity voltage as described in Appendix D.

** Note that this is approximately the latency between the onset of muscle-action potential and the beginning of acceleration for the quick hand movements displayed in Figs. 5-4 and 5-7. It also agrees with the results obtained by Hammond (Ref. 36), who measured the delay between EMG and a force which was elicited reflexly when a velocity disturbance was suddenly applied to the arm.

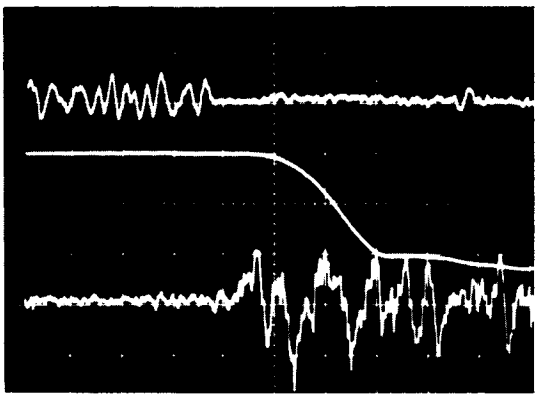

Subject: No. 4

Task:	Reverse direction of force in isometric contraction
Trace 1:	EMG from Pectoralis muscle 5×10^{-3} volt/cm
Trace 2:	Force 6 lb/cm
Trace 3:	EMG from Infraspinatus muscle 5×10^{-3} volt/cm
Time Base:	50×10^{-3} sec/cm

Fig. 5-8 Force and EMG Patterns for Rapid Isometric Force Change

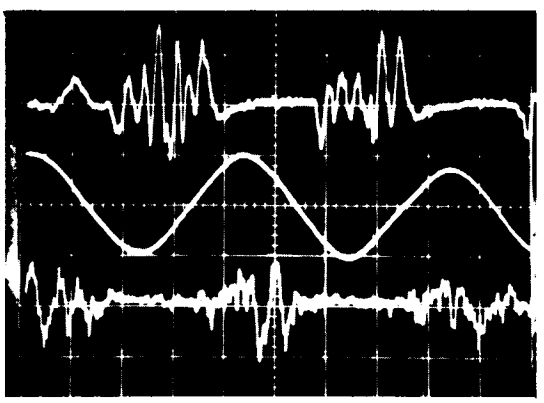

Subject: No. 4

Task:	Alternate direction of force in isometric contraction
Trace 1:	EMG from Pectoralis muscle 5×10^{-3} volt/cm
Trace 2:	Force 6 lb/cm
Trace 3:	EMG from Infraspinatus muscle 5×10^{-3} volt/cm
Time Base:	50×10^{-3} sec/cm

Fig. 5-9 Force and EMG Patterns for Alternating Isometric Force Change

The results of the foregoing measurements and analyses are summarized in Fig. 5-10. The input to the proposed model is the net algebraic activity of the agonist and antagonist muscles represented by two bursts each having a duration of T_2. After a transport delay of T_1 (associated with the muscle latency), the hand begins to accelerate;* this acceleration becomes manual displacement after two integrations. The transfer function relating the EMG signal input to the resulting hand displacement is given by Eq. 5.1.

$$\frac{X_h(s)}{EMG(s)} = \frac{4e^{-T_1 s}\left(1 - 2e^{-(T_2/2)s} + 2e^{-(3T_2/2)s} - e^{-2T_2 s}\right)}{T_2^3 s^3\left(1 - 2e^{-T_2 s} + e^{-2T_2 s}\right)} \qquad \begin{cases} T_1 \approx 65 \text{ msec} \\ T_2 \approx 70 \text{ msec} \end{cases} \tag{5.1}$$

This transfer function, together with results to be presented in the next subsection, will be used to derive the closed-loop frequency response of a human operator tracking random step inputs. In the process of deriving a model for hand displacement, experiments were conducted (see Figs. 5-8 and 5-9) which show that the transfer function from EMG activity to isometric muscle force is given by Eq. 5.2.

$$\frac{F(s)}{EMG(s)} = \frac{e^{-T_1 s}}{(T_3 s + 1)} \qquad \begin{cases} T_1 \approx 65 \text{ msec} \\ T_3 \approx 70 \text{ msec} \end{cases} \tag{5.2}$$

*The muscle and limb dynamics are not developed in any greater detail here because the intermediate variables (e.g., forces on the tendons) are not available for use as operator outputs in a tracking system. Evidence presented in Ref. 37, however, indicates that considerable viscosity (on the order of 0.25 lb-sec/in. referred to the hand) is present in the joint and/or muscles. This result is confirmed by Wilkie (Ref. 38) who used steady-state velocity measurements to derive the effective viscosity.

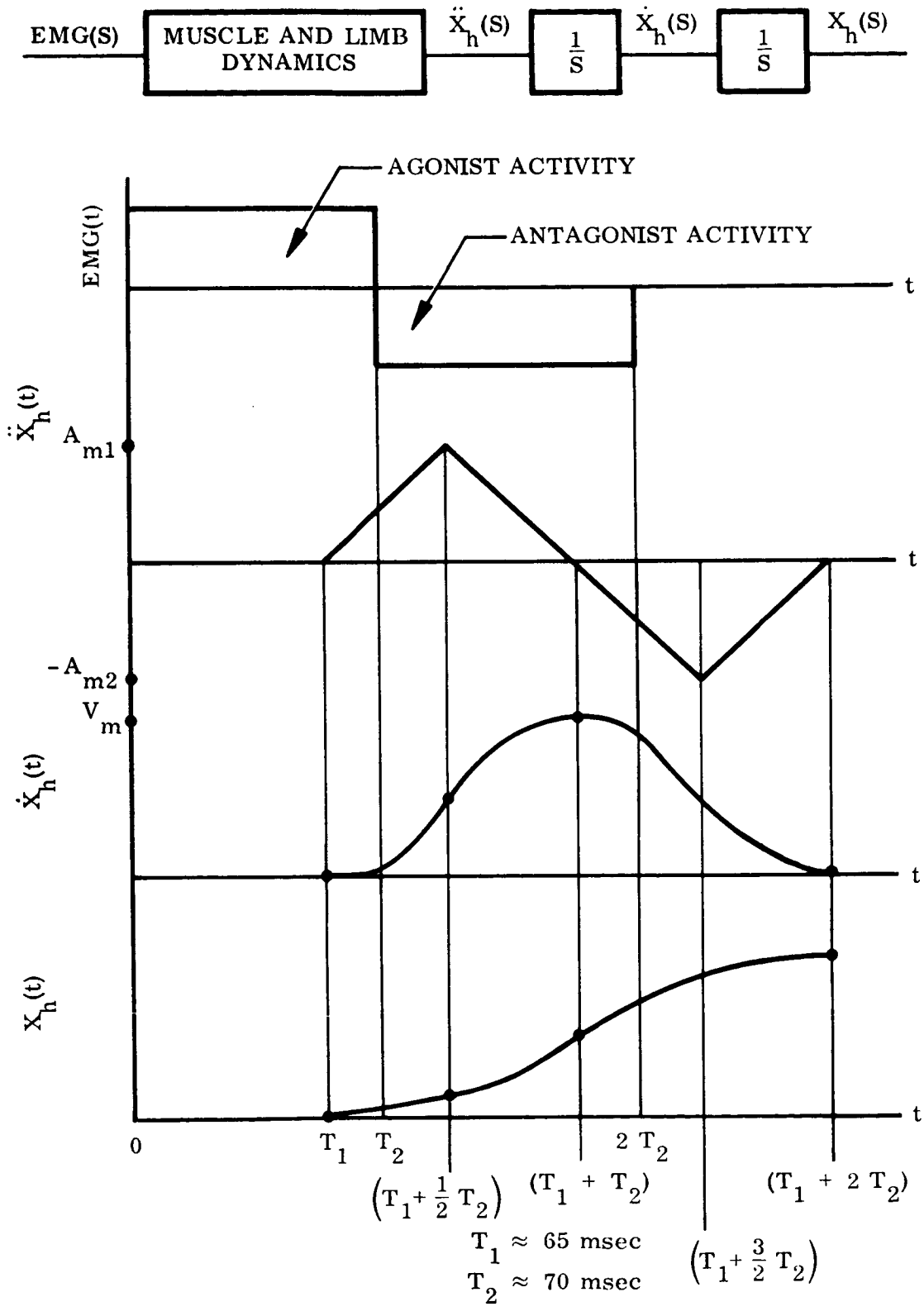

Fig. 5-10 Model of Motor Control System Applicable to Practiced, Rapid Moves

Comparison of Eqs. 5.1 and 5.2 indicates that muscle force is subject to much less phase lag than manual displacement. This is interpreted to mean that using a force control stick should result in a wider-bandwidth tracking loop than using a displacement control stick would.

5.2.3 Performance of the Human Operator in Tracking Random Step Inputs

The model to be developed in this section describes the behavior of the human operator in tracking a series of random step displacements. The input to the model is target displacement, and the outputs are EMG activity, angular eye movement, and acceleration, velocity, and position of the hand. This model contains latencies associated with generating appropriate muscle commands in addition to all elements of the model developed in the preceding subsection. The results to be presented here will be applied to:

(1) indicate ways in which delays in the operator's response can be reduced

(2) show the relationship between hand and eye movements in manual tracking

(3) derive a closed-loop transfer function for comparison with the transfer function (to be presented in Section 5.3) of an operator tracking a continuous random signal.

Experiments were performed using the configuration shown in Fig. 5-2 and the instrumentation described in Appendix D. The subjects (males between the ages of 20 and 40 without neurological disease) tracked by placing the tracking pole over the moving spot of light projected from behind the translucent tape. Each test lasted 48 sec, during which time the light spot made 48 random step jumps of $\pm$ 2, $\pm$ 4, $\pm$ 6, or $\pm$ 8 in. at random intervals of 0.6, 1.0 and 1.4 sec; the input program is given in Table D.1 of Appendix D.

The results of a typical tracking experiment are shown in Figs. 5-11 and 5-12. Table 5.1 lists the displayed variables and outlines how each was obtained. The one variable in Table 5.1 which may require further explanation is X_e, the position of eye fixation.

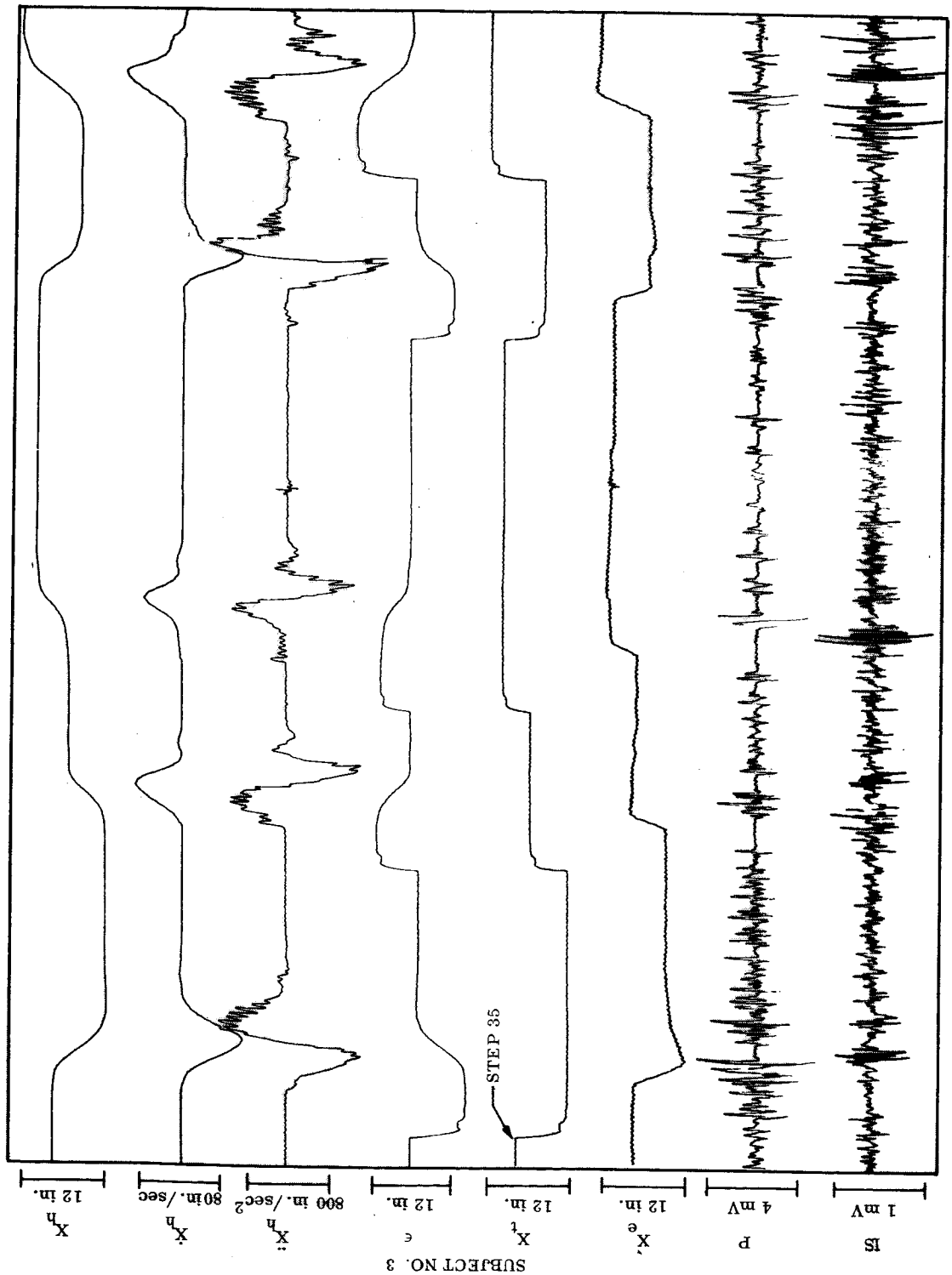

Fig. 5-11 Section from Typical Tracking Experiment-Moves 35 through 39

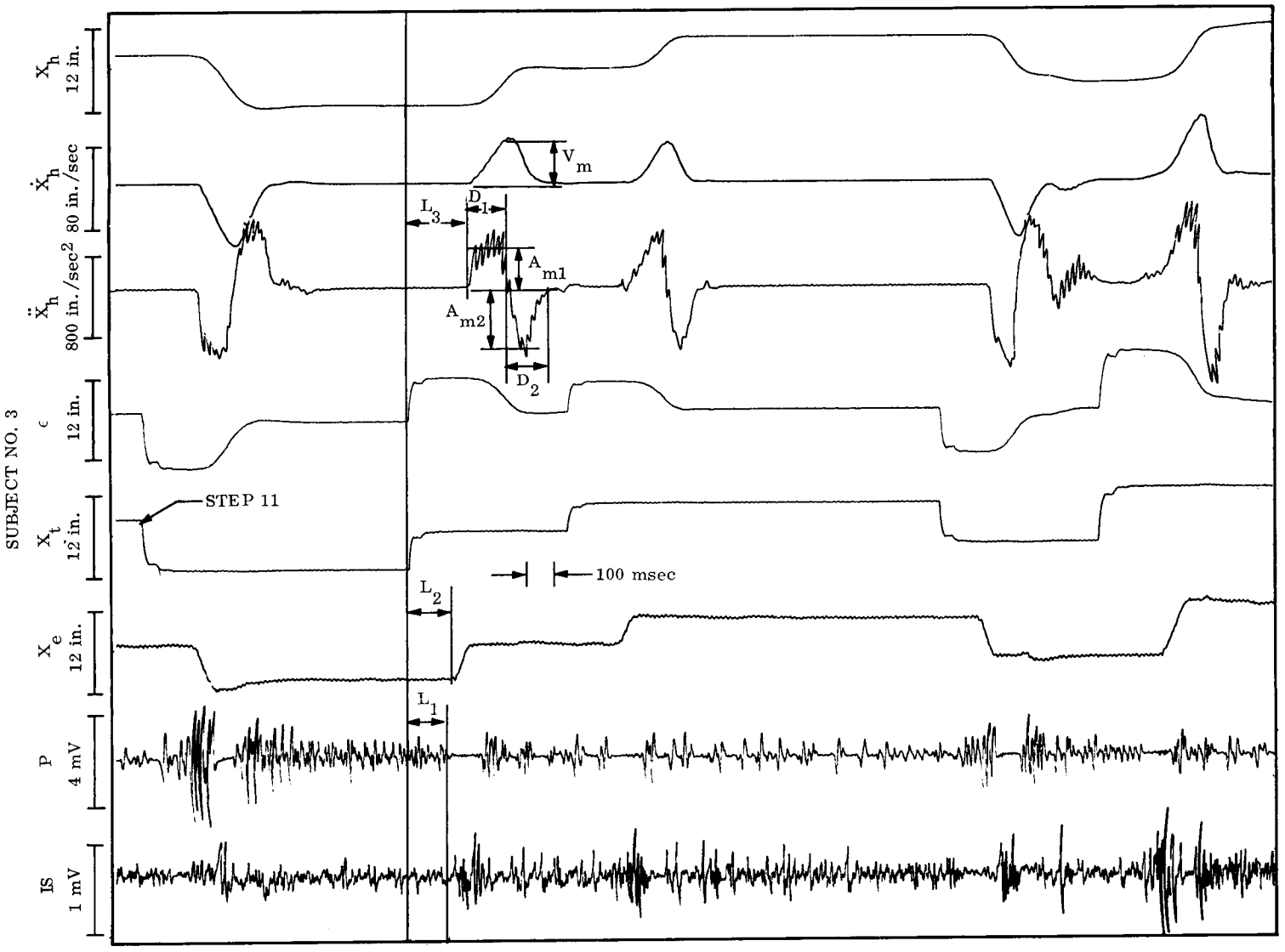

Fig. 5-12 Section from Typical Tracking Experiment-Moves 11 through 15

Although their specific task was to track the moving target with the tracking pole, all of the subjects also tracked the target with their eyes. The instantaneous position of gaze was measured using surface electrodes which detect steady corneoretinal potential (Refs. 39 and 40) and its field alternations with eye movement;* the electrodes were placed near the inner and outer canthus of the right eye.

Table 5.1

Listing of Variables Recorded During Step-Input Tracking Experiments

Channel	Variable	Method Used to Obtain Variable
1	X_h - Position of the hand	Potentiometer mounted on the Hand Monitor
2	$\dot{X}_h$ - Velocity of the hand	Variable capacitor mounted on Hand Monitor
3	$\ddot{X}_h$ - Acceleration of the hand	Electrical differentiation of velocity voltage
4	ϵ - Distance between light spot and tracking pole	Subtracting position output voltage of the Hand Monitor from output voltage of light spot programmer
5	X_t - Position of light	Output voltage of light spot programmer
6	X_e - Position of eye fixation	Electro-oculogram (EOG) using surface electrodes
7	P - Muscle action potentials of Pectoralis muscle	Electromyograph (EMG) using surface electrodes
8	IS - Muscle action potentials of Infraspinatus muscle	Electromyograph (EMG) using surface electrodes

*It should be emphasized that this signal (EOG) is a measure of eye rotation and is not the signal which causes the eye to rotate, as would be the case for EMG from the eye muscles.

One of the more interesting characteristics of the tracking records is the consistency of all aspects of the operator's response to a given sequence of target displacements. The input program (see Table D.1) was composed of two identical sections, to facilitate such comparisons as that shown in Figs. 5-11 and 5-12. These figures show that, although there is some variation in latencies between the input step and the time that commands come down from the central nervous system, the transients in each of the operator's outputs are quite similar to the transients following that step in the previous sequence 24 sec before. This similarity was also observed between tests made at different times and, to a lesser extent, between experiments involving different subjects.

Figures 5-11 and 5-12 show that the sequence of events following a step displacement of the target is as follows:

(1) A volley of muscle action potential appears in the agonist and activity in the antagonist is inhibited almost simultaneously
(2) The eye tracks the target with a saccadic movement
(3) The hand begins to accelerate
(4) A volley of muscle action potential appears in the antagonist and the agonist activity is inhibited almost simultaneously
(5) The hand begins to decelerate
(6) The move is completed, often with small corrections until the final position is attained.

The tracking records of five different subjects were analyzed to determine the eight quantities defined with respect to Fig. 5-12 and listed in the Notation. The reduced data are presented and discussed in subsequent paragraphs in order to define explicitly the various components of delay in the tracking response of the human operator.

From Figs. 5-13, 5-14 and 5-15 it can be seen that the time between the target movement and onset of agonist EMG activity is more or less randomly distributed between 100 and 200 msec. The average values, computed from 48 moves, for each of three typical subjects were 150, 166, and 134 msec. Barlow (Ref. 41) has shown that step displacements of a light spot evoke an EEG response at the visual cortex after an average latency of 80 to 90 msec. The time required for a nerve impulse to

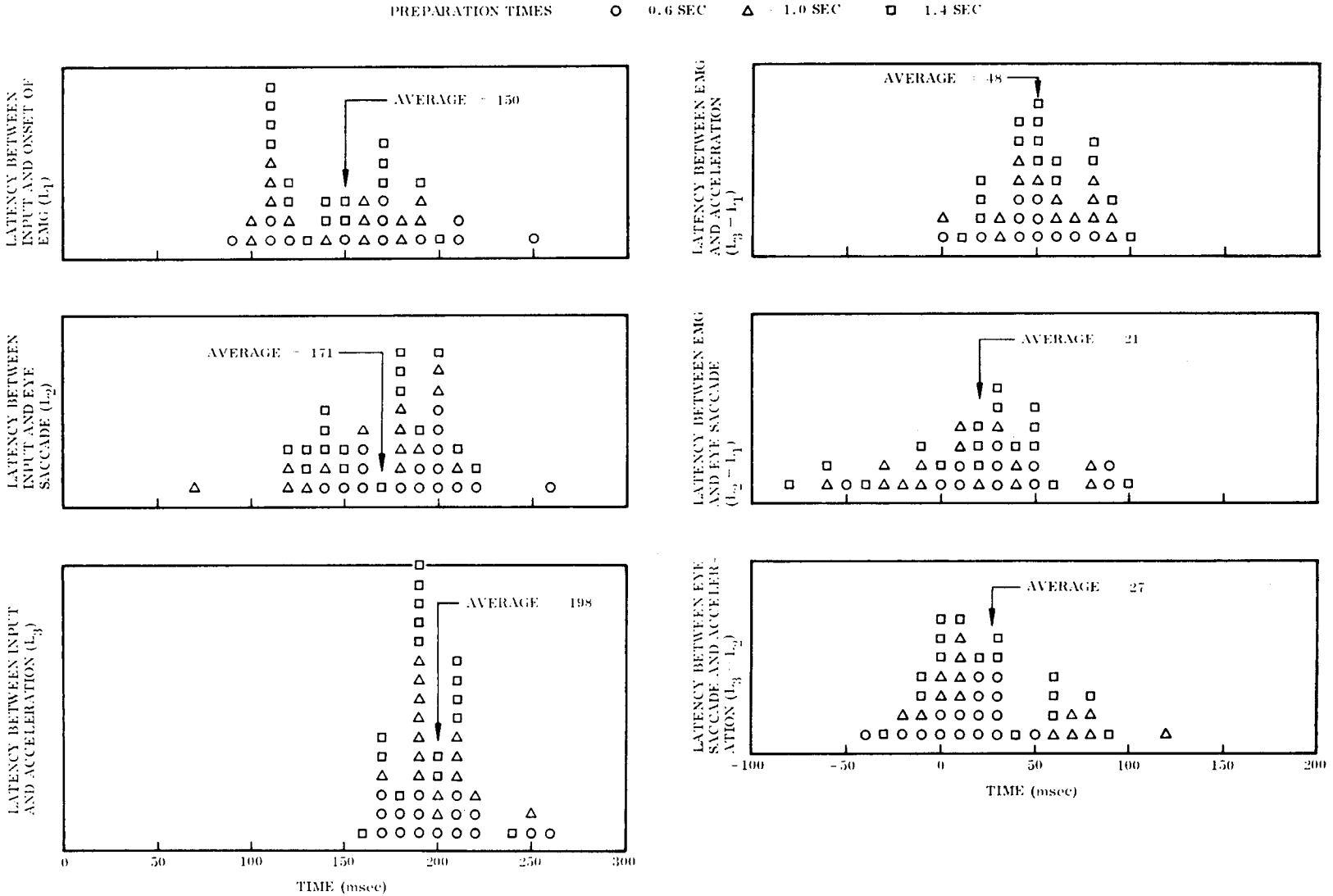

Fig. 5-13 Distribution of Tracking Latencies - Subject No. 1

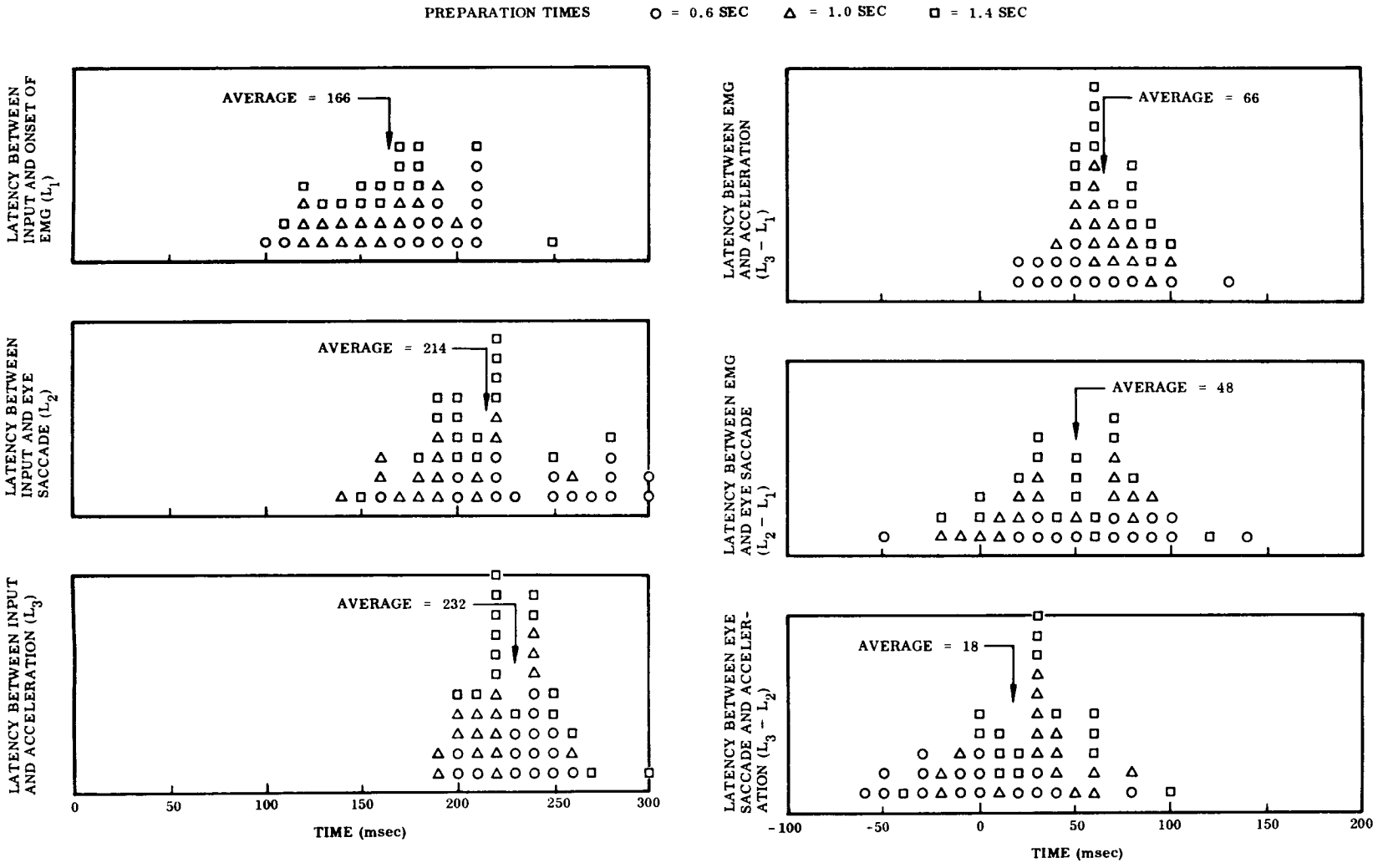

Fig. 5-14 Distribution of Tracking Latencies - Subject No. 2

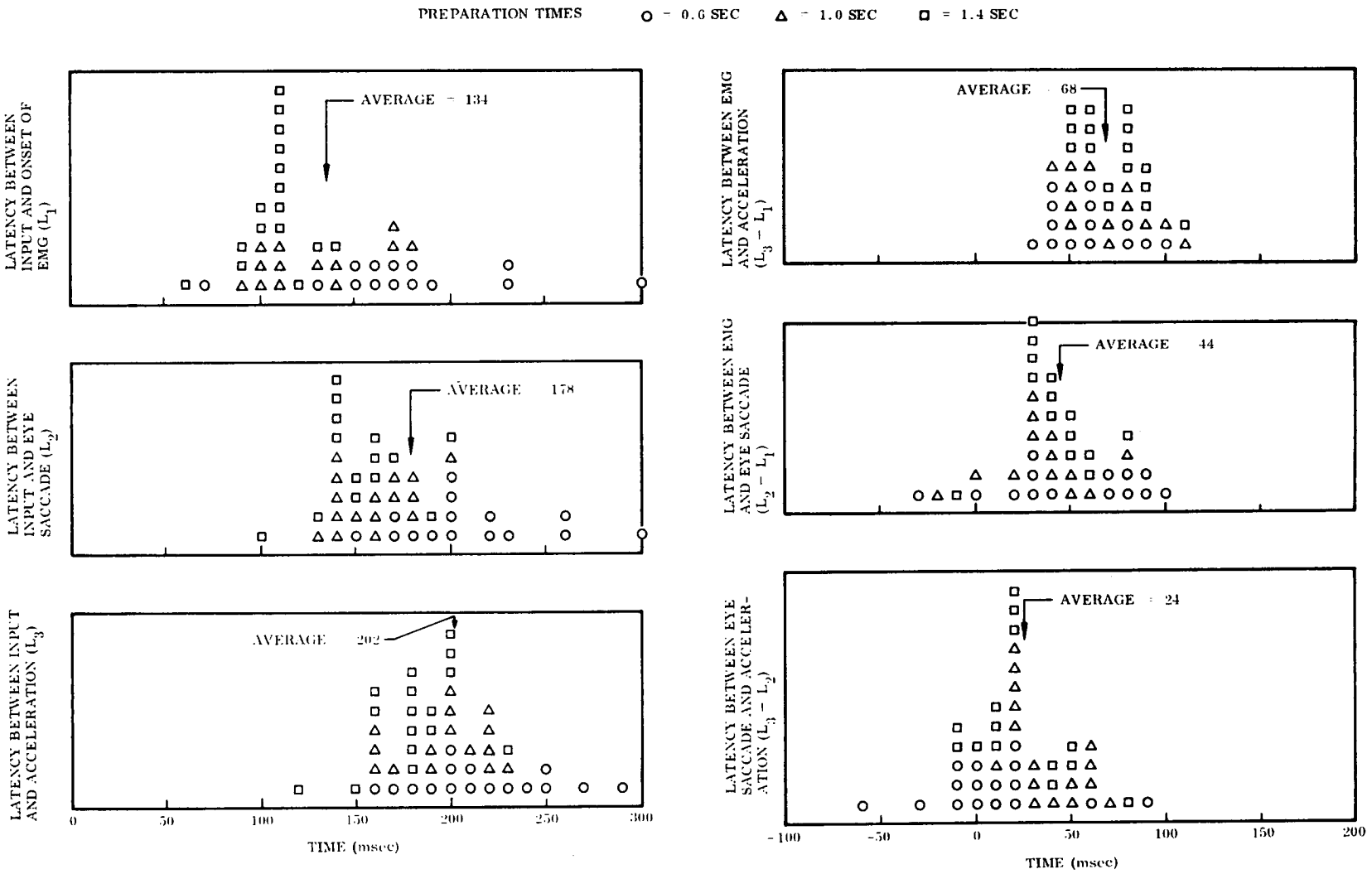

Fig. 5-15 Distribution of Tracking Latencies - Subject No. 3

travel from the motor cortex and be converted into EMG activity is on the order of 12 msec. This assumes one spinal synapse with a delay of 1.0 msec and a corticospinal conduction velocity of 300 ft/sec; the conduction time from cervical cord to EMG activity has been measured as 8 msec. From these measurements and estimates it follows that the time between the evoked response at the visual cortex and the discharge of the cortical motor neurons is on the order of 50 msec. It may be inferred that the sensory data are processed and the appropriate commands are issued during this 50 msec interval.

Figures 5-13, 5-14 and 5-15 show that the latency between step target motion and the saccadic eye movement L_2 is a random variable having a distribution extending over approximately 100 msec. The range of this distribution appears to argue against the model developed by Young (Ref. 28) who proposed that the eye tracking system contains a sampled data section operating on samples taken every 0.2 sec. If such a sampler operated asynchronously with the target motion, the distribution of response times would be rectangular and extend over a range of 200 msec. If the sampler is triggered by the stimulus, one would expect the latencies to vary over a range of less than 100 msec. The distribution of latencies to first acceleration L_1 given in Figs. 5-13, 5-14 and 5-15 similarly contradicts the sampled data model of the hand tracking system proposed by Bekey (Ref. 42).

Figures 5-13, 5-14 and 5-15 show the distribution of measured latencies between onset of agonist EMG activity and force as indicated by the beginning of acceleration. The average latencies for three typical subjects were 48, 66, and 68 msec. These averages are in good agreement with the values for practiced rapid moves as shown in Figs. 5-4 and 5-7 and for isometric contraction shown in Fig. 5-8.

Figures 5-13, 5-14 and 5-15 show that, on the average, the beginning of manual acceleration lagged the beginning of eye saccade by 27, 18 and 24 msec. Elkind, et al. (Ref. 43) observed that the average reaction time (presumably the latency between stimulus and the beginning of acceleration) measured for tracking experiments using step inputs is considerably greater than the transport lag derived from experiments using a continuous input signal. They conjecture that in the step input

case the eye must track the target before commands to the arm can be generated and they suggest that the latency of the cascaded eye-tracking system must be added to the latency of the hand-tracking system. Figures 5-13, 5-14 and 5-15 show that this is not the case. In three typical subjects, changing EMG activity in both agonist and antagonist is present 21, 48, and 44 msec before the eye saccade begins.

Measurements performed by Zuber, et al. (Ref. 44) show that visual input to the brain is inhibited for a period of approximately 60 msec starting 50 msec prior to the beginning of a saccadic eye movement; i.e., the brain does not receive visual information after the time $(L_2 - 50)$ msec. It was estimated previously that the motor cortex discharges approximately 12 msec before the muscle EMG activity changes; i.e., the brain issues commands to the muscles at the time $(L_1 - 12)$ msec. Figures 5-13, 5-14 and 5-15 show that the average value of the difference $[(L_2 - 50) - (L_1 - 12)]$ is less than 20 msec. From this it appears that these subjects issue muscle commands at approximately the time that their visual information is suppressed.

The interval during which the target is stationary prior to a step displacement is called the preparation time. For the histograms shown in Figs. 5-13, 5-14 and 5-15, different symbols are used to designate the three different preparation times; in this way the dependence of the various latencies on preparation time can be displayed explicitly. Although no formal statistical analysis of the data was performed, it appears from these figures that the various latency distributions are not significantly different for preparation times of 0.6, 1.0, and 1.4 sec. This is probably due to the fact that these preparation times are greater than the psychological refractory period. For easy to moderately difficult tasks, the psychological refractory period is in the range of 0.3 to 0.4 sec (Ref. 45).

In Fig. 5-16 various latencies are given as functions of the distance moved for the same three subjects represented in Figs. 5-13, 5-14 and 5-15. The value of latency plotted at each displacement is the average of six different moves (two for each of three different preparation times). The average value for that latency, computed

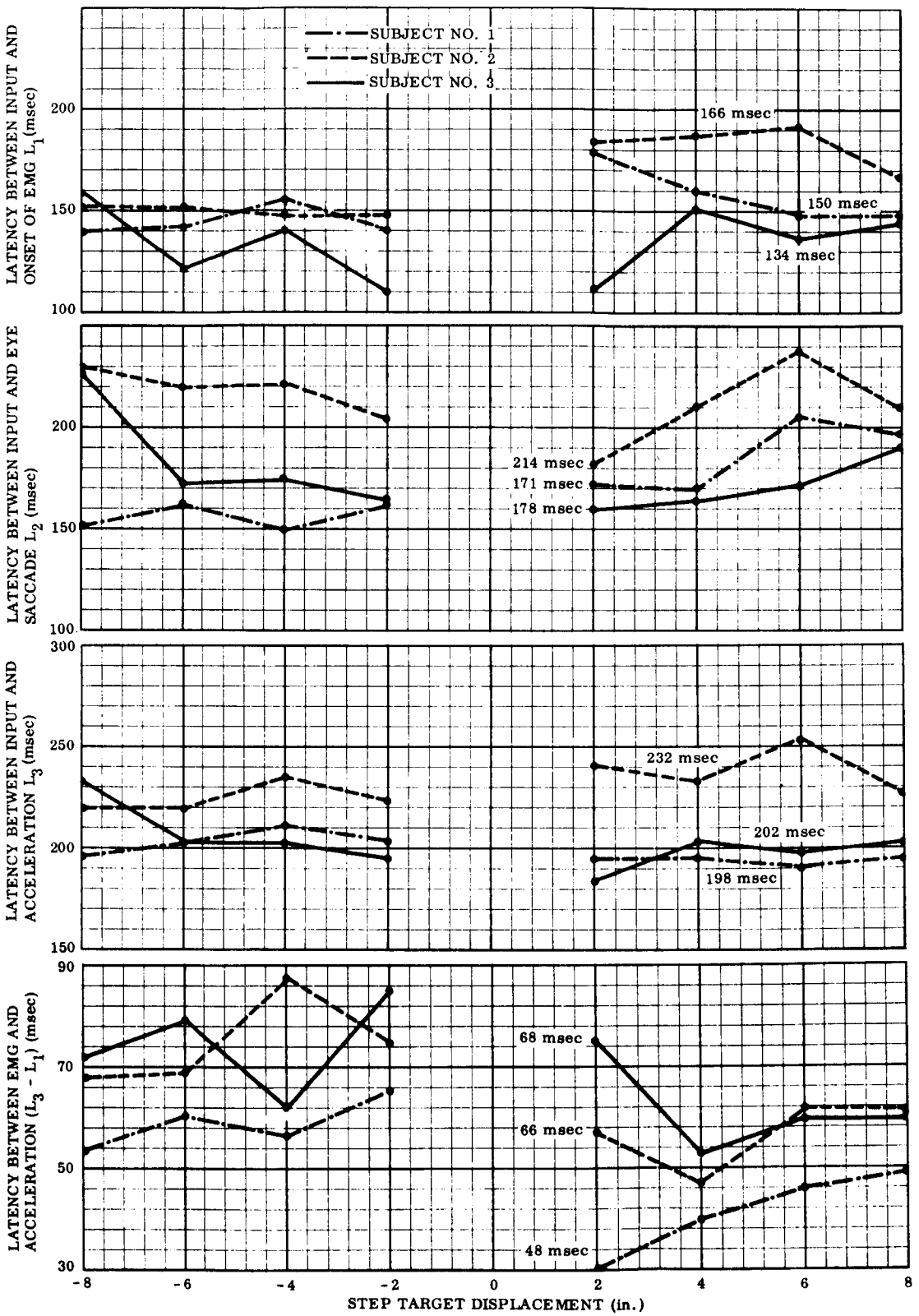

Fig. 5-16 Dependence of Latencies on Size of Input Step Function

using all 48 moves, is also given for each subject. Careful examination of Fig. 5-16 shows that, in nearly every case, a subject's average latency for a given step size varies randomly within ± 15 percent of his latency, averaged over all step sizes. This applies to step sizes from -8 to +8 in. and indicates that the various latencies are independent of the distance moved.

Figures 5-11 and 5-12 show that after the muscle commands have been given and the muscle action potentials converted into force, the arm experiences a period of acceleration followed by a period of deceleration. The waveform during each of these two phases is approximately triangular. The peak acceleration and peak deceleration (computed by averaging over six different moves) are given as functions of the input step size in Fig. 5-17. It is clear from this figure that the peak acceleration and deceleration are not linear functions of the input displacement. It also indicates that the model proposed by Smith (Ref. 46), in which the same force is used for moves of all distances so that they are accomplished in the minimum time, is not applicable for the low-inertia load used in these tests.

Reference to Figs. 5-4 and 5-7 indicates that the accelerations used for tracking a randomly moving target is only 25 percent to 35 percent of the acceleration used for practiced rapid moves. Another interesting characteristic is the asymmetry of the tracking moves. Comparison of the curves given in Fig. 5-17 indicates that, for all three subjects, the peak acceleration (deceleration) is almost always greater than the peak deceleration (acceleration) for negative(positive) displacements. This is probably due to the fact that the Pectoralis muscle used for acceleration (deceleration) is much stronger than the Infraspinatus muscle which causes deceleration (acceleration) in a move to the left (right).

Figure 5-18 gives the average durations of acceleration and deceleration computed from six moves for each of the input step sizes. This figure shows that the durations are not constant, but vary more or less systematically as much as 60 percent for a 4:1 range of input displacement. These results show that models which assume constant-duration force programs (Refs. 32 and 33) are not applicable where large displacements of the hand controller are required.

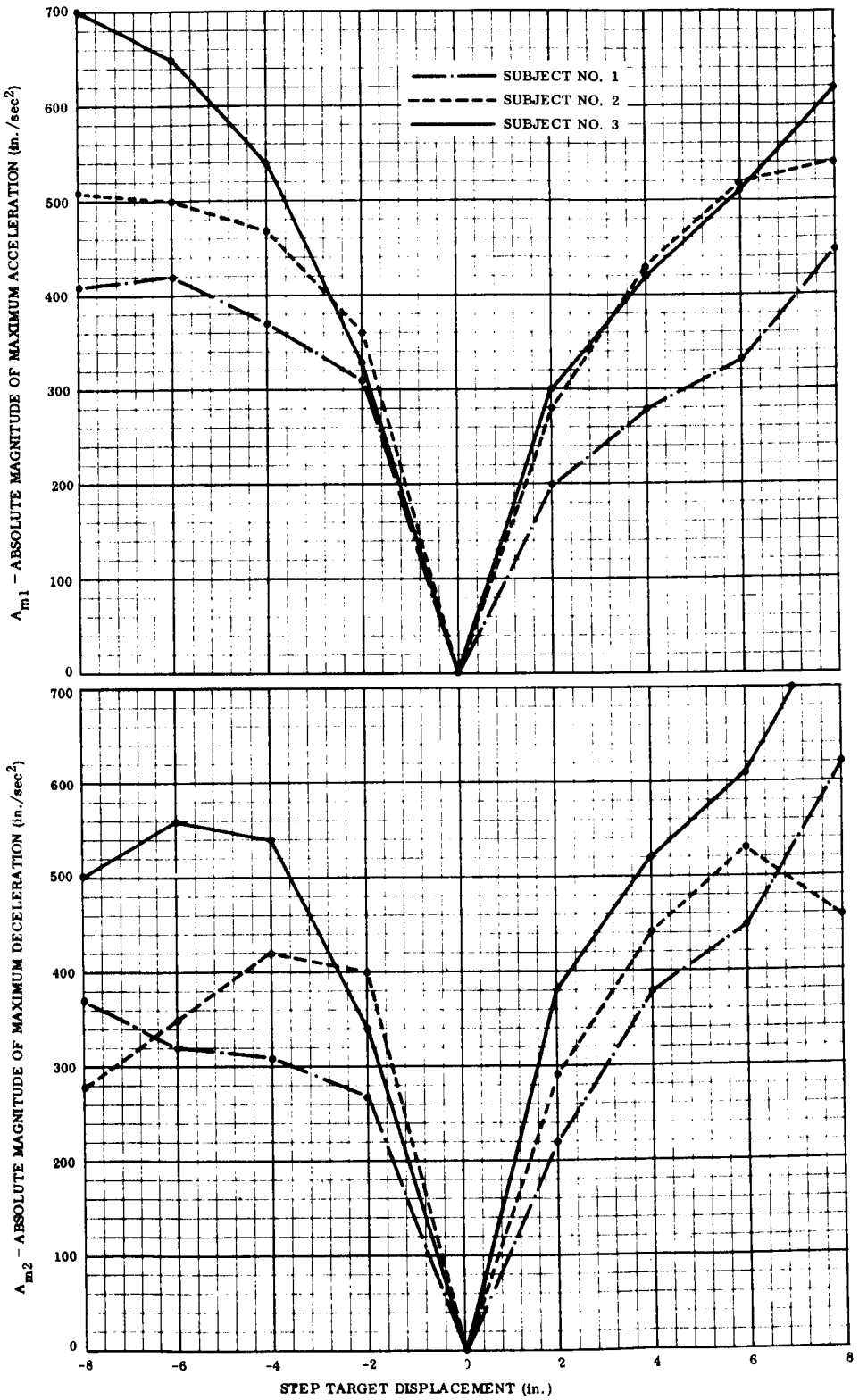

Fig. 5-17 Dependence of Maximum Acceleration and Deceleration on Size of Input Step Function

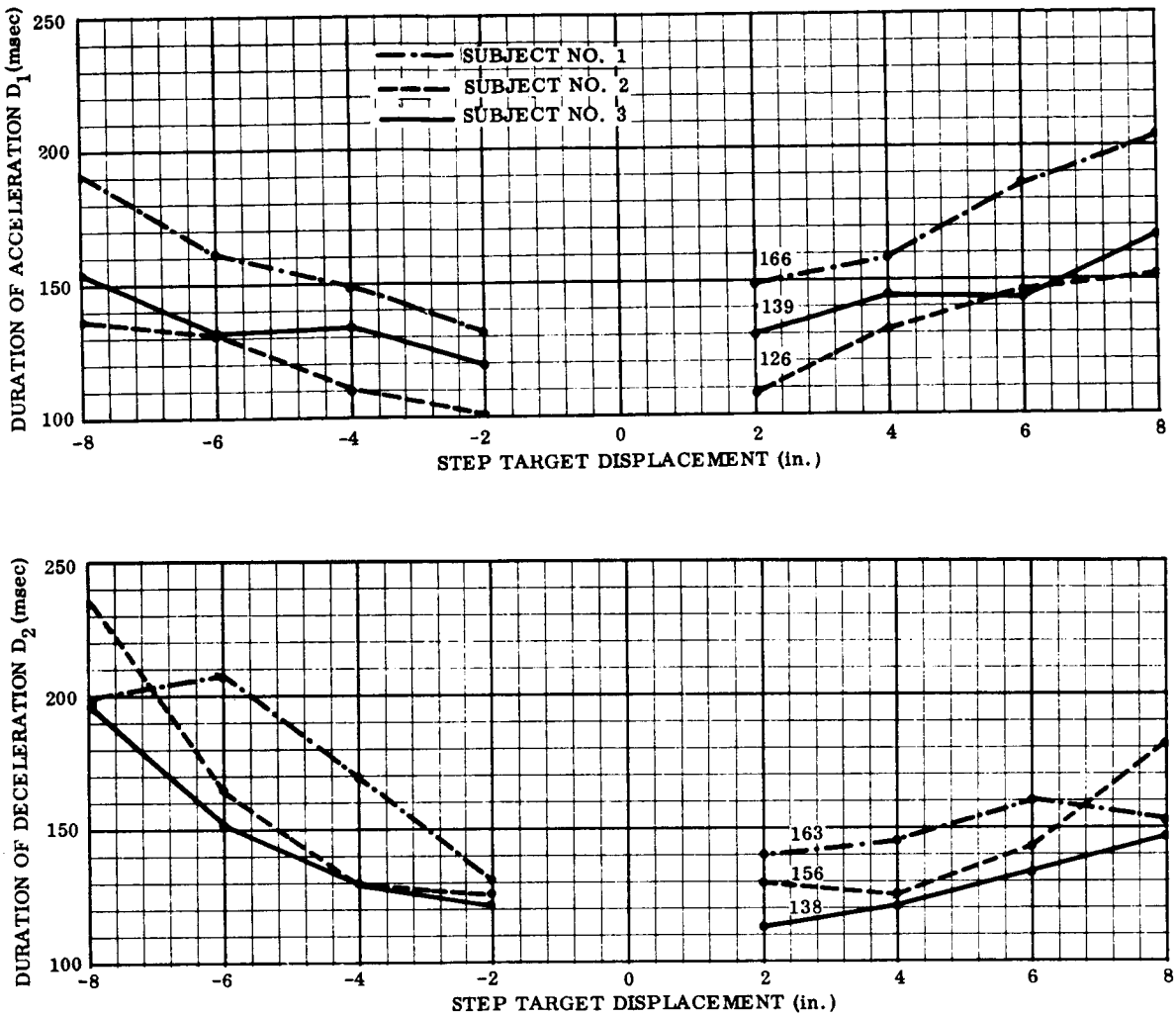

Fig. 5-18 Dependence of Duration of Acceleration and Deceleration on Size of Input Step Function

The durations given in Fig. 5-18 are approximately twice as long as the duration of moves shown in Figs. 5-4 and 5-7. This is consistent with the fact that the acceleration and deceleration are approximately a factor of four lower for the same displacement.

Figure 5-19 gives the peak velocity averaged over six moves as a function of input step size for the same three subjects. Like peak acceleration, the peak velocity is not linear with input displacement. It is also less than that measured for a practiced rapid move;

the peak velocity for a 6-in. move to the left by Subject No. 3 is only 49 in./sec compared with 85 in./sec for the move shown in Fig. 5-4. This is consistent with the fact that the acceleration is lower by a factor of four but the duration is greater by a factor of two.

5.2.4 Tracking Model Derived from Random-Step-Input Data

The results of the data presented in this section are summarized in Figs. 5-20a,b and c. Figure 5-20a gives a model which relates the various operator outputs to target displacement for the case of closed-loop pursuit tracking with a unity-gain plant. Figure 5-20b shows the transient response of each of the variables. It can be seen that this model is simply an extension of the one given in Fig. 5-10, in which the following two changes have been made:

(1) L_3 is substituted for T_1; i.e., the delay includes the time required to generate and transmit muscle commands in addition to the muscle latency in converting EMG activity into force.

(2) D_1 and D_2 are substituted for T_2; i.e., the durations of acceleration and deceleration are a factor of two greater for tracking a randomly moving target than for practiced rapid moves.

The transfer function relating hand displacement to target displacement is given by Eq. 5.3.* The frequency response is given by Eqs. 5.4 and 5.5** and is plotted in Fig. 5-20c using, as durations and latencies, values obtained by averaging over all three subjects.

---

* In order to simplify this equation, it has been assumed that the duration of acceleration and deceleration are equal. Because it has also been assumed that these durations are constant, this model is strictly applicable only for output displacement within the approximate range of $\pm$ 4 in. (See Fig. 5-18.)

** Notice that the phase lag would be the same for a rectangular force program (Refs. 32 and 33) or for any other waveshape symmetrical with respect to the time $(L_3 + D_1)$.

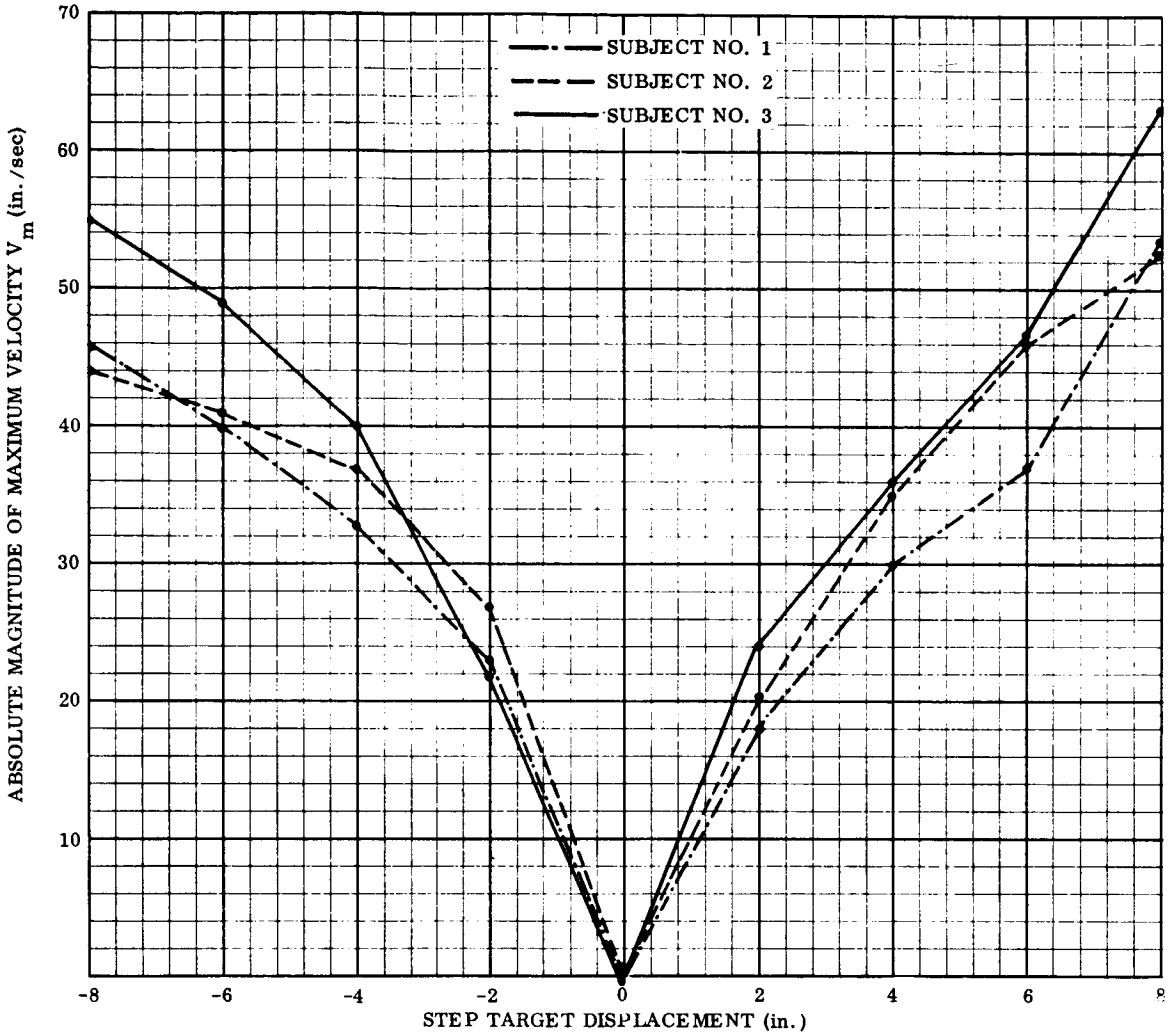

Fig. 5-19 Dependence of Maximum Velocity on Size of Input Step Function

$$\frac{X_h(s)}{X_t(s)} = \frac{4}{(D_1 s)^3}\left\{e^{+D_1 s} - 2e^{+(D_1 s)/2} + 2e^{-(D_1 s)/2} - e^{-D_1 s}\right\} e^{-(L_3 + D_1)s} \tag{5.3}$$

$$\left|\frac{X_h(\omega)}{X_t(\omega)}\right| = \frac{8(2 \sin D_1\omega/2 - \sin D_1\omega)}{(D_1\omega)^3} \tag{5.4}$$

$$\measuredangle \frac{X_h(\omega)}{X_t(\omega)} = -(L_3 + D_1)\,\omega \tag{5.5}$$

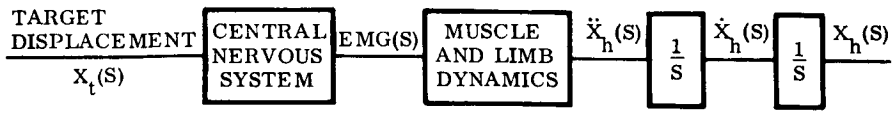

(a) Block Diagram

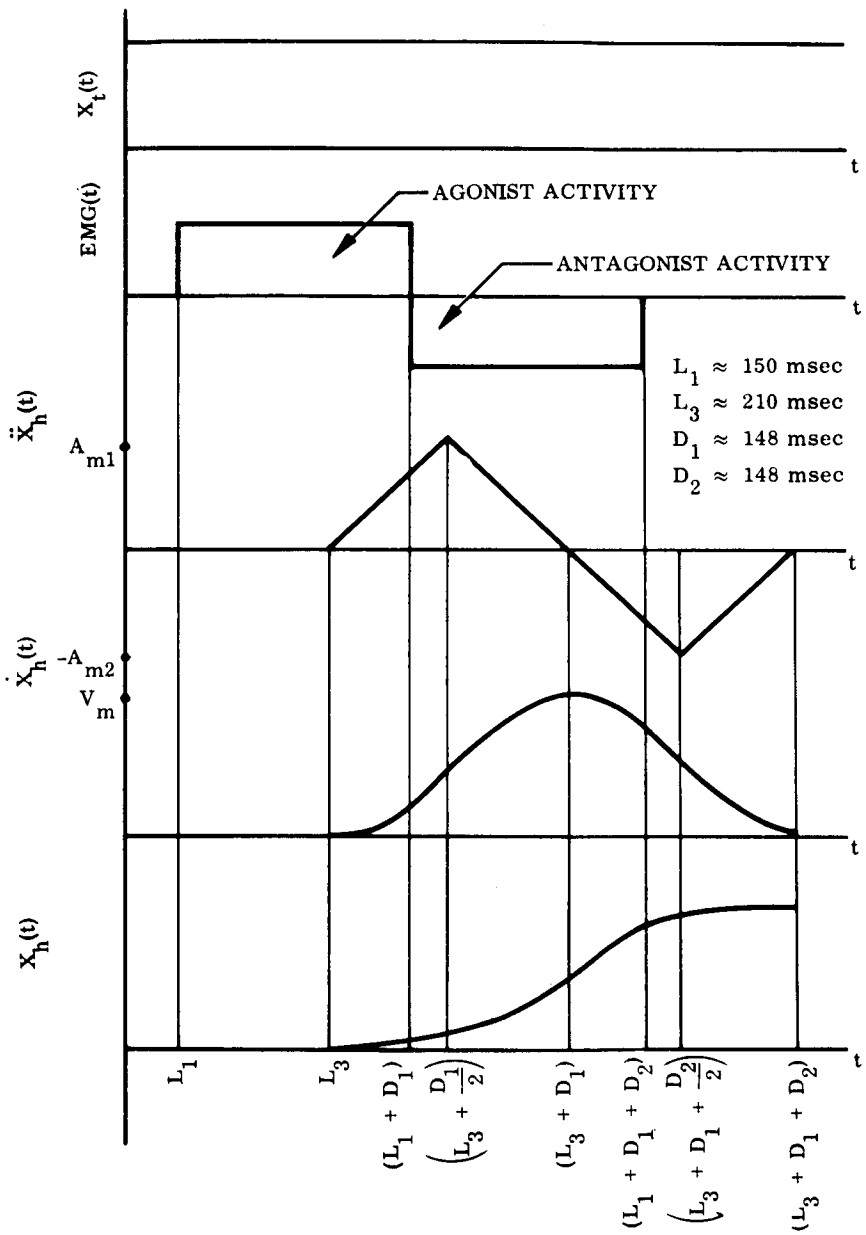

(b) Typical Transient Response

Fig. 5-20 Model of Motor Control System Applicable to Closed-Loop Pursuit Tracking with Unity-Gain Plant

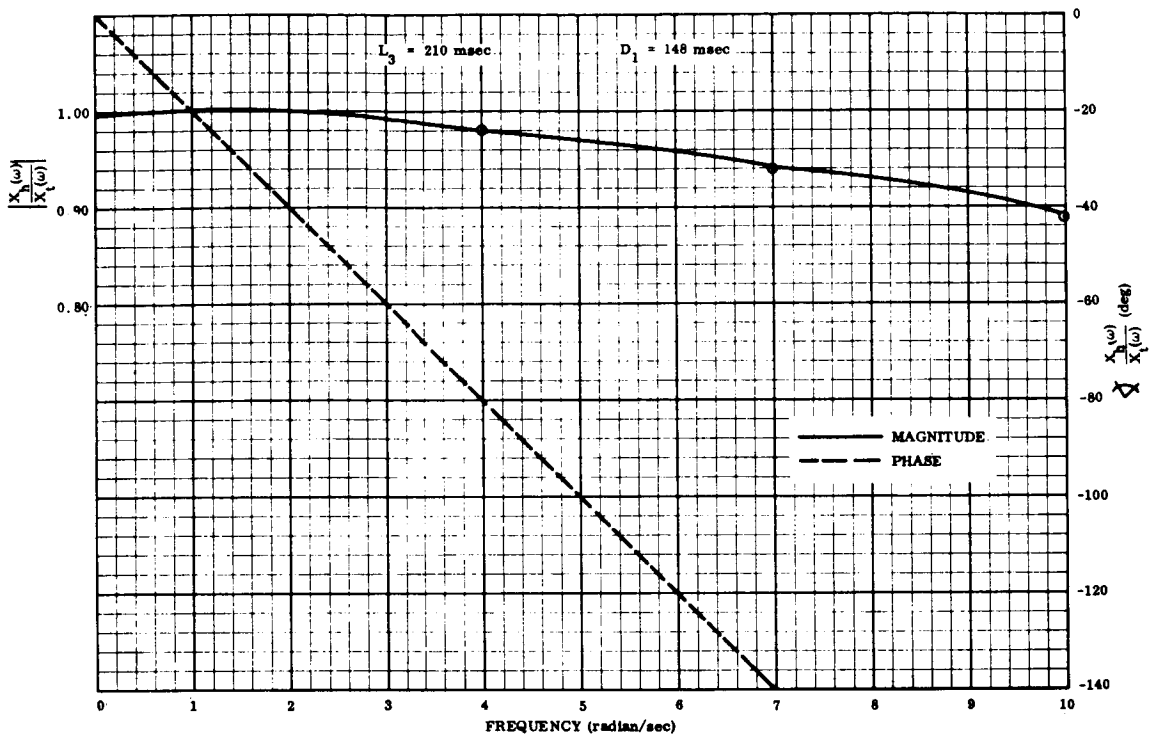

(c) Typical Frequency Response

Fig. 5-20 (cont.) Model of Motor Control System Applicable to Closed-Loop Pursuit Tracking with Unity-Gain Plant

Probably of greater importance than the transfer function is the detailed quantitative information on the latencies associated with each of the variables which can be considered as an operator output. In particular, data have been presented which demonstrate that the variables, ordered according to increasing latencies, are:

(1) Onset of EMG activity
(2) Beginning of eye movement
(3) Muscle force/acceleration of hand
(4) Final position of the hand

This ordering suggests that the bandwidth of the inner tracking loop of Fig. 2-2 can be extended by using some variable other than displacement as the controller output. Investigation of this conjecture is the topic of Section 5.3.

5.3 Tracking of Random Continuous Motion

5.3.1 Introduction

Data presented in the preceding section indicate that all of the potential operator outputs exhibit less delay in response to random step inputs than the commonly used manual displacement. This suggests that the bandwidth of the inner loop of Fig. 2-2 may be extended by using such quantities as (1) muscle force, (2) direction of gaze, or (3) muscle action potentials as the quantity which the operator uses to track the system errors. The various possible configurations are represented schematically in Fig. 5-21 by different positions of a switch which selects the follow-up quantity. The object of this section is to outline how such systems might be implemented and to determine their performance in tracking a random continuous input signal.

The performance of each tracking system is expressed in terms of the magnitude and phase of its measured closed-loop transfer function and the ratio of signal-to-noise in its output. The magnitude and phase information is further processed to obtain a pole-zero representation of the closed-loop tracking system which can be used for root-locus synthesis of the overall manned control system (see Fig. 2-2) in which it is embedded.

The results to be presented here differ from the extensive collection* of transfer functions available in the literature (Refs. 4, 5, 6 and 42) in that the parameter under investigation is the type of operator output used for feedback. The intended application of the results limited the scope of the investigation to deriving closed-loop transfer functions for pursuit tracking with a constant-gain plant.

---

*For example, Ref. 5 includes a tabulation of nineteen different open-loop transfer functions describing the performance of operators in a compensatory tracking task. These transfer functions apply to a wide variety of controlled element (plant) dynamics and most are specified for several different input spectra.

Only one input spectrum was used.*

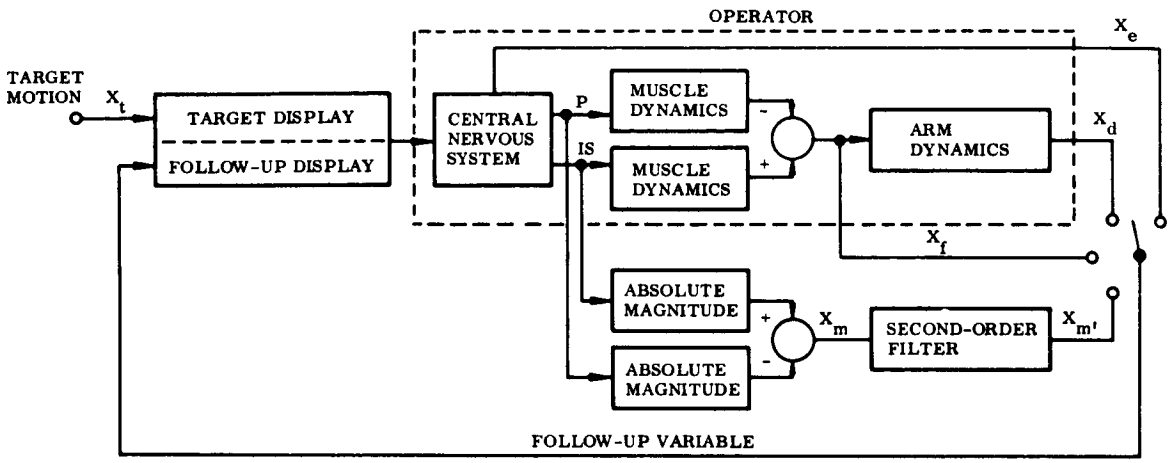

Fig. 5-21 Schematic Representation of Tracking Configurations to Be Investigated.

5.3.2 Instrumentation of Control Systems Using Various Operator Outputs

Probably the most widely used form of operator output is manual displacement. Hand controllers having one, two or three degrees of freedom are available in which control stick motions are used to control the plant directly (Ref. 11) or are converted into an electrical signal by potentiometers. Control force is another commonly used form of operator output. Like displacement, force is readily converted to a form suitable for input to the rest of the system. The proprioceptive feedback which displacement and force controllers provide to the operator is of considerable value in the case of high-order systems not employing Control Action Display.

*The input spectrum for this study was selected to satisfy two criteria:
(1) It contained enough energy in the higher frequencies to permit a meaningful determination of the transfer function over the frequency range of interest; more than 9% of the input power was in the spectrum beyond 6 rad/sec.
(2) It could be tracked with good fidelity by most operators; more precisely, it will be shown that the correlation between input and output signals was usually high.
This input spectrum was typical of spectra used for other studies reported in the literature.

Muscle action potential (EMG) is another quantity which can be used as the output variable in a manned system. Methods have been described for detecting the presence or absence of EMG activity in several groups of muscles in order to send commands to various controls. These systems use the techniques of binary logical design (Refs. 47 and 48) and/or pattern recognition (Ref. 49) to decode combinations and sequences of EMG bursts. Such systems have been designed primarily for persons who have lost the normal use of their limbs or who are operating in a high-acceleration environment.

In the approach investigated here, however, a continuous signal derived by processing the EMG activity was displayed to the operator; he tracked the target simply by contracting the appropriate muscle group (Pectoralis and Infraspinatus muscles were used) with the correct intensity. Such an approach seems feasible in the light of the following information:

(1) Basmajian (Ref. 50) found that after some practice a subject could exert very precise control over his muscles. This control was fine enough to permit the subject to select a single motor unit from among the several hundred (Ref. 31) that comprise a typical muscle.

(2) Lippold (Ref. 34) and Inman (Ref. 35) found that rectified/filtered EMG was proportional to the steady isometric force exerted by a subject. The results presented in Section 5.2 show that the EMG activity is also related to the transient muscle force.

A detailed description of the signal processing and display scheme used in this investigation is given in Appendix E. Briefly, the EMG signals from the two different muscles were separately detected using surface electrodes, rectified (Figs. 5-4, 5-7, 5-11 and 5-12 indicate that the EMG signals have an average value of zero) and filtered using a second-order filter having a natural frequency of 20 rad/sec and a damping ratio of 0.7. The difference between the two processed EMG signals was then applied to the display.

Another candidate for the output of a manned tracking loop is a signal measuring the operator's direction of gaze; in such a system the operator tracks the target simply by looking at it. It is apparent that this approach is susceptible to spurious outputs which would be caused when the operator is distracted and looks away from the target.

At least two types of instrumentation can be used to measure eye movement. One method requires that the operator wear a pair of goggles (Ref. 29) in which are mounted light sources and photocells which measure the difference in diffuse light reflected from the scalera and iris. A second method (the one used for measurements shown in Section 5.2) is to detect variations in corneoretinal potential (Refs. 39 and 40) using surface electrodes. The first method can presumably be used for tracking in both the horizontal and vertical directions but the second is limited to the horizontal direction only. The latter limitation is due to the fact that during blinks the eyeball is rotated upward (Ref. 40), which would cause a spurious output signal. Because both of these methods measure eye movement relative to the head, accurate tracking demands that the operator keep his head absolutely stationary; this is ordinarily accomplished by using a bite board.

Figure 5-22 shows the tracking performance of Subject No. 5 when displacement, force, and processed EMG are used as the output (i.e., tracking) variables. Careful study of Figs. 5-22a and b shows that the displacement output does not change as abruptly as the force output. This is an expected result because the arm dynamics act as a low-pass filter between muscle force and manual displacement. It can also be seen from these figures that the excursions of the follow-up variable, either displacement or force, were not as large as the excursions of the target; this was true even for long duration excursions. This point will be discussed in more detail later in this section.

Figure 5-22c shows the tracking results obtained when processed EMG is used as the follow-up variable. Despite relatively heavy* filtering,

*Over the frequency range of interest, the second-order filter can be represented as a simple time delay of $2\zeta/\omega_n$ = 70 msec. To decrease the natural frequency of the filter would defeat the purpose of the approach, which is to circumvent the time lags [see Eq. 5.2] between EMG activity and muscle force.

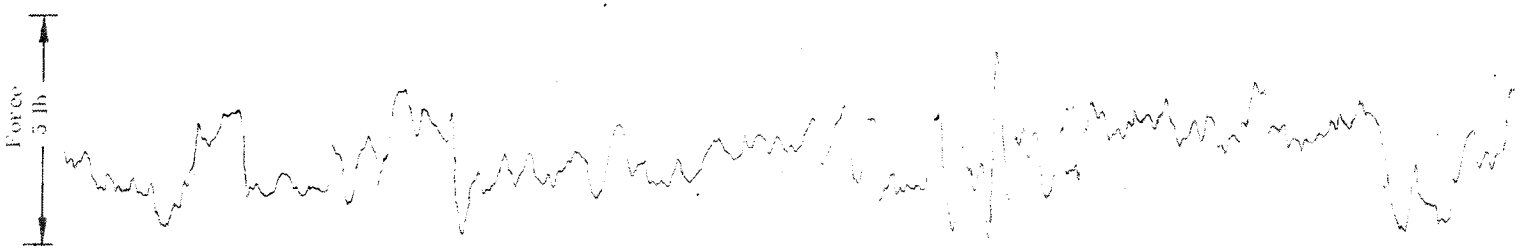

(d) Force Generated During EMG Tracking

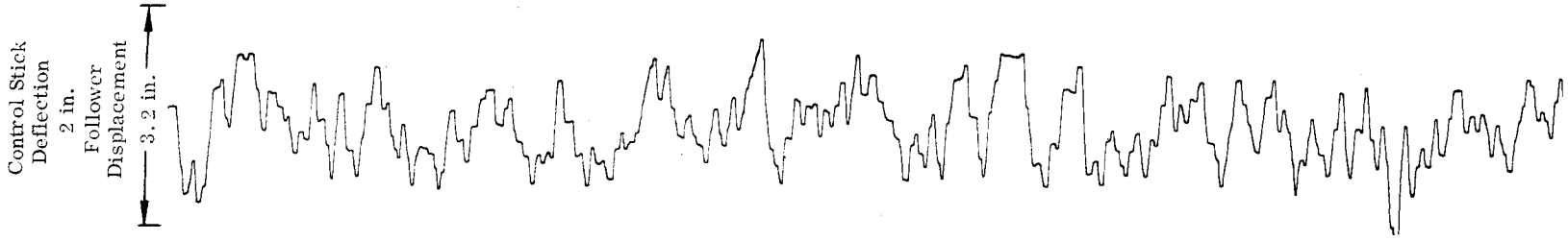

(a) Displacement Follow-Up

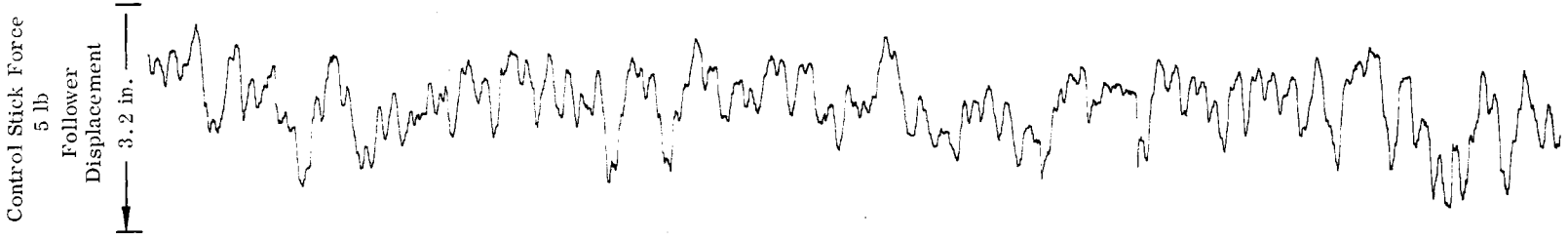

(b) Force Follow-Up

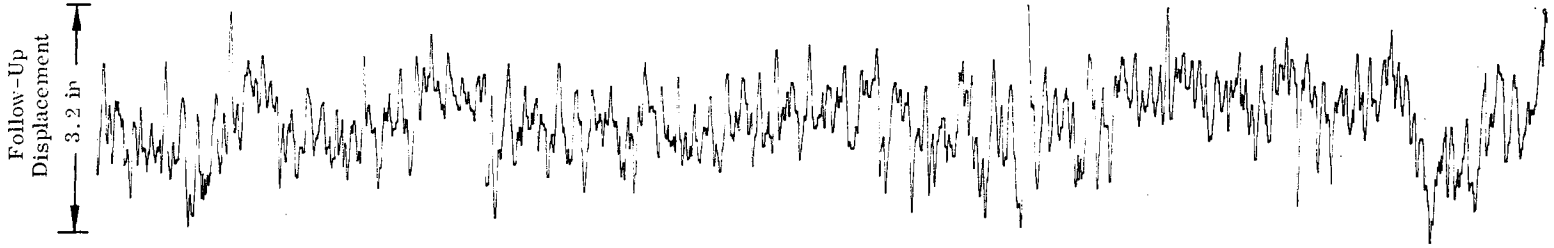

(c) Processed EMG Follow-Up

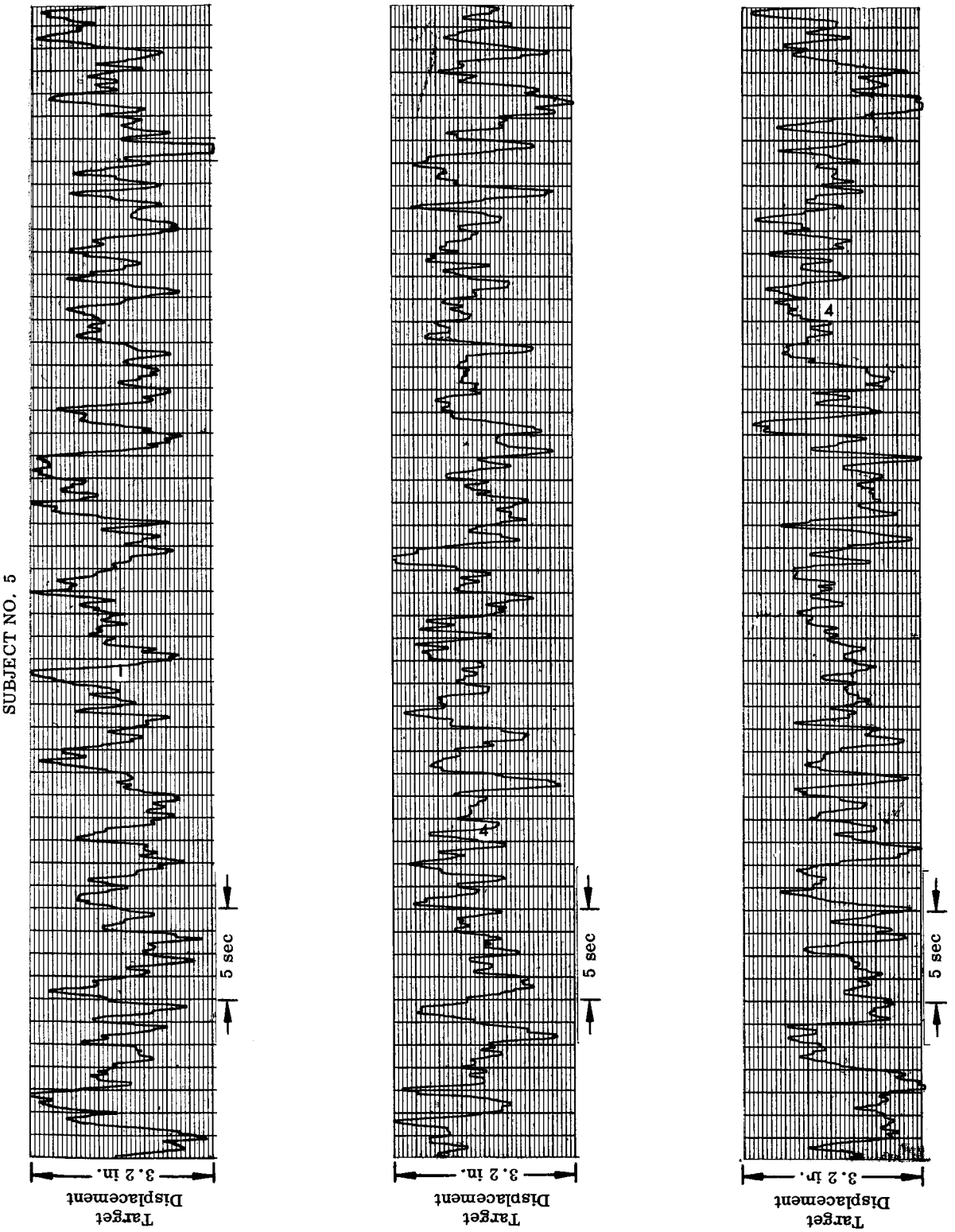

Fig. 5-22 Typical Tracking Performance for Displacement, Force, and EMG Follow-Up Signals

the EMG signal was quite noisy; it can be seen, however, that the trend of this signal corresponds to the target motion. It is particularly interesting to note that the force exerted by the subject (to cause the processed EMG signal to track the target) closely resembles* the delayed target motion.

Because the performance of the eye in tracking continuous random signals had already been investigated and well documented (Refs. 28 and 29) no such experiments were undertaken during this study. For this reason time traces for the system using eye position output are not included in Fig. 5-22.

5.3.3 Method Used for Determining Transfer Function and S/N Ratio

The transfer function and signal-to-noise ratio for each of the various tracking systems were evaluated using an approach described by Elkind (Ref. 51). This approach can be explained by referring to Fig. 5-23 which shows the operator tracking a target using the displacement follow-up signal in a pursuit display; typical time traces are shown in Figs. 5-22a and E-3. The performance of this closed-loop tracking system is characterized by the inpulse response $[h_{td}(\sigma)]$ of an equivalent linear system and a noise source (X_n) which is linearly uncorrelated with the input signal.

The input signal used for the tracking tests was a random variable having an autocorrelation function $\varphi_{tt}(\tau)$; the nominal value of $\varphi_{tt}(\tau)$ given by Eq. E.2 was used for all of the tests reported here. The actual measured values of input and output autocorrelation and cross-correlation functions $[\varphi_{tt}(\tau)$, $\varphi_{dd}(\tau)$ and $\varphi_{td}(\tau)$, respectively] were derived using calculations outlined in Appendix E; typical results are shown in Fig. E-4. These correlation functions are important for at least two reasons:

(1) The impulse response of the linear system which approximates (with the least mean squared error)(Ref. 5) the behavior of the closed-loop tracking system is given by Eq. 5.6.

*In fact, for all three subjects the correlation coefficient (ρ_{max} defined in the next subsection) between force and target motion is higher than between processed EMG and target motion, even though the loop was closed using the processed EMG signal.

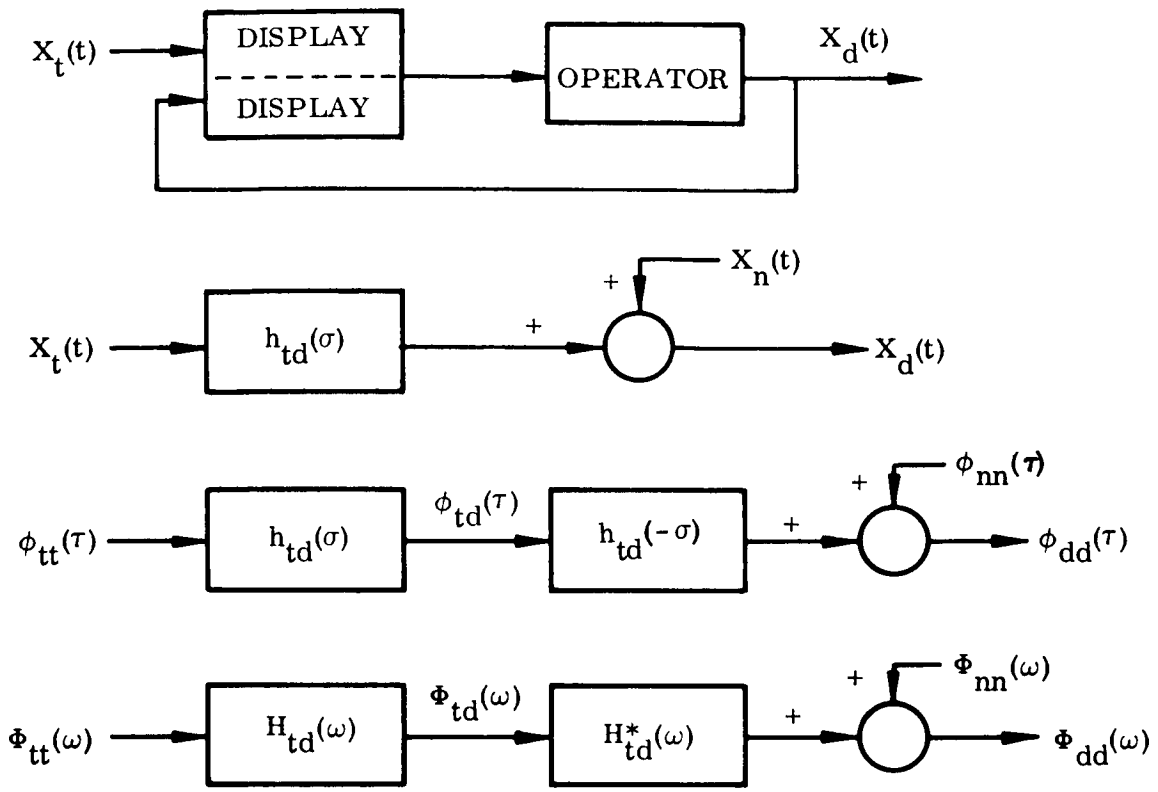

Fig. 5-23 Steps Followed in Deriving Transfer Function and Signal-to-Noise Ratio for Closed-Loop Tracking Systems

(2) The values of τ_{max} and ρ_{max} given by Eq. 5.7 provide a good measure of the operator's response time and the correlation between input and output, respectively.

$$\varphi_{td}(\tau) = \int_{-\infty}^{\infty} h_{td}(\tau - \sigma)\, \varphi_{tt}(\sigma)\, d\sigma \qquad (5.6)$$

$$\rho(\tau_{max}) = \rho_{max} = \text{Maximum}[\rho(\tau)] \qquad (5.7)$$

where

$$\rho(\tau) = \frac{\varphi_{td}(\tau)}{\sqrt{\varphi_{tt}(o)\, \varphi_{dd}(o)}}$$

The solution of Eq. 5.6 for $h_{td}(\sigma)$ is simplified by converting it into the Fourier transform domain. In this case the transfer function of the equivalent linear system is expressed in terms of the various spectral densities of the input and output according to Eq. 5.8. This formulation also leads to the expression for signal-to-noise ratio given by Eq. 5.9.

$$H_{td}(\omega) = \frac{\Phi_{td}(\omega)}{\Phi_{tt}(\omega)} \tag{5.8}$$

$$\frac{S}{N}(\omega) = \frac{1}{\dfrac{\Phi_{tt}(\omega)\,\Phi_{dd}(\omega)}{|\Phi_{td}(\omega)|^2} - 1} \tag{5.9}$$

The necessary power spectral density functions were computed from their respective correlation functions using the computational techniques outlined in Appendix E; typical results are shown in Fig. E-5.

To summarize, the performance of the closed-loop tracking system containing the operator is described in terms of its transfer function $[H(\omega)]$ and signal-to-noise ratio $[(S/N)(\omega)]$. Other measures of special interest are the value of the maximum correlation coefficient (ρ_{max}) and the time shift at which it occurs (τ_{max}). These quantities are computed from Eqs. 5.7 to 5.9 using correlation functions and power spectral densities (defined for the case of displacement feedback in Fig. 5-23) derived from the measured data (e.g., Fig. 5-22), using procedures described in Appendix E.

5.3.4 Presentation of Experimental Data

The tracking performance of three different subjects using displacement, force and processed EMG follow-up signals is summarized in Figs. 5-24 to 5-26. They show the magnitude and phase of the closed-loop transfer function and the signal-to-noise ratio as functions of frequency, and tabulate the values of ρ_{max} and τ_{max} for each system.

The results of experiments using random-step-function inputs described in Section 5.2 indicated that the latency of force output is greater than for EMG activity and that manual displacement lags muscle force. It is clear from Figs. 5-24 to 5-26 that these same conclusions apply in the case of operators tracking a random continuous input signal. For all three subjects, the value of τ_{max} (which is a measure of the subject's average reaction time) decreased as the variable used to close the tracking loop was changed from displacement to force and from force to processed EMG. For all three subjects, and over almost all of the frequency range of interest, the phase lag of the closed-loop transfer functions decreased according to this same ranking.

Unfortunately, however, the increased bandwidth (or more accurately, the reduced phase lag) obtained by using force or processed EMG follow-up signals is accompanied by an increase in the noise component of the output signal at almost all frequencies. This is particularly true in the case of processed EMG signals, where the noise is apparent even in the time domain (see Fig. 5-22). Figures 5-24 to 5-26 show that at most frequencies $[(S/N)(\omega)]$ decreases for all three subjects as the output variable is changed from displacement to force and from force to processed EMG. This is also verified in all except one case (the change from displacement to force by Subject No. 5) by a decreasing value of correlation coefficient, ρ_{max}.

Another important result displayed in Figs. 5-24 to 5-26 is that all tracking systems had a closed-loop gain of less than unity at low frequencies; this effect was noted in discussing the tracking performance shown in Fig. 5-22. This is an important difference from the step-function tracking results (in which the steady-state hand displacement always equals the step input displacement), and will be discussed in more detail in the next subsection.

During the tracking tests in which processed EMG was used as the follow-up signal, the force exerted by the subject (to cause the EMG to follow the target) was measured and recorded. The correlation function and power spectral density between processed EMG and force, and between the input signal and force, were computed in order to derive the transfer functions given in Figs. 5-27 and 5-28, respectively.

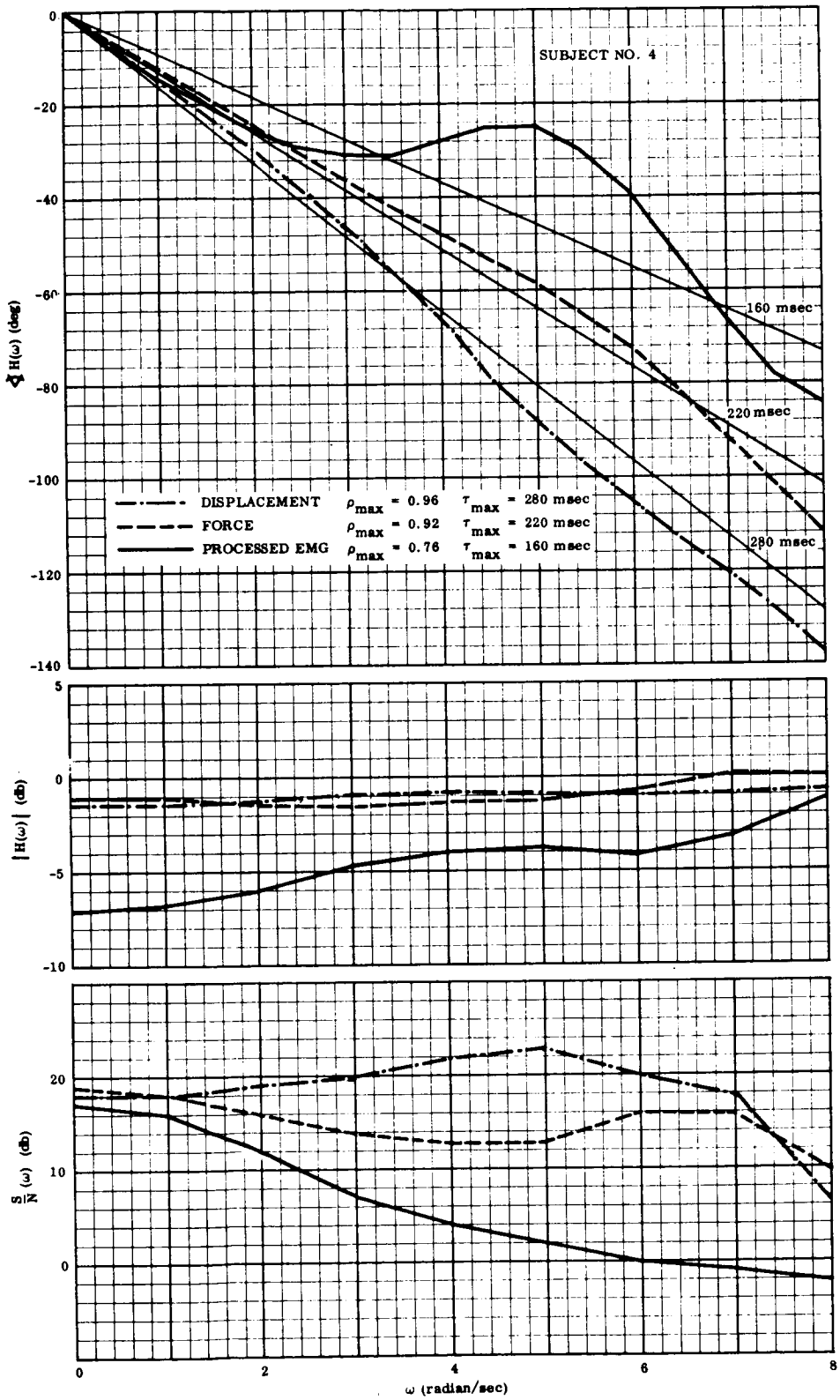

Fig. 5-24 Transfer Functions and Signal-to-Noise Ratios for Subject No. 4

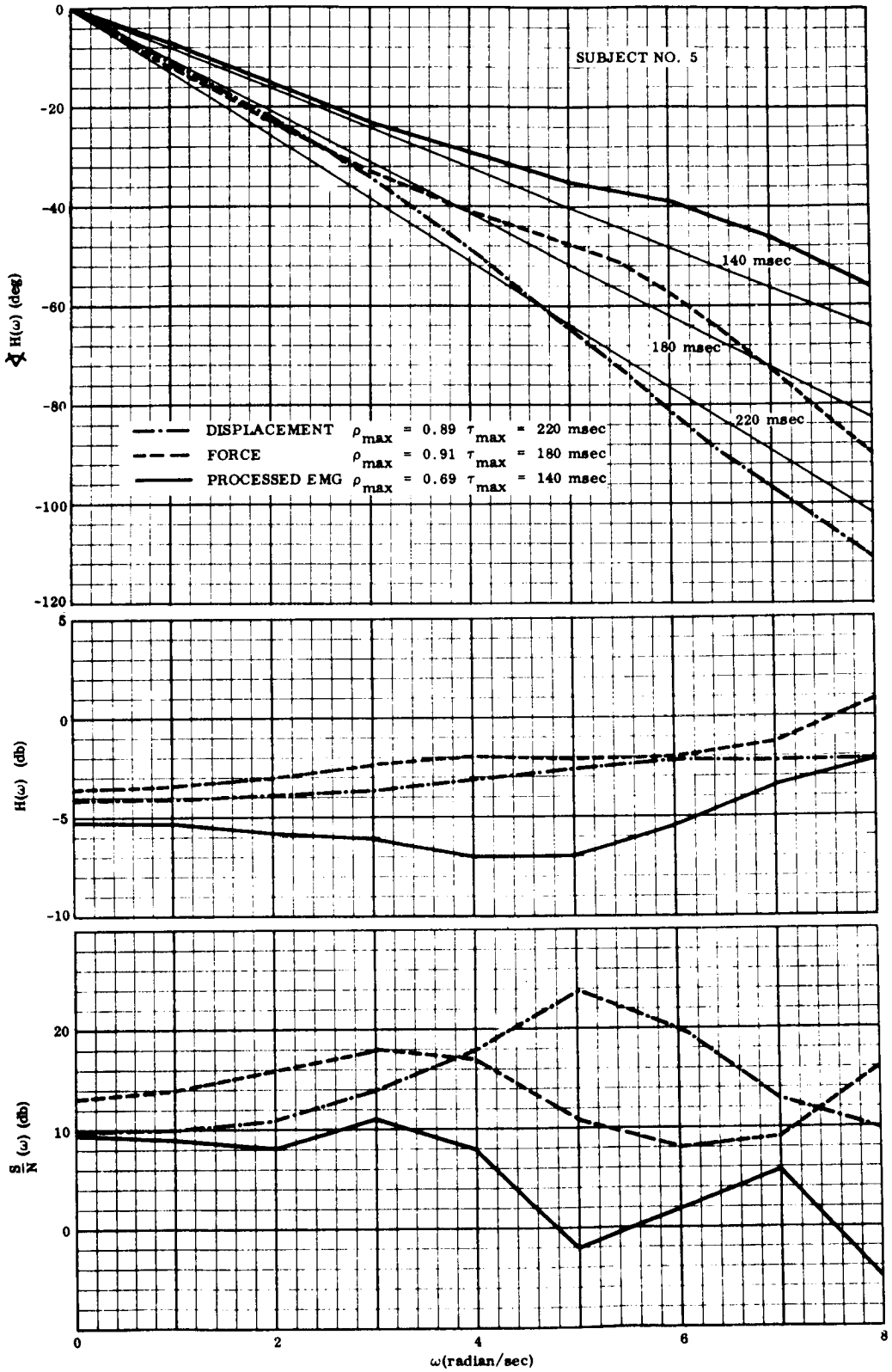

Fig. 5-25 Transfer Functions and Signal-to-Noise Ratios for Subject No. 5

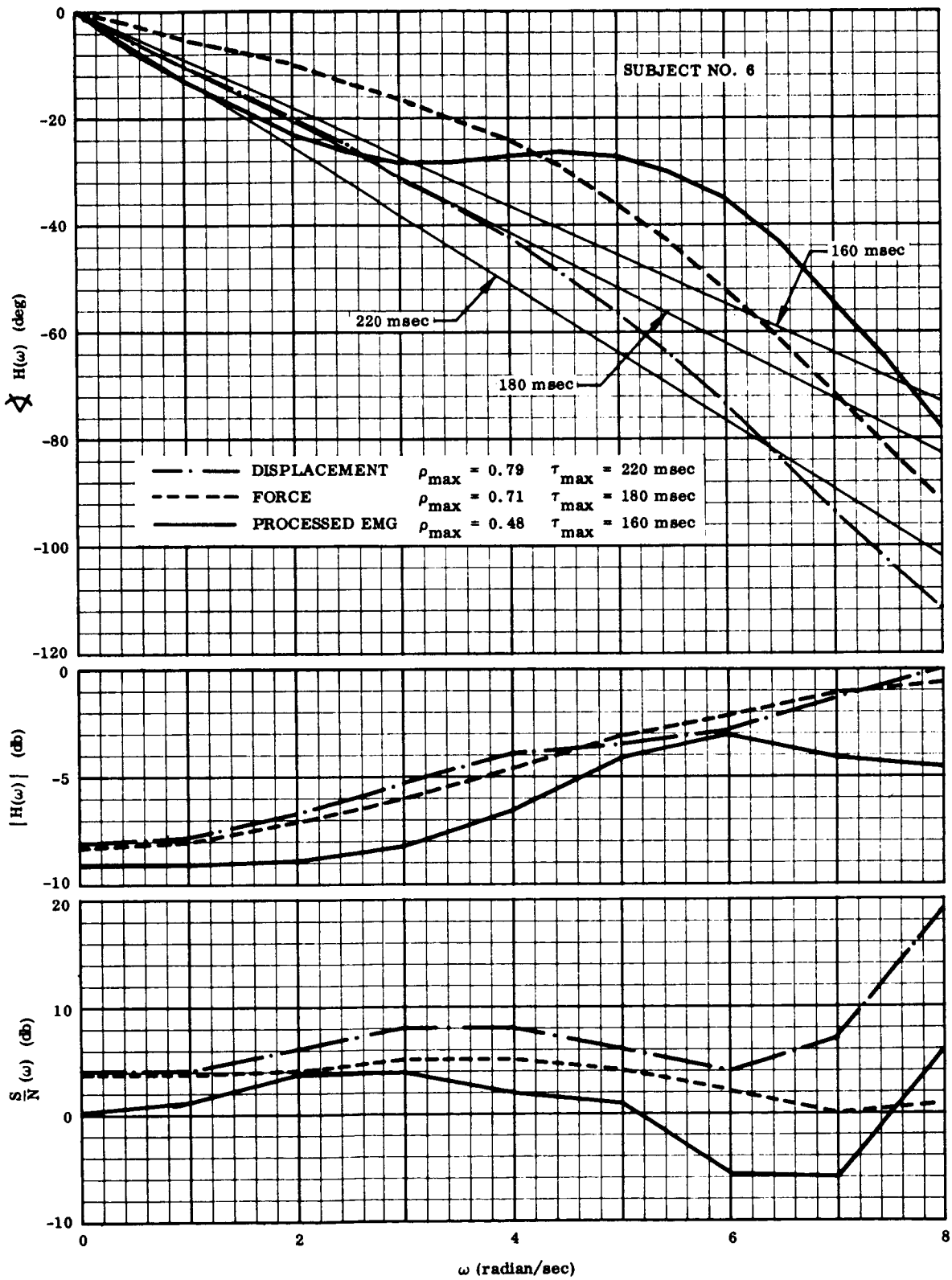

Fig. 5-26 Transfer Functions and Signal-to-Noise Ratios for Subject No. 6

Figure 5-27 shows the transfer function between EMG activity and muscle force for a tracking test using a random continuous input signal. It can be seen from Fig. 5-21 that the transfer function between processed EMG and force must be multiplied by the filter transfer function in order to compensate for the dynamics that this filter introduces. This makes it possible to derive the transfer function relating the unfiltered absolute magnitude of EMG to the net muscle force it causes; this is the function plotted in Fig. 5-27. Also plotted in the same figure is the transfer function given by Eq. 5.2 which relates the EMG activity to muscle force for step isometric force application (see Fig 5-8). Comparison of these two functions indicates that the latency between EMG and force is approximately 90 msec greater for continuous tracking than for a step force application. This same result was confirmed for Subject No. 5, but could not be verified in the case of Subject No. 6 because of a very low signal-to-noise ratio.

Figure 5-28 gives the transfer function of the dynamics between input displacement and muscle force for two of the situations shown in Fig. 5-21:

(1) Force is used as the follow-up variable, and EMG is inside the closed tracking loop.

(2) Processed EMG is used as the follow-up variable and Force is outside the closed tracking loop.

It can be seen from Fig. 5-28 that the force latency is approximately 60 msec less when force is used as the follow-up variable than when processed EMG is used as the follow-up variable; this latency difference was 60 and 80 msec for Subjects 5 and 6, respectively. This is interpreted to mean that human operators are capable of applying force (and therefore muscle action potential) at a higher rate than they actually use in EMG tracking. Stated another way, it appears that subjects do not make full use of the latency reduction which feedback of the processed EMG signal affords.

Prior work in the field was reviewed in order to determine the tracking performance obtained when eye position is used as the output variable. Figure 5-29, taken from Refs. 28 and 29, shows the transfer

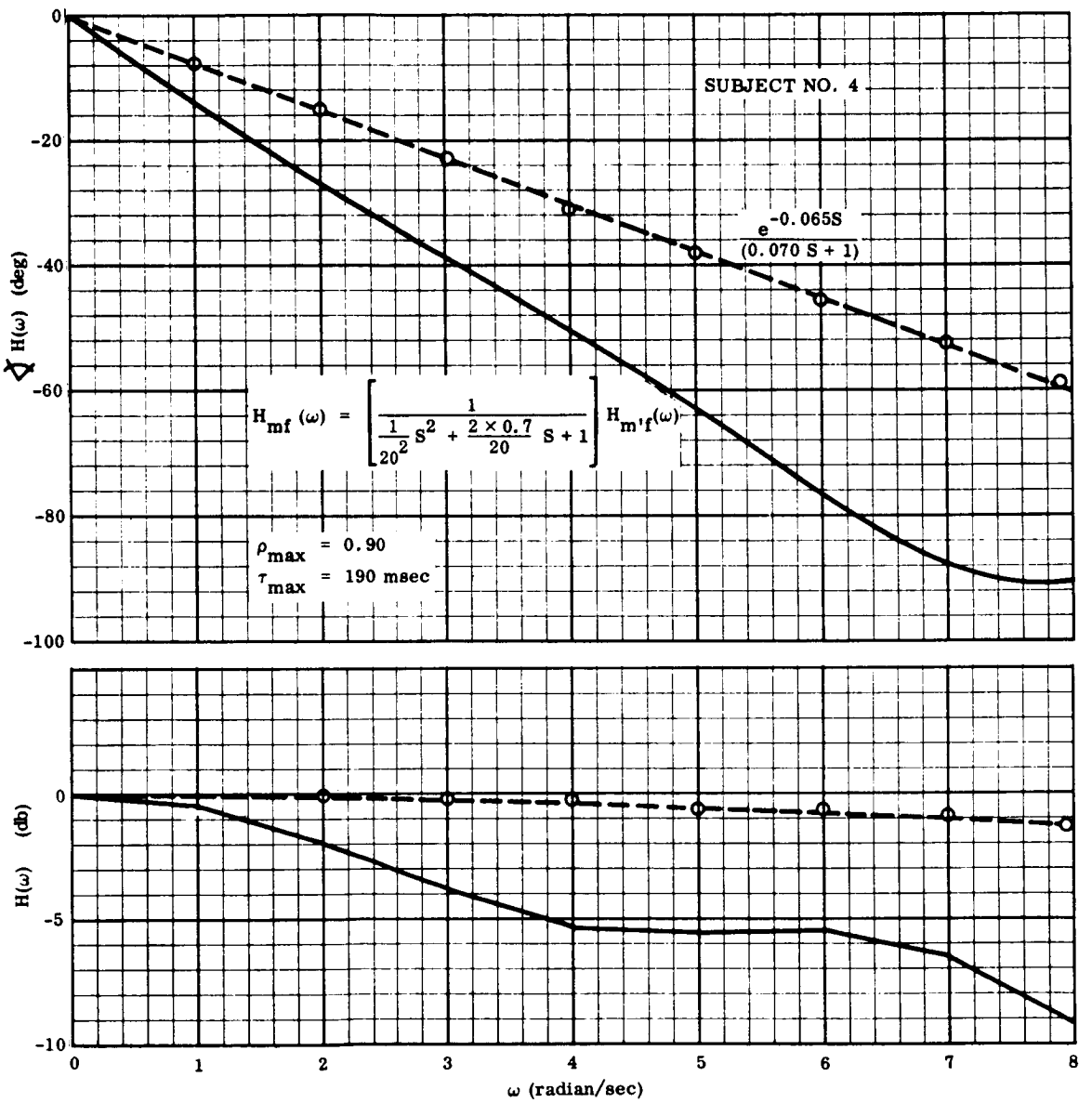

Fig. 5-27 Transfer Functions Between EMG and Force

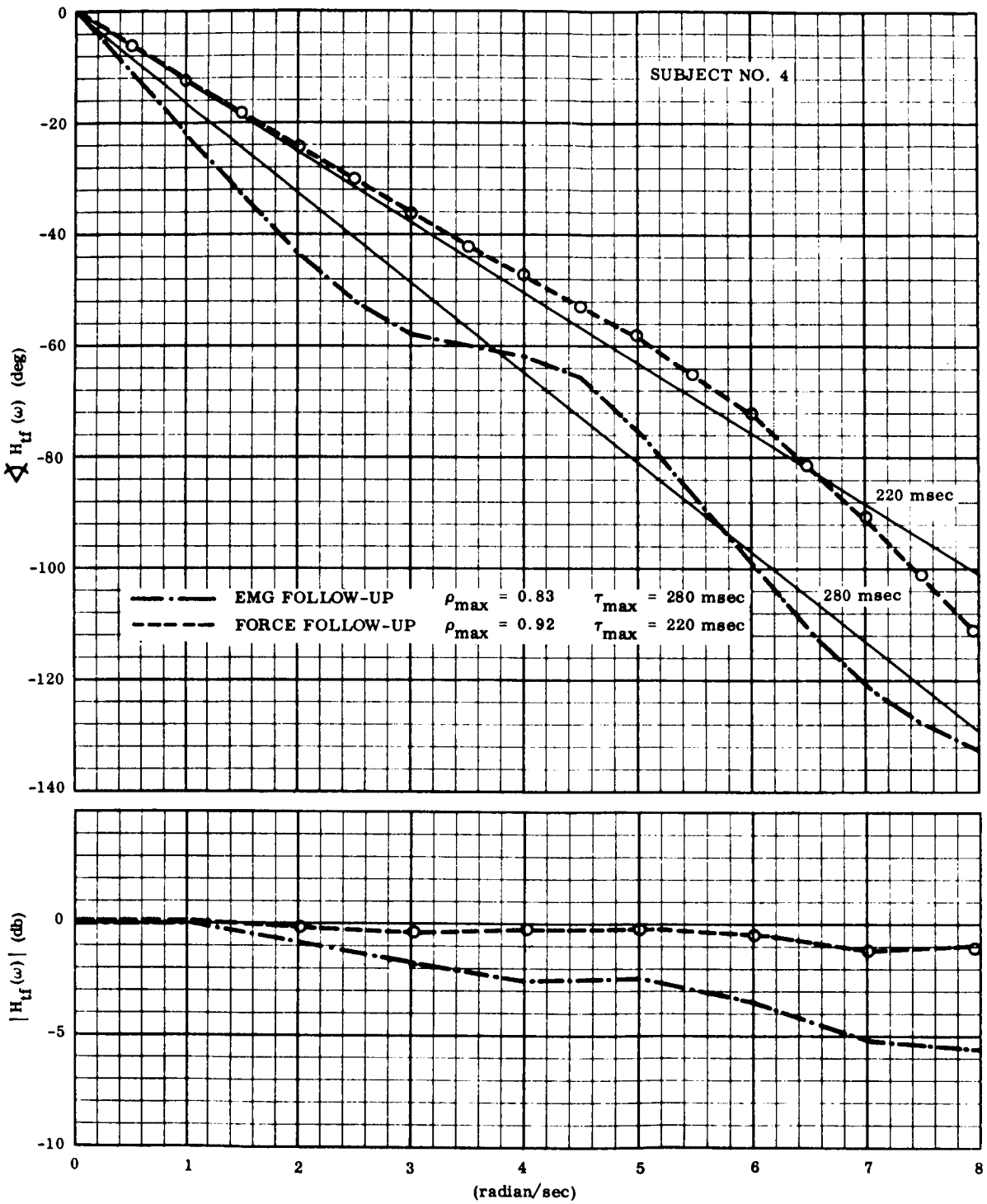

Fig. 5-28 Transfer Function Between Input Displacement and Force for EMG Follow-Up and for Force Follow-Up

function between target displacement and direction of gaze for a typical tracking run by an experienced subject. The performance of Subject No. 5 using force as the follow-up variable is plotted on this same graph for comparison. It appears* that the transfer functions of these two tracking systems are quite similar; this agrees with the results of tracking tests using random step inputs, which showed (see Figs. 5-13, 5-14 and 5-15) that the average latency of eye movements and the onset of force are comparable.

5.3.5 An Analytical Representation of Closed-Loop Tracking Behavior

Thus far in this section results have been presented in the form of measured magnitude and phase of the closed tracking loop as a function of input frequency. This form of data is convenient if the overall manned control system (in which the closed tracking loop is embedded; see Fig. 2-2) is to be designed using frequency domain synthesis techniques, as in Chapter 3. However, in order to design the control system using the root-locus approach it is necessary to derive an analytical model which fits the empirical data; that is the object of this section.

Wilde and Westcott (Ref. 32) analyzed tracking behavior in the time domain and concluded that for a compensatory display the human operator's output rate is proportional to the delayed error; the proportionality constant and transport delay are approximately 3.0 sec^{-1} and 125 msec, respectively. McRuer, et al. (Ref. 6) independently discovered that for a compensatory display, a relationship of this form provided a useful approximation to their frequency response data; they call this model the "crossover" model. The starting point for the analytical model to be derived here is a somewhat more general form of the Wilde-Westcott/Crossover model and is given by the block diagram in Fig. 5-30a. This figure suggests that an operator using a pursuit display (where he

*Unfortunately a rigorous comparison cannot be made between these two transfer functions because they were obtained using different subjects and different input signal spectra.

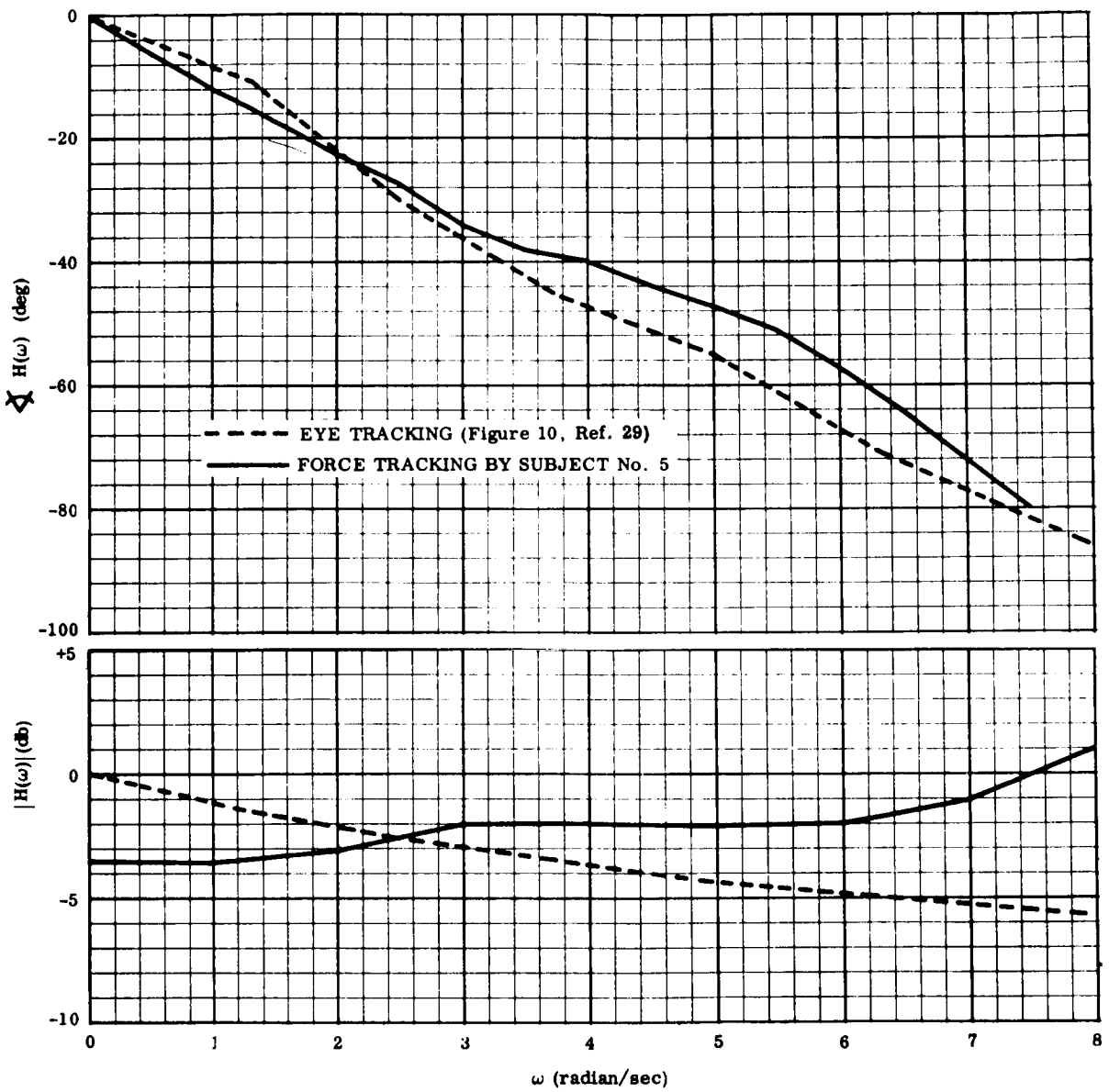

Fig. 5-29 Comparison of Transfer Functions for Eye and Force Tracking

can see both the target and the follower independently) tries to follow a scaled-down version of the input signal. This modification must be included to make the model consistent with the fact (noted in discussing Figs. 5-22, 5-24, 5-25 and 5-26) that the closed-loop response does not approach unity gain at low frequencies.

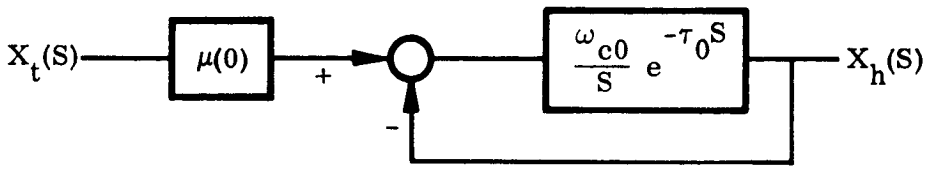

(a) Modified Wilde-Westcott/Crossover Model

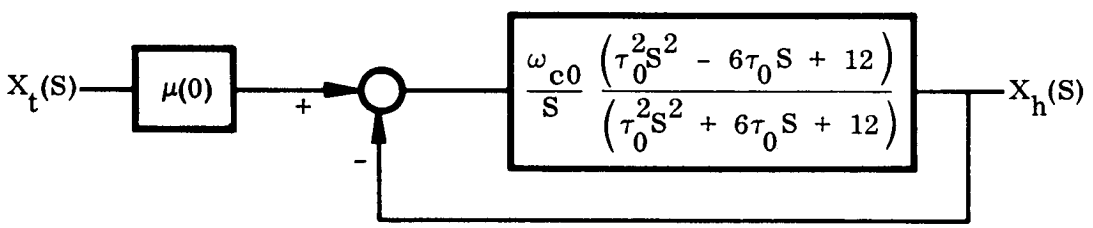

(b) Model Using Second-Order Padé Approximation

Fig. 5-30 Block Diagram Showing Analytical Approximation to Human Operator's Closed-Loop Tracking Behavior

The next step in deriving the desired model is to determine the constants $\mu(o)$, ω_{co}, and τ_o. The value of $\mu(o)$ is readily determined from Figs. 5-24, 5-25 and 5-26 as the magnitude of the transfer function at low frequencies. The values of ω_{co} and τ_o are determined by a trial-and-error procedure in order to obtain the best match to the measured transfer functions, particularly the phase data. It can be shown that the value of ω_{co} dictates the slope of the phase curve at low frequencies, which in turn is approximated by

τ_{max}^{-1}. These two facts are used to derive an initial estimate of ω_{co} given by Eq. 5.10*

$$\omega_{co} = \left\{ \left[- \frac{d}{d\omega} \not\leq H(\omega) \right]_{\omega=0} \right\}^{-1} \approx \tau_{max}^{-1} \qquad (5.10)$$

It was determined that values for $\mu(o)$, ω_{co} and τ_o could be found which caused the closed-loop transfer function of the model to approximate the measured closed-loop transfer functions obtained using both displacement and force follow-up signals and also using the transfer function derived from step input data (Fig. 5-20c). The resulting values are given in Table 5.2, and Fig. 5-31 shows how nearly the model can be made to fit the experimental data.** It was found, however, that the model could not be used to fit the data for any subject using processed EMG as the follow-up signal.

Two interesting features of the various subjects' tracking performance are evident from Table 5.1:

(1) The value of τ_{max}^{-1} gives an initial estimate of ω_{co} which is within approximately 20 percent of the value that best fits the measured data.

(2) Each subject exhibits approximately the same steady-state gain $\mu(o)$ for force tracking as for displacement tracking. In an attempt to track as rapidly as possible, a subject adjust his follow-up motion to a certain percentage of the input excursion; this scale factor is the same (for a given subject and input spectrum) for both force and displacement outputs.

---

* Note that the value of ω_{co} determines the low-frequency phase shift in the frequency domain and that the value of τ_o dictates the latency between step-function input and model output in the time domain.

** Note that this does not mean that the correct open-loop transfer function has been found. It does mean, however, that any difference between the true and derived open-loop transfer functions is unimportant in modeling the inner tracking loop (see Fig. 2-2) and in designing the overall control system in which it is embedded. In fact one of the reasons for using Control Action Display is to reduce the closed-loop dependence on open-loop variations by providing feedback around the inner loop.

Table 5.2

Comparison of Various Tracking Results in Terms of Models Shown in Figs. 5-30a and 5-30b

Situation	$\mu(o)$	τ_o (sec)	ω_{co} (rad/sec)	τ_{max}^{-1} (sec^{-1})	Z_1 (rad/sec)	P_1 (rad/sec)	P_2 (rad/sec)	Increase in Bandwidth (%)
Subject No. 4-Displacement	0.86	0.157	3.9	3.6	19.1 + j11.0	-4.21 + j6.22	-33.7	33
Subject No. 4-Force	0.89	0.116	5.1	4.5	25.6 + j14.9	-5.91 + j8.15	-45.0	
Subject No. 5-Displacement	0.62	0.136	5.3	4.5	22.1 + j12.7	-4.01 + j8.11	-41.4	25
Subject No. 5-Force	0.65	0.105	6.0	5.6	28.6 + j16.5	-6.05 + j9.62	-51.1	
Subject No. 6-Displacement	0.39	0.143	5.6	4.5	21.0 + j12.1	-3.33 + j8.34	-40.8	20
Subject No. 6-Force	0.39	0.125	7.2	5.6	24.0 + j13.8	-3.16 + j10.2	-48.9	
Derived from Average Step Response (Fig. 5-20c)	1.00	0.165	3.3	-	18.2 + j10.5	-4.45 + j5.29	-30.8	-
Wilde-Westcott Results (Ref. 32)	1.00	0.125	3.0	-	24.0 + j13.9	-7.80 + j1.38	-36.0	-

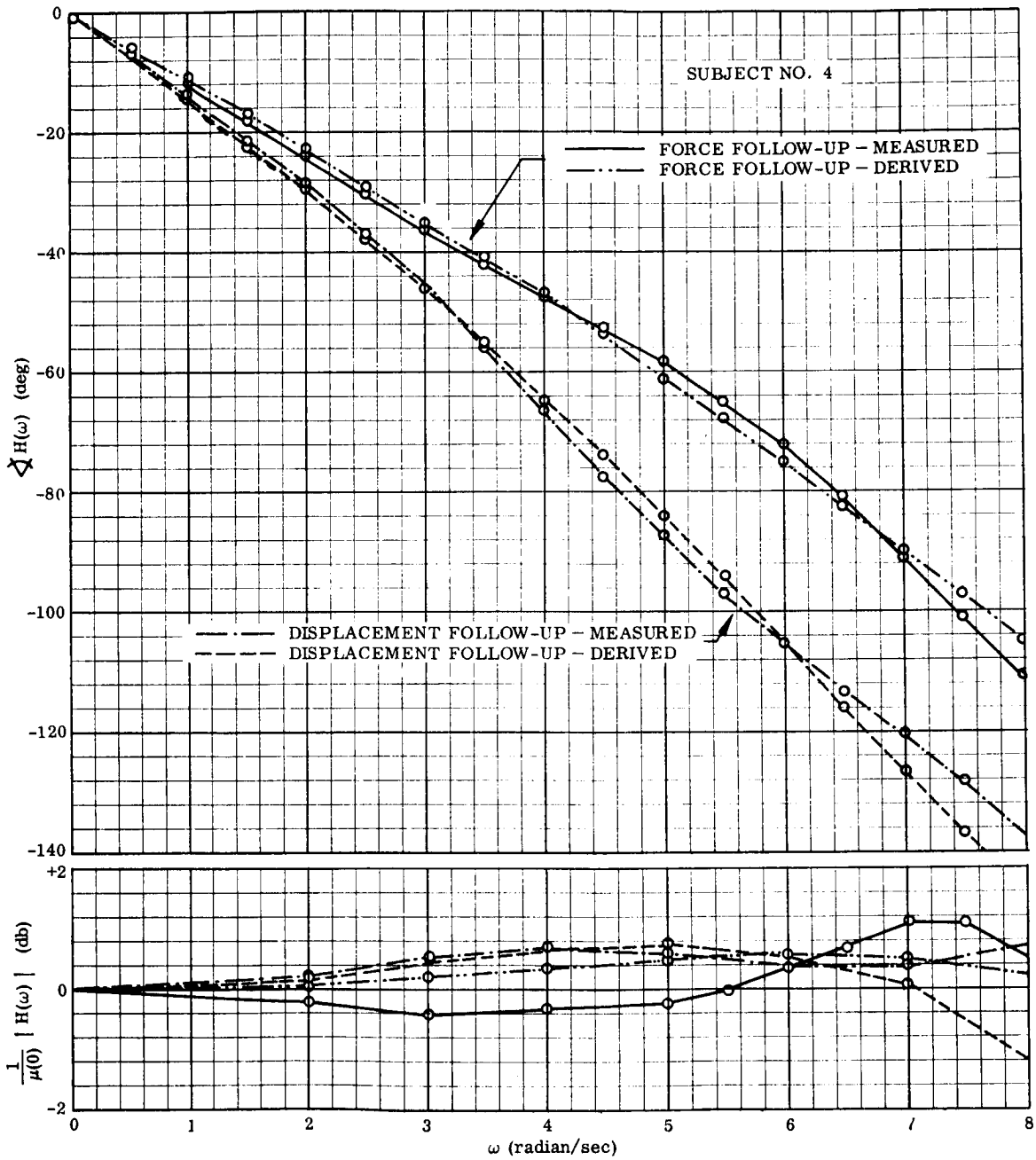

Fig. 5-31 Comparison of Measured and Derived Closed-Loop Transfer Functions

The next step in deriving the desired model is to approximate $e^{-\tau_o s}$ as a rational function. It has been found convenient to use the second-order Padé (Ref. 52) approximation given by Eq. 5.11 and the block diagram of Fig. 5-30b:

$$e^{-\tau_o s} \approx \frac{\tau_o^2 s^2 - 6\tau_o s + 12}{\tau_o^2 s^2 + 6\tau_o s + 12} \tag{5.11}$$

By making use of such an approximation, the closed-loop transfer function of the modified Wilde-Westcott/Crossover model can be expressed as a rational polynomial given by

$$H(s) = \mu(o) \frac{|P_1|^2 \, |P_2|}{|Z_1|^2} \frac{(s - Z_1)(s - \bar{Z}_1)}{(s - P_1)(s - \bar{P}_1)(s - P_2)} \tag{5.12}$$

in which the poles and zeros for each of the various cases are given in Table 5.2. It was found that magnitude and phase computed from Eq. 5.12 match the closed-loop magnitude and phase of the model shown in Fig. 5-30a within 0.1 db and 1 deg over a frequency range of 0 to 8 rad/sec for all of the cases given in Table 5.2.

The tracking results for each of the various cases can now be compared in terms of their poles and zeros by referring to Table 5.2. The effect of changing from displacement to force feedback is to increase the real and imaginary parts of all poles and zeros (i.e., to increase the closed-loop bandwidth) by approximately 33, 25, and 20 percent for Subjects 4, 5 and 6, respectively. It is also apparent that the pole-zero representation derived from the average step function results (Fig. 5-20c) does not differ appreciably from that of Subject No. 4 tracking a random continuous input using displacement feedback.

The model shown in Fig. 5-30b is readily mechanized on an analog computer according to Fig. 5-32; in this way the performance of a typical operator in a tracking loop with Control Action Display can be simulated. By using this mechanization, together with the analog computer representation of the compensation and plant dynamics (see Fig. 2-2), a preliminary determination of the overall system performance can be obtained.

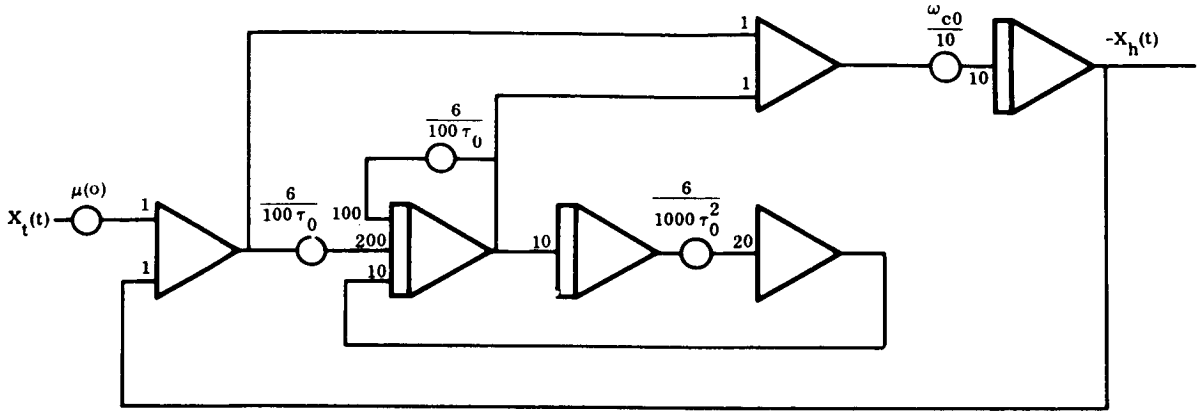

Fig. 5-32 Analog Computer Representation of Human Operator's Closed-Loop Tracking Behavior

5.3.6 Comparison of Responses of Models Derived in Sections 2 and 3

At this point it is of interest to compare the results obtained in Sections 5.2 and 5.3 as follows:

(1) Compare the transfer functions measured using a random continuous input signal in Section 5.3 with the transfer function derived from the response to random step inputs in Section 5.2.

(2) Compare the step function response measured using random step inputs in Section 5.2 with the step function response derived from the response to a random continuous input signal in Section 5.3.

Examination of Fig. 5-20c and Figs. 5-24, 5-25 and 5-26 indicates that an operator tracks a random continuous input signal with less phase lag than he does a signal composed of random step inputs. This means that the operator responds with less delay in the case of a continuous signal, probably because a certain amount of extrapolation (i.e., prediction) is possible. In an attempt to follow as rapidly as possible, the operator tends to track a scaled-down version of the continuous input signal; for a series of random step inputs, however, full-scale displacement was almost always achieved.

Figure 5-33 shows the step function response of the model given in Fig.5-30b and Fig. 5-32 using the values of τ_o and ω_{co} derived for Subject No. 4 (see Table 5.2). It can be seen that the velocity reaches a maximum of $V_m = \omega_{co} X_t$ at the time $2\tau_o$. The response obtained from the model shown in Fig. 5-30a is given by the dotted curve in Fig. 5-33; note that after a delay of τ_o, the velocity jumps to a value $V_m = \omega_{co} X_t$ and remains constant until the time $2\tau_o$.

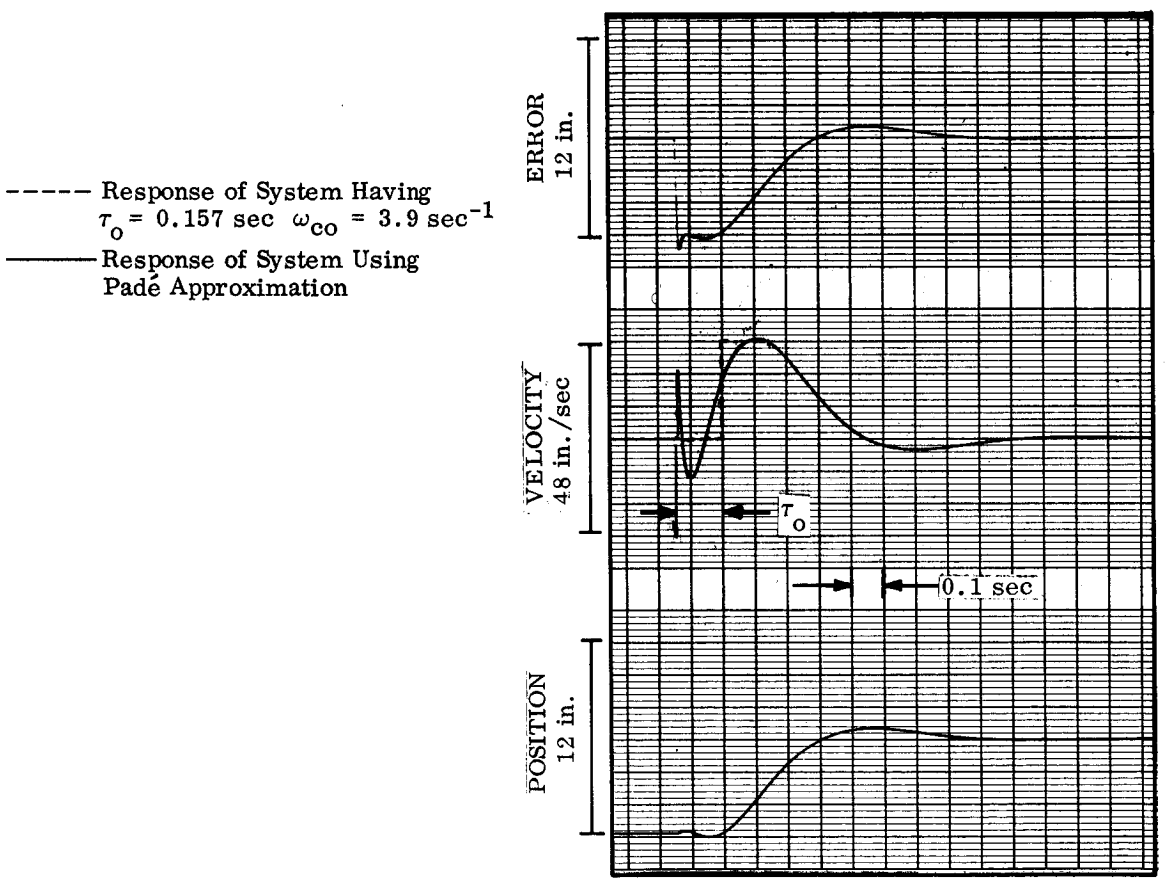

Fig. 5-33 Step Function Response of Derived Closed-Loop Model

Figure 5-20b shows the average measured response for the case of random step inputs. This response differs from Fig. 5-33 in two respects:

(1) The latency between the input step and the first motion is 0.157 sec for the continuous input signal compared with 0.210 sec for the case of random step inputs.

(2) For a given magnitude of displacement, the models shown in Fig. 5-30 exhibit a considerably smaller value of V_m. In fact Fig. 5-19 shows that $\omega_{co} = V_m/X_t$ is on the order of 10 sec^{-1} for the case of random step inputs, compared with 4 to 6 sec^{-1} (given in Table 5.2) for random continuous inputs.

These findings indicate that the model derived in Section 5.2 requires a longer time to initiate a response, but a shorter time to accomplish a move, than the model derived in Section 5.3.

5.4 Summary

The data presented in this chapter support the following detailed conclusions regarding the performance of a human operator in closed-loop tracking using pursuit display:

(1) Figures 5-13, 5-14 and 5-15 show that the sequence of events following a step target displacement is as follows: (i) Electrical activity within the muscles (EMG) indicates that a command has been received from the central nervous system. (ii) The eye begins a saccadic move to the new position. (iii) A force is generated by the agonist muscles.

(2) The values of these latencies appear to be independent of the amplitude of the step function displacement (see Fig. 5-16).

(3) The hand tracking system is not in series with the eye tracking system; in fact, Figs. 5-13, 5-14 and 5-15 show that commands reach the muscles before the beginning of eye movement. Past confusion on this point has been caused by the time delay between muscle commands and the resulting force and acceleration (see Figs. 5-4, 5-7, 5-8 and 5-9).

(4) Figures 5-17 and 5-18 show that neither the duration nor the magnitude of acceleration is constant for step-function moves of varying distances.

(5) Results of tests using a random continuous input signal indicate that the bandwidth of the closed tracking loop is increased as the follow-up variable is changed from displacement to force and from force to processed EMG. Unfortunately, however, the signal-to-noise ratio of the closed tracking loop generally decreases in the same order, throughout the frequency range of interest for Control Action Display. These results* are displayed in Figs. 5-24, 5-25 and 5-26 and in Table 5.2.

(6) Figure 5-29 shows that eye tracking does not provide an increase in closed-loop bandwidth compared with force tracking; no signal-to-noise ratio data are available for eye tracking performance.

(7) The model given in Fig. 5-30b and Table 5.2 accurately represents the performance of an operator using displacement or force feedback to track a random continuous input signal. This closed-loop model yields a particularly simple pole-zero representation, Eq. 5.12, which can be used to design the overall system (in which it is embedded) by root-locus techniques.

The overall conclusion of this study is that the increased bandwidth of the closed tracking loop obtained by using eye position or processed EMG as the follow-up variable probably does not warrant the increased random noise output and instrumentation complexity which these approaches impose. Use of force as the follow-up variable can increase the closed-loop bandwidth as much as 30 percent (compared with displacement feedback) without significantly increasing the output noise or system complexity, and should be considered for applications which do not require a steady-state controller output.

---

*It is not possible to determine from these results what closed-loop delays would result in the case of EMG tracking if the filtering (within the loop) were chosen to give a signal-to-noise ratio comparable to those obtained using displacement or force feedback. Such a determination could be the subject of an extensive investigation, as it would require repeating the EMG-tracking tests using different filters until an acceptable signal-to-noise ratio was obtained.

Chapter 6

CONCLUSIONS AND SUGGESTIONS FOR FUTURE STUDY

6.1 Conclusions

The technique of Control Action Display is implemented by providing:

1) An auxiliary display superimposed on the display normally employed; the operator's control action is instantaneously presented on this auxiliary display.
2) Compensation networks (either preceding the display or following the operator's response) as required to give the desired overall system performance.

The technique appears to be applicable to a wide variety of manned control systems; its use was demonstrated in experimental simulations for such diverse problems as controlling a spacecraft and maintaining balance on a tightrope.

Use of the Control Action Display technique makes it possible to design manned systems by using the conventional, straightforward analytical techniques of automatic control system theory. Overall system performance can be estimated without recourse to extensive testing and subjective evaluation by many operators. The operator can easily control nonlinear, high-order, multidimensional systems using Control Action Display, because he always knows what control action he is exerting and what is required.

Control Action Display makes it possible for the operator to respond with any one of his several different output variables. Tests indicated that tracking bandwidth increased as responses nearer in space and time to the operator's central nervous system were used for the follow-up variable. Unfortunately, however, the noise component of the operator's output also increased in approximately the same order. It is concluded therefore that use of such operator responses as EOG or processed EMG signals is probably not warranted in most applications.

6.2 Suggestions for Future Study

Adams (Ref. 53) and Braisted (Ref. 54) have studied a system in which an operator on earth drives a vehicle around on the surface of the moon using a television picture returned from the vehicle. The operator's task is complicated by a 2.6 sec delay (i.e., time required for radio transmission to the moon and back) between his steering commands and the response of the television picture.

The approach used by Adams and Braisted was to simulate the system by constructing a small cart which carried a closed circuit television system. System parameters and performance were established empirically.

It appears* that the design procedure given in Chapter 2 is applicable to this problem. In this case an indication of the operator's instantaneous control action (rotation of the steering wheel) is superimposed on the television picture returned from the cart. The operator's response is processed by a compensation network specified analytically using frequency domain or Z-transform** synthesis techniques. The maximum vehicle velocity can be related to the complexity of the course (represented in terms of a Fourier series giving the required steering commands as a function of distance along the course) through the system closed-loop transfer function.

Another area of continuing interest is the investigation of the human motor-control system. Reference 37 describes results of experiments (conducted during the course of research for this dissertation) to study the response of the central nervous system during the transient following a load disturbance. This and other such experiments could be used to derive a model of the human motor-control system which might provide a basis for the diagnosis and treatment of various neurological diseases.

---

* Meissinger (Ref. 9) has applied elements of the recommended analytical approach to the problem of remotely controlling a lunar landing vehicle.

** In some cases a sampled television picture is transmitted intermittently to reduce the required-data-link bandwidth. In this case the Z-transform approach is particularly appropriate.

Appendix A

DERIVATION OF LINE-OF-SIGHT ANGLES

The object of this appendix is to derive equations relating body rates about the principal axes to the rate of change of star angles observed in the vehicle-fixed coordinates defined by Fig. 3-2. Equation (A.1) states the assumption that the angular velocity of the line of sight (with respect to inertial space) to a distant star may be neglected.

$$\vec{\Omega}_{LOS} = \vec{\Omega}_V + \vec{\Omega}_{LV} = 0 \tag{A.1}$$

The angular velocity of the vehicle relative to inertial space and the angular velocity of the line of sight relative to the vehicle are given by Eqs. (A.2) and (A.3), respectively.

$$\vec{\Omega}_V = \omega_1 \vec{I}_1 + \omega_2 \vec{I}_2 + \omega_3 \vec{I}_3 \tag{A.2}$$

$$\vec{\Omega}_{LV} = (\dot{\rho} \cos\alpha \cos\epsilon - \dot{\epsilon} \sin\alpha) \vec{I}_1 + (\dot{\rho} \sin\alpha \cos\epsilon + \dot{\epsilon} \cos\alpha) \vec{I}_2 + (-\dot{\rho} \sin\epsilon + \dot{\alpha}) \vec{I}_3 \tag{A.3}$$

Equations (A.4) through (A.9) are obtained by solving the three scalar equations which result when Eqs. (A.2) and (A.3) are substituted into Eq. (A.1).

$$\omega_1 = -\dot{\rho} \cos\alpha \cos\epsilon + \dot{\epsilon} \sin\alpha \tag{A.4}$$

$$\omega_2 = -\dot{\epsilon} \cos\alpha - \dot{\rho} \sin\alpha \cos\epsilon \tag{A.5}$$

$$\omega_3 = -\dot{\alpha} + \dot{\rho} \sin\epsilon \tag{A.6}$$

$$\dot{\alpha} = - \omega_3 - (\omega_1 \cos \alpha + \omega_2 \sin \alpha) \tan \epsilon \tag{A.7}$$

$$\dot{\epsilon} = - \omega_2 \cos \alpha + \omega_1 \sin \alpha \tag{A.8}$$

$$\dot{\rho} = - \omega_1 \frac{\cos \alpha}{\cos \epsilon} - \omega_2 \frac{\sin \alpha}{\cos \epsilon} \tag{A.9}$$

Appendix B

COMPUTER WIRING DIAGRAM

The computer wiring diagram and Table B.1 have been included because they are the most complete and accurate description of the simulation studies which were performed.

Figure B-1 shows the way in which components of the reticle line are derived by resolving a triangular-pulse waveform. The cathode ray tube display of the reticle and two different stars is generated by multiplexing the appropriate variables with a two-pole electromechanical commutator; the details of the commutator and control stick connections are shown in Fig. B-2. Figures B-3, B-4, and B-5 show the way in which the controller outputs are processed to obtain vehicle body rates in the cases of proportional and on-off thrusters. The mechanization of Eqs. (3.40) and (3.41) for deriving the azimuth and elevation angles of two different stars is given by Fig. B-6.

Table B.1

Potentiometer Settings

Potentiometer Number	Control Action/Proportional		Control Action/On-Off		Quickening/Proportional		Rate Reticle/Proportional	
	Value	Setting	Value	Setting	Value	Setting	Value	Setting
00	*[a]	0.239	*	0.334	$3\,D_{11}/\pi\ 10$	0.239	$3\,D_{11}/\pi\ 10$	0.334
01	$K_{n1}/10\ \tau_1$	0.127	$K_{n1}/10\ \tau_1$	0.800	*	0.127	*	0.127
02	$(K_{n1} - 1)/10\ \tau_1$	0.114	$(K_{n1} - 1)/10\ \tau_1$	0.720	0	0.000	0	0.000
03	*	0.047	*	0.000	$D_{21}\ K_{m1}/10\ K_{c1}\ I_1$	0.047	0	0.000
04	*	0.320	$A_{o1} = -50\ M_{o1}/I_1 = -6$	0.320	*	0.320	*	0.320
05	$K_{n2}/10\ \tau_2$	0.159	$K_{n2}/10\ \tau_2$	0.800	*	0.159	*	0.159
06	$(K_{n2} - 1)/10\ \tau_2$	0.143	$(K_{n2} - 1)/10\ \tau_2$	0.720	0	0.000	0	0.000
07	*	0.090	*	0.000	$D_{22}\ K_{m2}/10\ K_{c2}\ I_2$	0.090	0	0.000
08	$K_{m2}/K_{c2}\ I_2$	0.800	*	0.160	$K_{m2}/K_{c2}\ I_2$	0.320	$K_{m2}/K_{c2}\ I_2$	0.160
09	–	–	–	–	–	–	–	–
10	$(K_{n3} - 1)/10\ \tau_3$	0.143	$(K_{n3} - 1)/10\ \tau_3$	0.720	0	0.000	0	0.000
11	*	0.090	*	0.000	$D_{23}\ K_{m3}/10\ I_3\ K_{c3}$	0.090	0	0.000
12	$K_{m3}/K_{c3}\ I_3$	0.800	*	0.160	$K_{m3}/K_{c3}\ I_3$	0.320	$K_{m3}/K_{c3}\ I_3$	0.160
13	*	0.100	$20\ K_{c2}\ \psi_{o2}$	0.100	*	0.100	*	0.100
14	$2\epsilon_1(0)$	0.800	$2\epsilon_1(0)$	0.800	$2\epsilon_1(0)$	0.800	$2\epsilon_1(0)$	0.800
15	$2\alpha_1(0)$	0.800	$2\alpha_1(0)$	0.800	$2\alpha_1(0)$	0.800	$2\alpha_1(0)$	0.800
16	$\pi\ K_{m1}/3\ I_1\ K_{c1}$	0.524	*	0.524	$\pi\ K_{m1}/3\ I_1\ K_{c1}$	0.140	$\pi\ K_{m1}/3\ I_1\ K_{c1}$	0.070
17	*	0.115	$30\ K_{c1}\ \psi_{o1}/\pi$	0.115	*	0.115	*	0.115
18	*	0.115	$30\ K_{c1}\ \psi_{o1}/\pi$	0.115	*	0.115	*	0.115
19	*	0.057	$A_{43} = +20\ M_{o2}/I_2 = +1.6$	0.057	*	0.057	*	0.057
20	$2\epsilon_2(0)$	1.000	$2\epsilon_2(0)$	1.000	$2\epsilon_2(0)$	1.000	$2\epsilon_2(0)$	1.000
21	$2\alpha_2(0)$	1.000	$2\alpha_2(0)$	1.000	$2\alpha_2(0)$	1.000	$2\alpha_2(0)$	1.000
22	*	0.200	*	0.250	$D_{12}/10$	0.200	$D_{12}/10$	0.250
23	$K_{n3}/10\ \tau_3$	0.159	$K_{n3}/10\ \tau_3$	0.800	*	0.159	*	0.159
24	*	0.057	$A_{43} = -20\ M_{o2}/I_2 = -1.6$	0.057	*	0.057	*	0.057
25	*	0.200	*	0.250	$D_{13}/10$	0.200	$D_{13}/10$	0.250
26	$0.273\ K_{c1}$	0.820	$0.273\ K_{c1}$	0.820	$0.273\ K_{c1}$	0.820	$0.273\ K_{c1}$	0.820
27	1/2	0.500	1/2	0.500	1/2	0.500	1/2	0.500
28	*	0.100	$20\ K_{c3}\ \psi_{o3}$	0.100	*	0.100	*	0.100
29	*	0.061	$A_{35} = -20\ M_{o3}/I_3 = -1.6$	0.061	*	0.061	*	0.061
30	Null A_{24}	0.004	Null A_{24}	0.004	Null A_{24}	0.004	Null A_{24}	0.004
31	Null A_{25}	0.009	Null A_{25}	0.009	Null A_{25}	0.009	Null A_{25}	0.009
32	Null A_{26}	0.007	Null A_{26}	0.007	Null A_{26}	0.007	Null A_{26}	0.007
33	$0.571\ K_{c2}$	0.714	$0.571\ K_{c2}$	0.714	$0.571\ K_{c2}$	0.714	$0.571\ K_{c2}$	0.714
34	*	0.320	$A_{o1} = +50\ M_{o1}/I_1 = 6$	0.320	*	0.320	*	0.320
35	$0.571\ K_{c3}$	0.714	$0.571\ K_{c3}$	0.714	$0.571\ K_{c3}$	0.714	$0.571\ K_{c3}$	0.714
36	*	0.200	1/5	0.200	*	0.200	*	0.200
37	*	0.100	$20\ K_{c3}\ \psi_{o3}$	0.100	*	0.100	*	0.100
38	*	0.100	$20\ K_{c2}\ \psi_{o2}$	0.100	*	0.100	*	0.100
39	*	0.060	$A_{35} = 20\ M_{o3}/I_3 = +1.6$	0.060	*	0.060	*	0.060

(a) * indicates potentiometer is not used in that particular case and may be set to any convenient value.

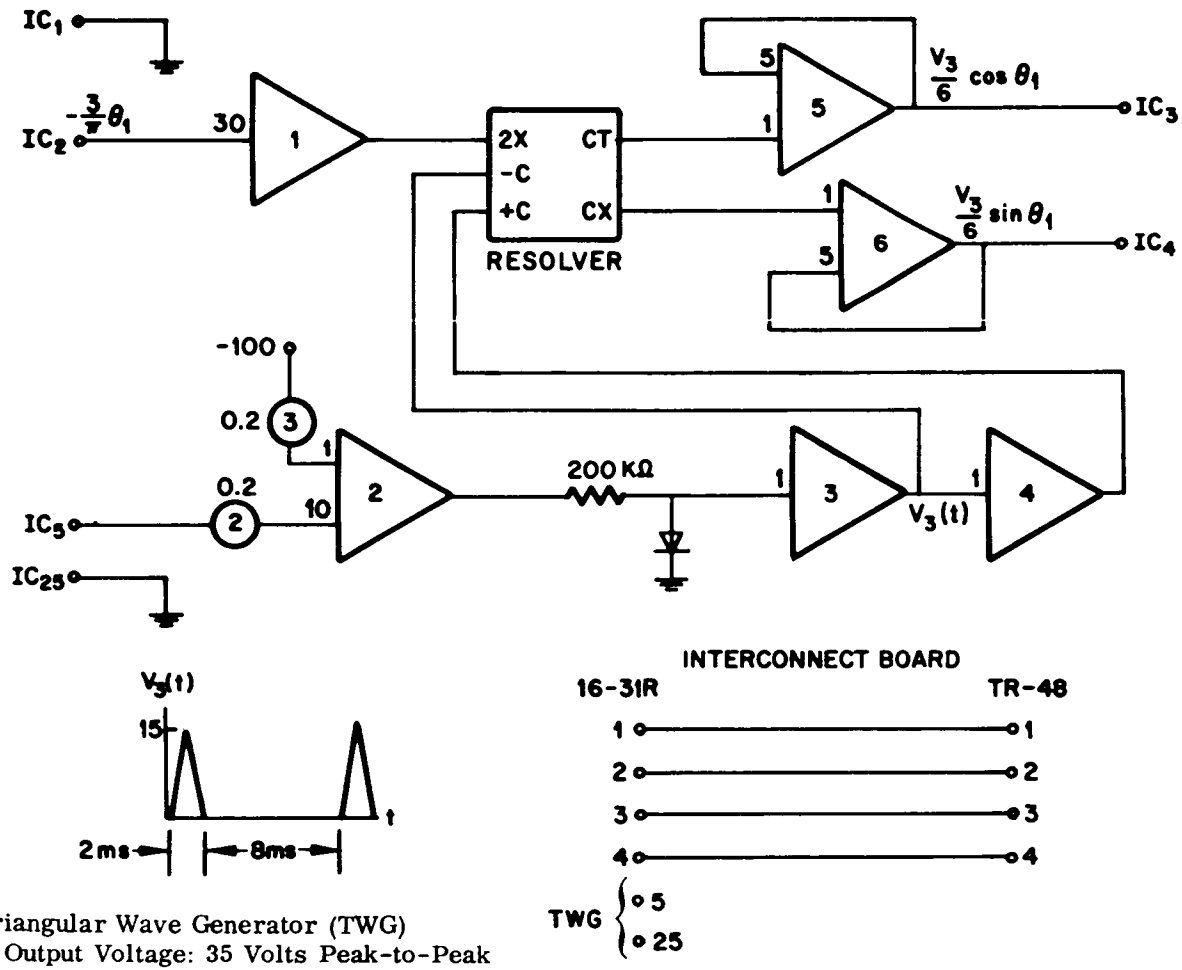

Triangular Wave Generator (TWG)
Output Voltage: 35 Volts Peak-to-Peak
Frequency: 100 cps

Fig. B-1 Generation of Radial Line for Reticle Display

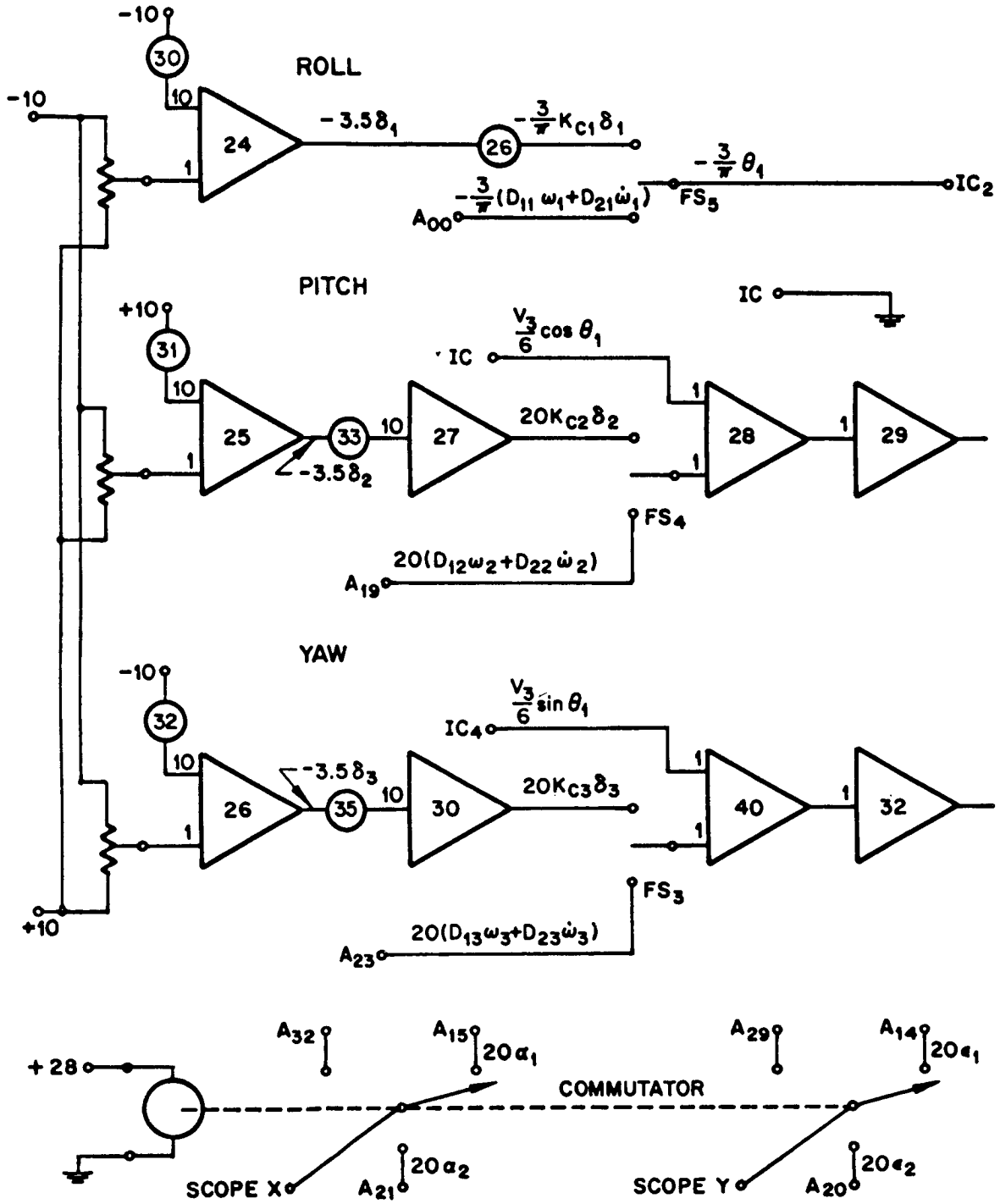

Fig. B-2 Controller and Display Sections

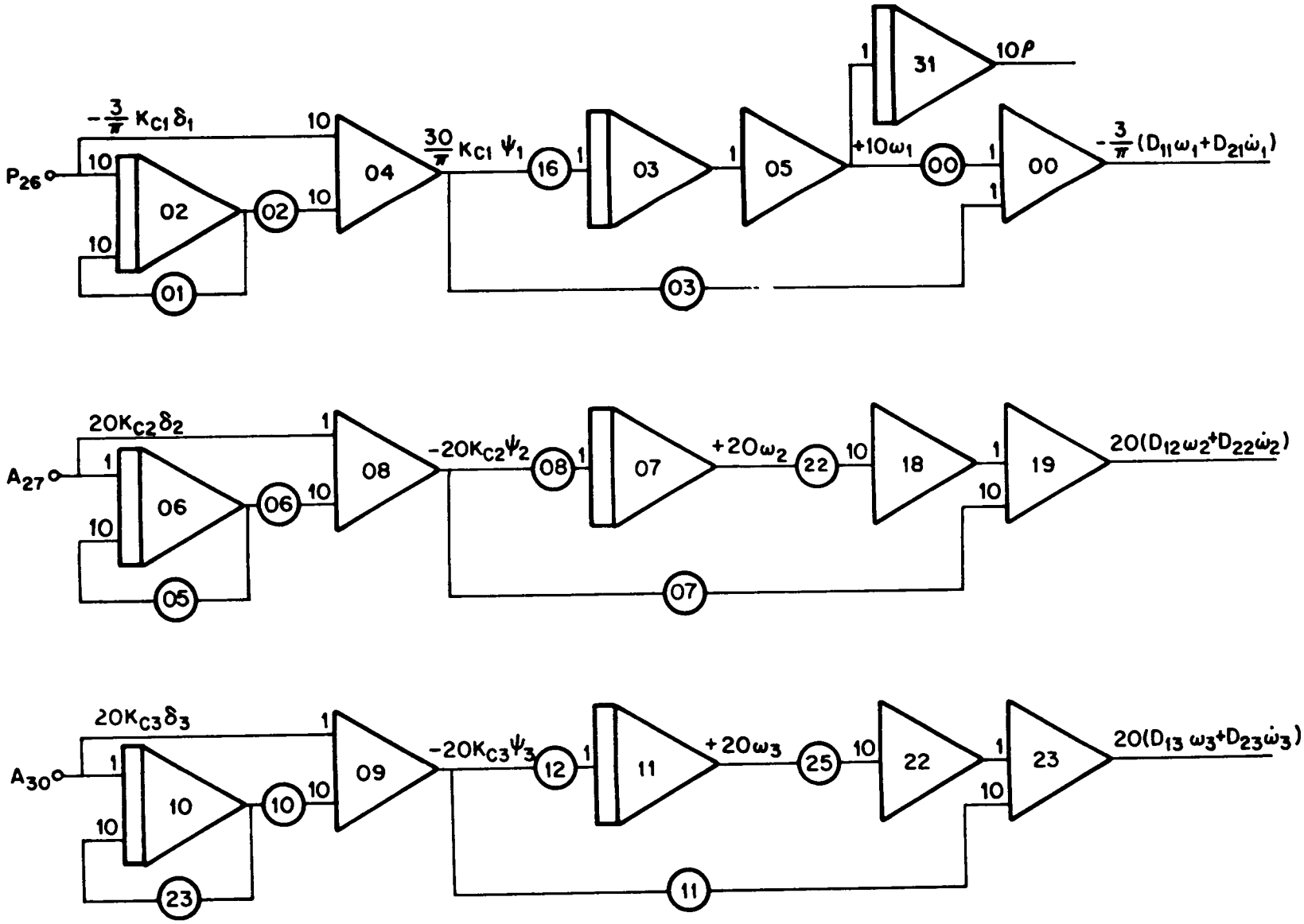

Fig. B-3 Body Rates for Proportional Control

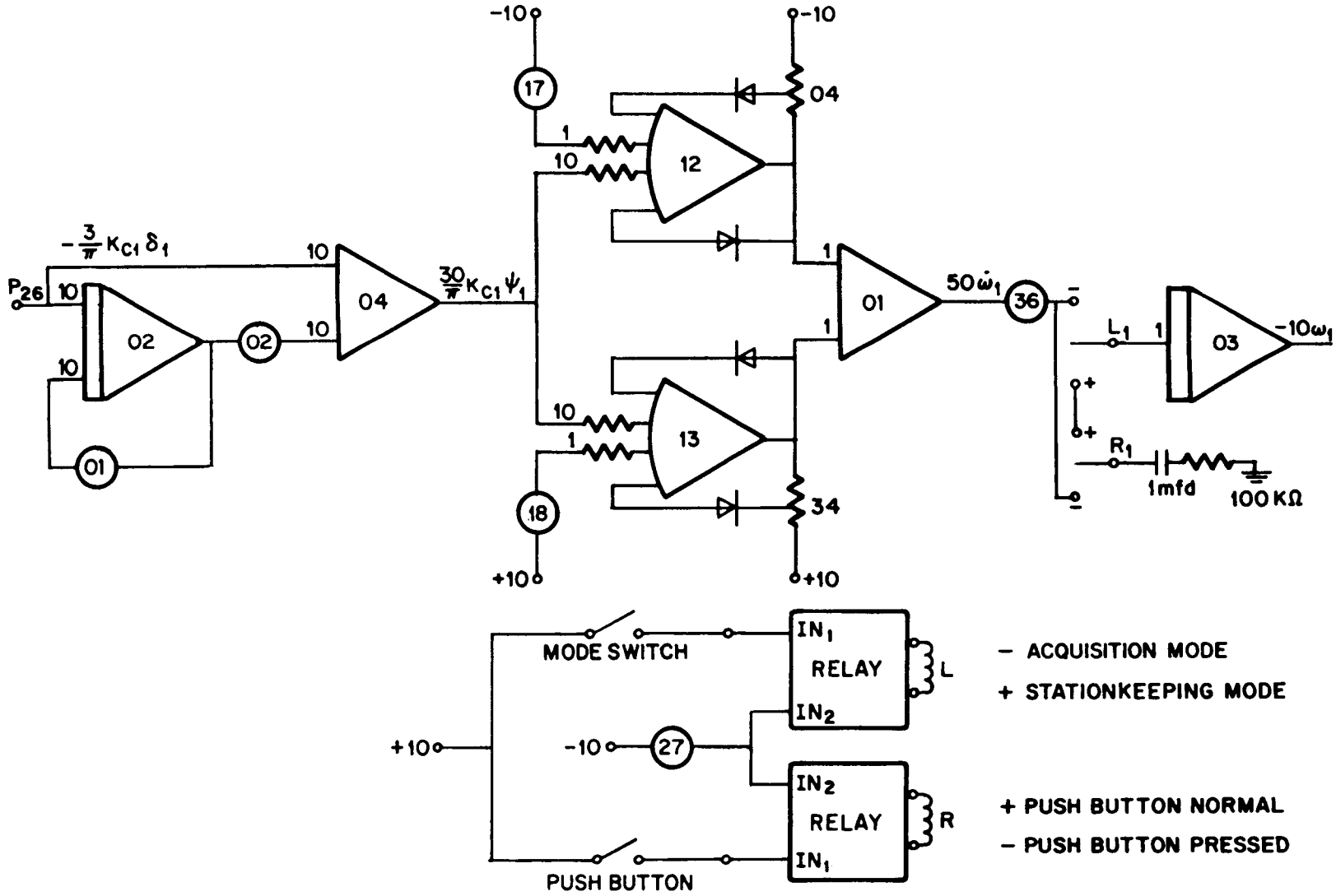

Fig. B-4 Roll Rate for On-Off Control

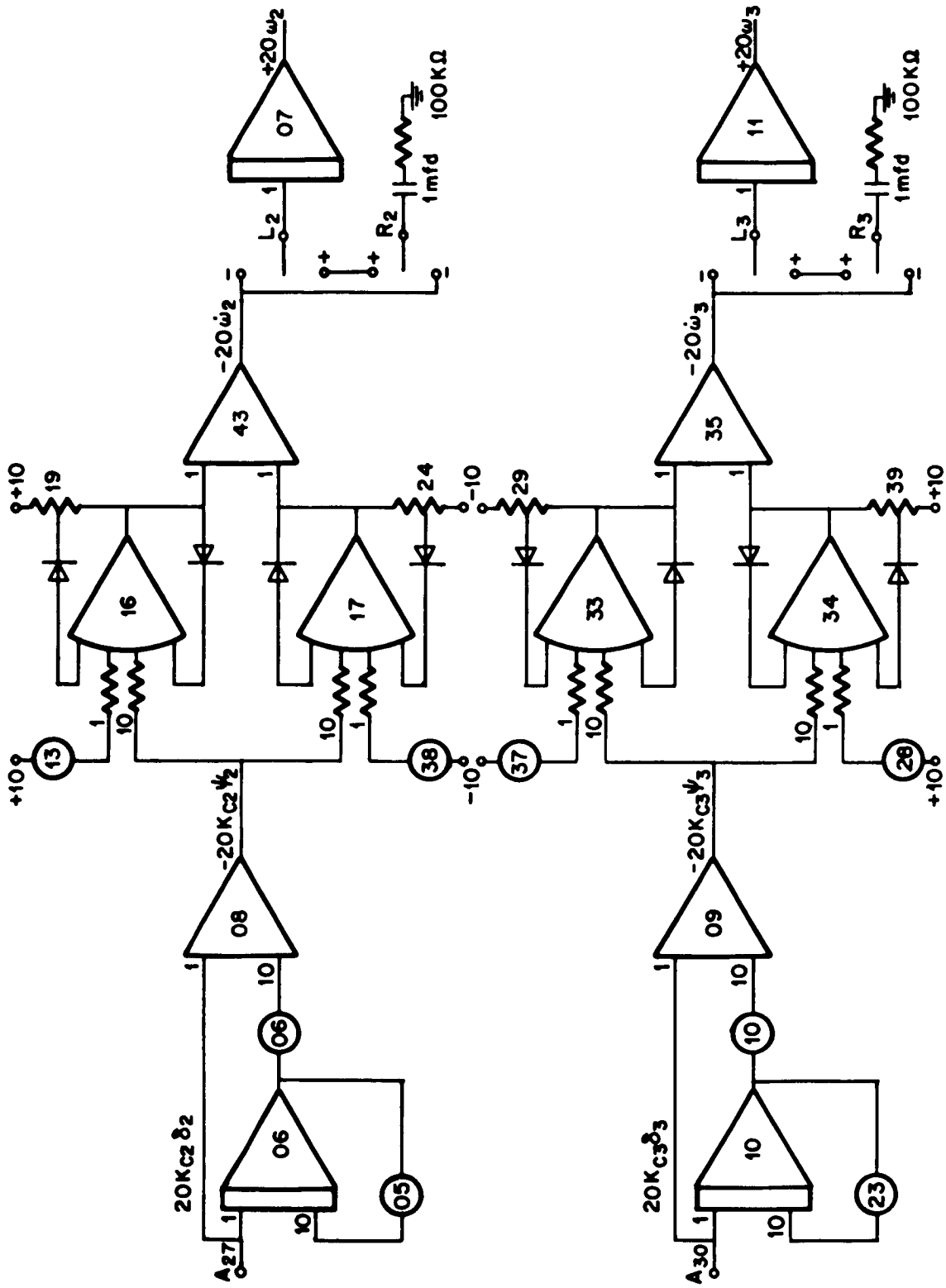

Fig. B-5 Yaw and Pitch Rates for On-Off Control

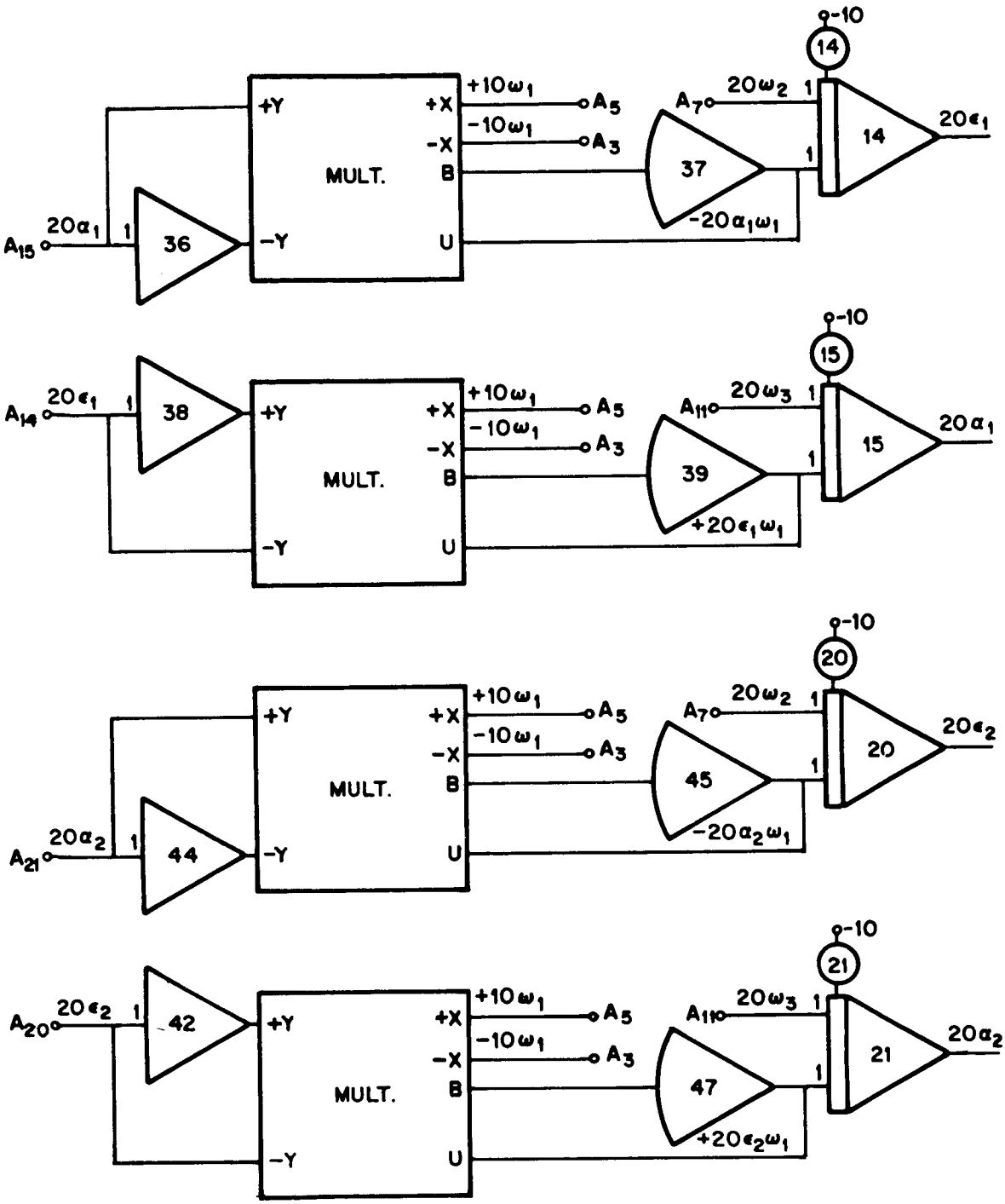

Fig. B-6 Computation of Azimuth and Elevation Angles

Appendix C

DERIVATION OF TIGHTROPE WALKER MODEL

C.1 Object

The purpose of this appendix is to derive the model used in Chapter 4 for describing the dynamic behavior of a tightrope walker. This treatment includes a derivation of the equations of motion of the plant and the specification of an appropriate display function.

C.2 Background

The model to be presented here was formulated after an interview* with Mr. Manfred Fritsch, a professional tightrope walker who performs for Ringling Bros. and Barnum & Baily Circus. Mr. Fritsch was highly articulate and very well versed in the theoretical aspects of his skill. The author is indebted to him for providing the background information cited in this section.

Tightrope walkers can be divided into two different categories, depending on whether or not they carry a balancing pole. Those who do not carry a pole maintain their balance by controlling the position of their center of mass (relative to the rope) with rapid arm movements and body bending. In some cases (e.g., when he is connected to and/or carries other performers) the tightrope walker is not allowed any bending motion; in this case he maintains equilibrium by moving a long, heavy balancing pole. This is the case treated here and in Chapter 4.

The length and weight of the balancing pole vary, depending on the magnitude of the disturbance torques which must be accommodated

---

*This interview, held in San Francisco, California on August 29, 1964, was made possible by the generous cooperation of Mr. Henry Ringling North.

(i.e., the size of the tightrope walker and the number of persons he must support). Typically, the balancing pole may be 20 ft long and weigh between 25 and 50 pounds; often the weight is concentrated near the ends to increase the moment of inertia.

The motion used by the tightrope walker to maintain his equilibrium is a combination rotation and translation of the balancing pole. Although Mr. Fritsch could not explicitly define this motion (i.e., write a control law), he was able to provide certain qualitative information that was useful in formulating the model. He indicated that large angular displacement of the pole is considered bad form; it is clear that rotations of $\pm 90°$ are not allowed. While performing outdoors he observed that the translation of the balancing pole closely followed wind gusts indicating that this translation is used to compensate for transient torque disturbances.

It is well known (for example, see Ref. 55) that the vestibular canals of the inner ear are a primary source of feedback used to maintain postural orientation. Mr. Fritsch indicated that this feedback is particularly important in tightrope walking, and cited the case of a friend who could not perform because of an infection of the inner ear.

Visual data is another indispensible source of orientation feedback; according to Mr. Fritsch, a tightrope walker cannot maintain his balance in total darkness. This is interpreted to mean that the necessary position data cannot be derived with sufficient accuracy (i.e., free of accumulated drift) by double integration of acceleration feedback from the vestibular canals. Visual data is more important for tightrope walking than for normal postural control (e.g., a normal person has no difficulty standing with his eyes closed for extended periods of time) because the tightrope walker cannot obtain position information by the normally available proprioceptive and tactile feedback.

According to Mr. Fritsch, considerable practice and expert coaching are necessary to learn to walk on a tightrope. For example, he indicated that this skill was several times more difficult to acquire than that of riding a bicycle. In view of this fact, the results (see Fig. 4-6) achieved by complete novices using Control Action Display are especially significant.

C.3 Equations of Motion

The information cited in the preceding section provides the basis for deriving the equations of motion. In particular, the tightrope walker is assumed to translate and rotate the balancing pole while keeping his body (except for arms) absolutely rigid. The desired equations of motion express the angular rotation of the body (output variable) as a function of the balancing pole translation and rotation (control variables).

Figure C-1b shows a simplified model of the actual situation represented by Fig. C-1a. The tightrope walker, regarded as a composite of arms and armless-body, and the balancing pole, move in a common plane perpendicular to the rope through the fixed point O. The two arms have been combined into a single equivalent arm attached to the torso at shoulder height.

Formulating the necessary equations of motion is quite straightforward,* and involves simply equating the time derivative of the total angular momentum of the system about the fixed point O to the sum of external moments about that point (Ref. 56). Let $\vec{i}$, $\vec{j}$, $\vec{k}$ be unit vectors directed horizontally to the tightrope walker's left, vertically upward and along the wire in the direction faced by the tightrope walker, respectively. The position vectors from the fixed point O to the center of mass of the armless-body, the equivalent arm and the balancing pole are $\vec{r}_1$, $\vec{r}_2$, and $\vec{r}_3$, respectively.

$$\vec{r}_1 = (\ell_1 \sin\alpha)\vec{i} + (\ell_1 \cos\alpha)\vec{j}$$

$$\vec{r}_2 = (\ell_3 \sin\alpha - \ell_2 \sin\theta)\vec{i} + (\ell_3 \cos\alpha - \ell_2 \cos\theta)\vec{j} \qquad \text{(C.1)}$$

$$\vec{r}_3 = (\ell_3 \sin\alpha - \ell_4 \sin\theta)\vec{i} + (\ell_3 \cos\alpha - \ell_4 \cos\theta)\vec{j}$$

*An alternate approach using Lagrange's equations was also considered. This formulation leads to three equations (one for each of the three generalized coordinates α, θ and ρ) which must be combined to eliminate the generalized torques which are of no interest. Because this approach is computationally tedious and does not provide any additional insight it was not selected for this presentation.

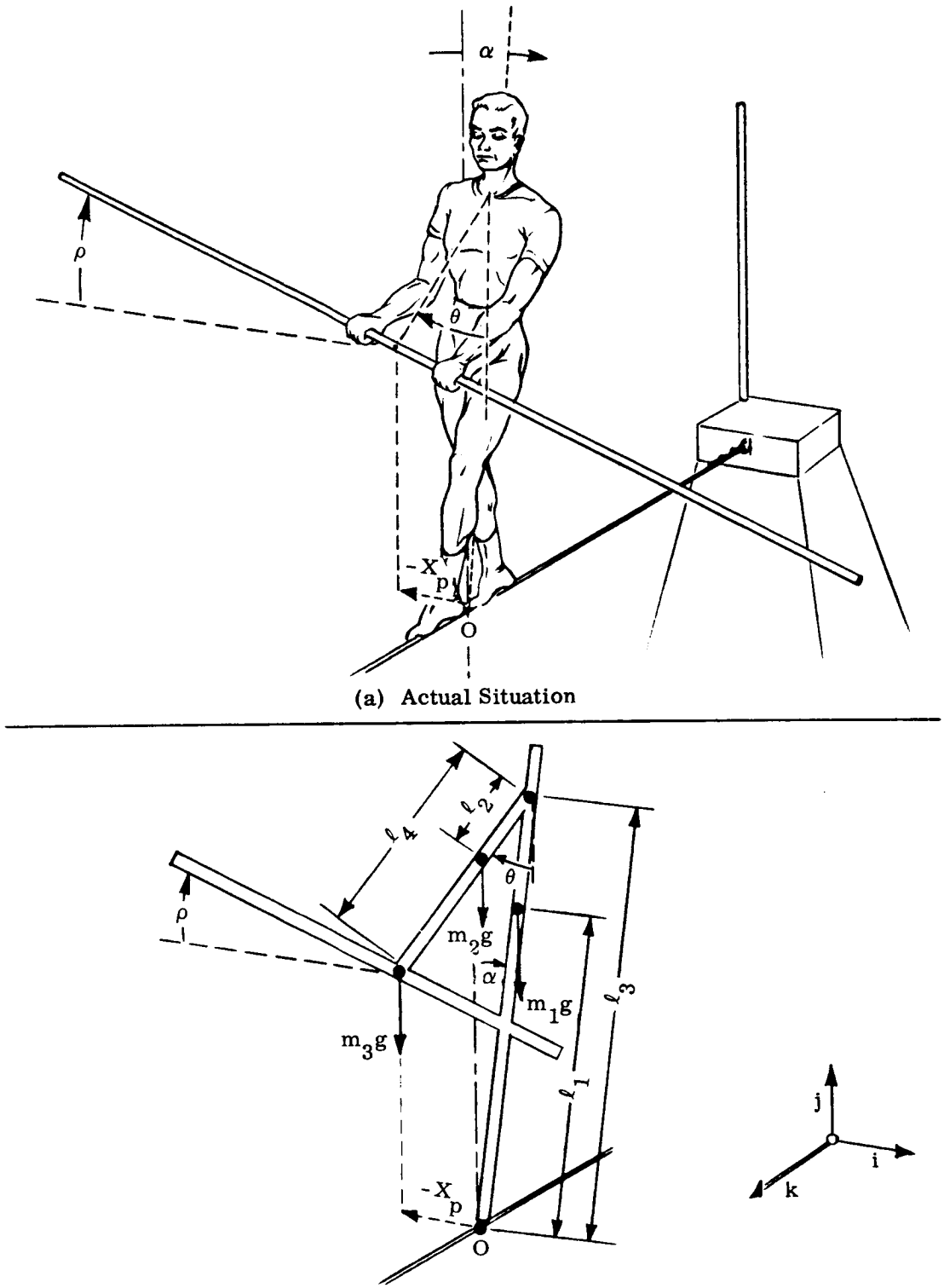

Fig. C-1 Representation of Tightrope Walker Used in Deriving Equations of Motion

The total angular momentum of the system about the fixed point O is given by

$$\vec{H}_o = m_1\vec{r}_1 \times \dot{\vec{r}}_1 + m_2\vec{r}_2 \times \dot{\vec{r}}_2 + m_3\vec{r}_3 \times \dot{\vec{r}}_3 - (I_1\dot{\alpha} + I_2\dot{\theta} + I_3\dot{\rho})\vec{k} \qquad (C.2)$$

The sum of external moments about the fixed point O is given by

$$\vec{M}_o = \vec{r}_1 \times (-m_1 g)\vec{j} + \vec{r}_2 \times (-m_2 g)\vec{j} + \vec{r}_3 \times (-m_3 g)\vec{j} \qquad (C.3)$$

Equating the time derivative of the total angular momentum to the sum of external moments about O gives

$$\dot{\vec{H}}_o = \vec{M}_o \qquad (C.4)$$

Substituting Eqs. C.1, 2 and 3 into C.4 directly yields the desired equation of motion

$$\begin{aligned}
&\{I_1 + m_1\ell_1^2 + [m_2 + m_3]\ell_3^2 - [m_2\ell_2 + m_3\ell_4]\ell_3 \cos(\alpha - \theta)\}\ddot{\alpha} \\
&+ \{[m_2\ell_2 + m_3\ell_4]\ell_3 \sin(\alpha - \theta)\}\dot{\alpha}^2 - \{g[m_1\ell_1 + (m_2 + m_3)\ell_3]\} \sin\alpha \\
&+ \{I_2 + m_2\ell_2^2 + m_3\ell_4^2 - [m_2\ell_2 + m_3\ell_4]\ell_3 \cos(\alpha - \theta)\}\ddot{\theta} \\
&- \{[m_2\ell_2 + m_3\ell_4]\ell_3 \sin(\alpha - \theta)\}\dot{\theta}^2 + \{g[m_2\ell_2 + m_3\ell_4]\}\sin\theta + I_3\rho = 0
\end{aligned} \qquad (C.5)$$

Equation C.5 can be further simplified by the usual small-angle approximations

$$\begin{aligned}
&\{I_1 + m_1\ell_1^2 + m_2\ell_3(\ell_3 - \ell_2) + m_3\ell_3(\ell_3 - \ell_4)\}\ddot{\alpha} - \{g[m_1\ell_1 + (m_2 + m_3)\ell_3]\}\alpha \\
&+ \{I_2 + m_2\ell_2(\ell_2 - \ell_3) + m_3\ell_4(\ell_4 - \ell_3)\}\ddot{\theta} \\
&+ \{g[m_2\ell_2 + m_3\ell_4]\}\theta + I_3\ddot{\rho} \approx 0
\end{aligned} \qquad (C.6)$$

Equation C.6 defines the given plant, because it expresses the output variable α in terms of the two control variables θ and ρ; i.e., the tightrope walker maintains his orientation by translating and rotating the balancing pole to compensate for non-zero initial conditions and for disturbance torques.

C.4 Investigation of Various Forms of Control Action

The object of this section is to derive a control law which will stabilize the given plant described by Eq. C.6. This will be a specification of the control action which the tightrope walker should apply in any given condition. This specification is an expression giving θ and ρ as functions of α.

Typical values for the system parameters are

$$\begin{array}{lll} m_1 = 6.0 \text{ slug} & \ell_1 = 3.25 \text{ ft} & I_1 = 18.0 \text{ slug-ft}^2 \\ m_2 = 0.5 \text{ slug} & \ell_2 = 0.75 \text{ ft} & I_2 = 0.2 \text{ slug-ft}^2 \\ m_3 = 1.0 \text{ slug} & \ell_3 = 5.0 \text{ ft} & I_3 = 16.6 \text{ slug-ft}^2 \\ & \ell_4 = 2.0 \text{ ft} & \end{array} \qquad \text{(C.7)}$$

Substituting these values into Eq. C.6 gives (for small angles)

$$107\,\ddot{\alpha} - 870\,\alpha - 7.4\,\ddot{\theta} + 76.5\,\theta + 16.6\,\ddot{\rho} = 0 \qquad \text{(C.8)}$$

One type of control action which might be considered is to keep the arms fixed relative to the body (i.e., $\theta = \alpha$) and simply rotate the balancing pole to maintain equilibrium; the equation of motion for this case is:

$$\ddot{\alpha} - 7.94\,\alpha + 0.166\,\ddot{\rho} = 0 \qquad \text{(C.9)}$$

It can be seen from Eq. C.9 that a stable second-order system results if the balancing pole is rotated so that

$$\ddot{\rho} = \frac{1}{0.166}\left[2\xi\omega_n\dot{\alpha} + (\omega_n^2 + 7.94)\alpha\right] \qquad (C.10)$$

In terms of the root-locus analysis shown in Fig. C-2, the transfer function of the plant is given by

$$\frac{\alpha(s)}{\rho(s)} = \frac{-0.166s^2}{(s + 2.82)(s - 2.82)} \qquad (C.11)$$

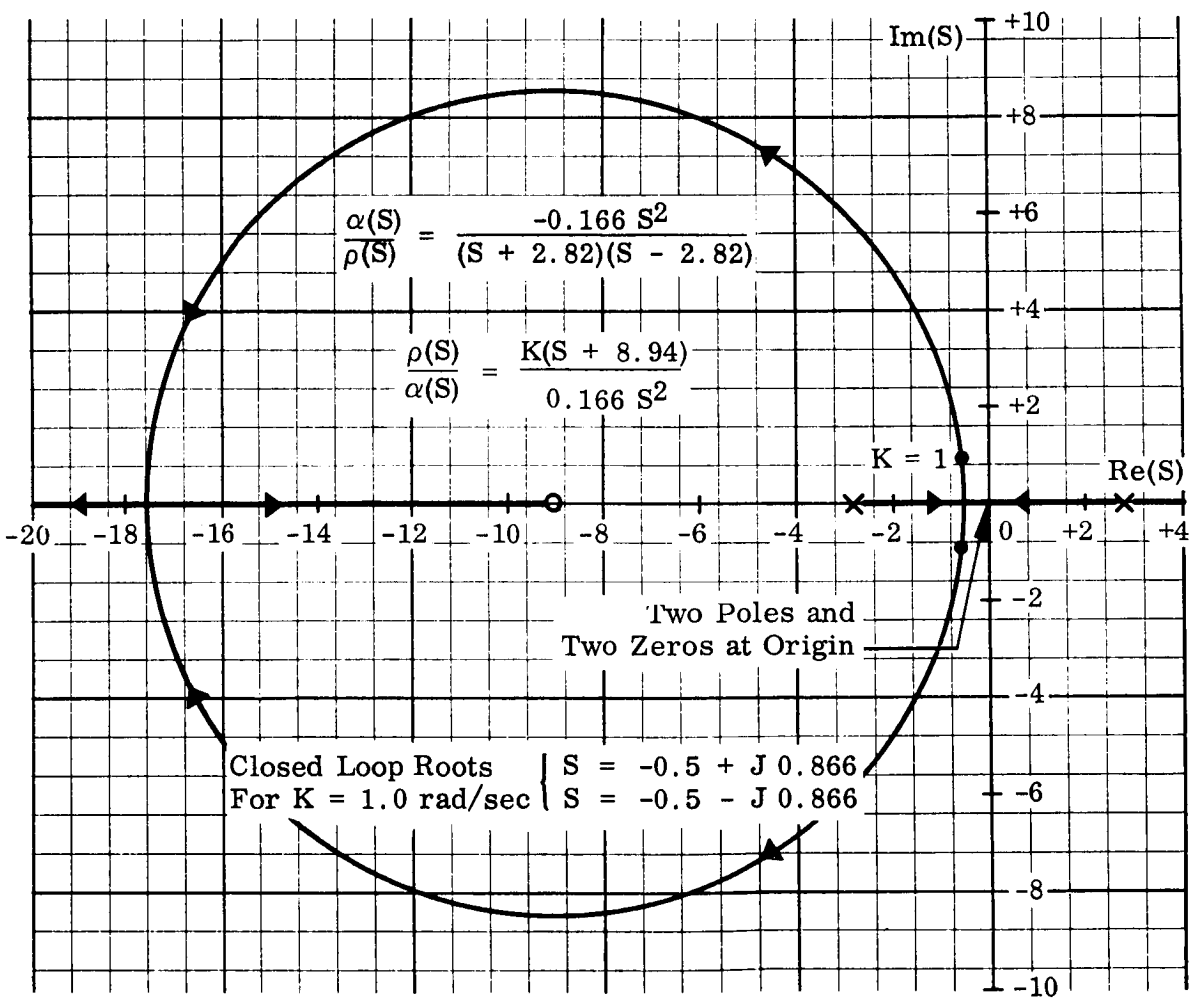

Fig. C-2 Root-Locus Analysis for Case $\theta = \alpha$

For typical operating values ($\zeta = 0.5$, $\omega_n = 1.0$ rad/sec), the control law is given by

$$\frac{\rho(s)}{\alpha(s)} = \frac{K(s + 8.94)}{0.166s^2} \qquad (C.12)$$

where K is unity as shown in Fig. C-2. On the basis of Fig. C-2 it appears that Eq. C.12 is an appropriate control law. However it can be shown by solving Eqs. C.9 and C.10 that a steady-state angular velocity of the balancing pole is required to compensate for non-zero initial conditions; for $\zeta = 0.5$ and $\omega_n = 1.0$ rad/sec the steady-state angular velocity is

$$\dot{\rho}(\infty) = 54[\dot{\alpha}(0) + \alpha(0)] \qquad (C.13)$$

It is clear that the initial angular momentum and the integral of gravity torques (during the time that the system is out of balance) are transferred to the balancing pole. Because the balancing pole cannot be rotated more than $\pm$ 90° the control law given by Eq. C.12 is unacceptable; i.e., the tightrope walker cannot stabilize himself by (only) rotating the balancing pole.

Another type of control action to be considered is a combination of rotation and translation of the balancing pole; according to Mr. Fritsch, this is the kind of motion employed by tightrope walkers who cannot use body bending to maintain their balance. In order to simplify the control action required of the subjects, this motion was reduced to a single dimension by imposing the constraint

$$\rho = \theta \qquad (C.14)$$

According to Eq. C.14 and the simplified model shown in Fig. C-1b, the tightrope walker rotates the poles with respect to inertial space to keep it always perpendicular to his (equivalent) arms as he translates the center of mass from side to side.

The transfer function of the plant, derived by combining Eqs. C.8 and C.14 is given by

$$\frac{\alpha(s)}{\theta(s)} = -\frac{9.2}{107}\ \frac{(s + j2.88)(s - j2.88)}{(s + 2.85)(s - 2.85)} \qquad (C.15)$$

From the root-locus diagram of Fig. C-3 it is clear that there is no difficulty moving the unstable root into the left-half plane. Use of the control law given by

$$\frac{\theta(s)}{\alpha(s)} = K\ \frac{107}{9.2}\ \frac{(s + 2.0)}{(s + 10.0)} \qquad (C.16)$$

and analyzed in Fig. C-3 results in a well-damped system and does not require that the balancing pole have a steady-state angular velocity to compensate for non-zero initial conditions.

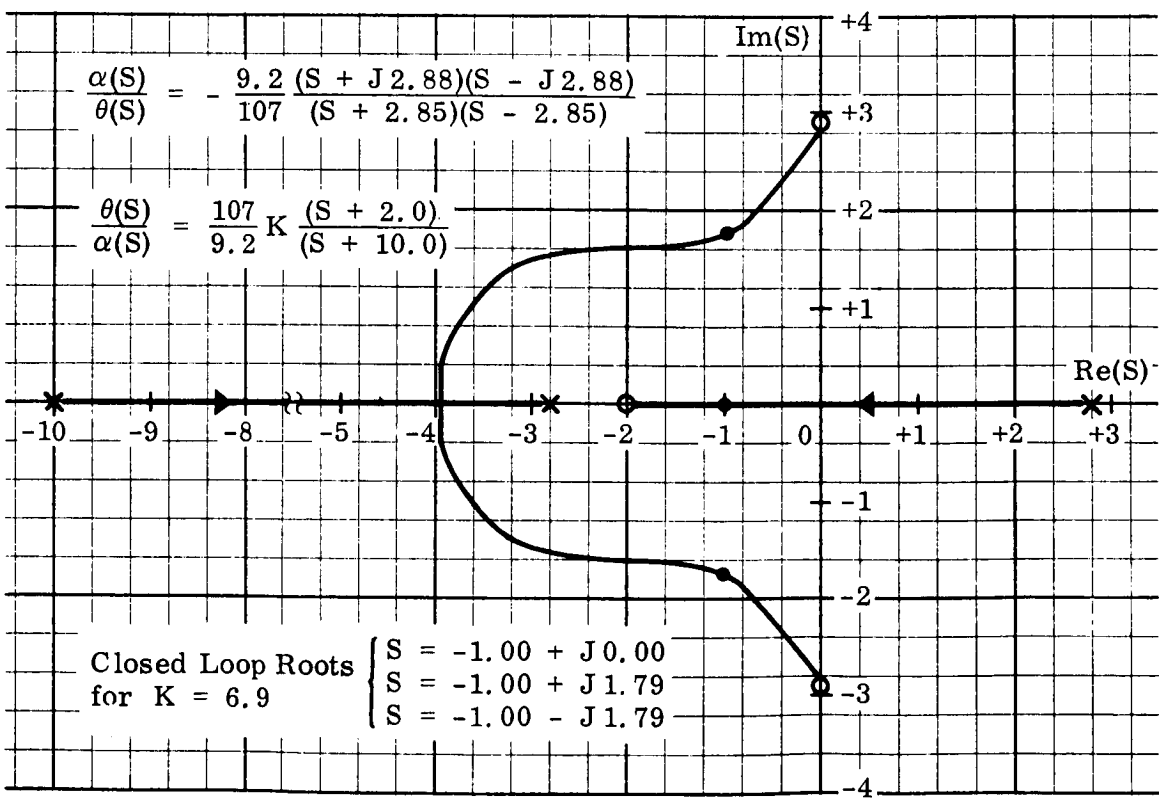

Fig. C-3 Root-Locus Analysis for Case $\rho = \theta$

C.5 Model and Control Law Used in Chapter 4

Although the control law expressed by Eq. C.16 causes the system to exhibit an acceptable dynamic response, it is not in a form which is well-suited for Control Action Display. In particular, the subject cannot directly observe the angle θ. For this reason, the one-dimensional command is displayed as the linear horizontal displacement of the center of mass of the balancing pole. This quantity is designated x_p in Fig. C-1b and (for small angles) is approximated by

$$x_p = \ell_3\alpha - \ell_4\theta \tag{C.17}$$

Substituting Eqs. C.6 and C.14 into Eq. C.17 gives the transfer function of the plant in terms of the new one dimensional control variable. In the notation of Chapter 4

$$\frac{\alpha(s)}{X_p(s)} = \frac{K_p(s + jZ_2)(s - jZ_2)}{(s + P_3)(s - P_3)} \tag{C.18}$$

where

$$K_p = \frac{[I_2 + I_3 - m_2\ell_2(\ell_3 - \ell_2) - m_3\ell_4(\ell_3 - \ell_4)]}{[\ell_4(I_1 + m_1\ell_1^2) + \ell_3(I_2 + I_3) + m_2\ell_3(\ell_3 - \ell_2)(\ell_4 - \ell_2)]}$$

$$Z_2 = \left\{ \frac{[g(m_2\ell_2 + m_3\ell_4)]}{[I_2 + I_3 - m_2\ell_2(\ell_3 - \ell_2) - m_3\ell_4(\ell_3 - \ell_4)]} \right\}^{1/2}$$

$$P_3 = \left\{ \frac{g[m_1\ell_1\ell_4 + m_2\ell_3(\ell_4 - \ell_2)]}{[\ell_4(I_1 + m_1\ell_1^2) + \ell_3(I_2 + I_3) + m_2\ell_3(\ell_3 - \ell_2)(\ell_4 - \ell_2)]} \right\}^{1/2}$$

Typical values for these parameters are obtained by substituting the constants of Eq. C.7 into Eq. C.18.

$$K_p = 3.54 \times 10^{-2} \text{ rad/ft}; \qquad Z_2 = 2.88 \text{ rad/sec};$$
$$P_3 = 2.28 \text{ rad/sec} \tag{C.19}$$

An appropriate control law can be expressed in terms of the readily observable, one-dimensional variable x_p; in the notation of Chapter 4

$$\frac{X_p(s)}{\alpha(s)} = -\frac{K_c \omega_f (s + \omega_c)}{\omega_c (s + \omega_f)} \tag{C.20}$$

For $K = 6.9$ (and for the particular values of Eq. C.7) the control law given in Eq. C.16 can be expressed in the form of Eq. C. 20 where

$$K_c = 27 \text{ ft/rad} = 5.6 \text{ in./deg}; \qquad \omega_c = 1.74 \text{ rad/sec};$$
$$\omega_f = 10.0 \text{ rad/sec} \tag{C.21}$$

In summary Eq. C.18 gives the tightrope walker's transfer function and Eq. C.20 gives an acceptable control law subject to two assumptions:

1) The tightrope walker keeps his body (except for arms) perfectly rigid
2) The control motion he uses is a combination of translation and rotation of the balancing pole, with the constraint (given by Eq. C.14) that the pole is kept perpendicular to his (equivalent) arms.

The plant and control law are expressed in terms of a readily observable, one-dimensional control variable. They were formulated using information provided by a professional tightrope walker and are the basis for the experimental work described in Chapter 4.

Appendix D

MEASUREMENT METHOD—SECTION 5.2

D.1 Objective

The purpose of this appendix is to describe the instrumentation used to make the measurements reported in Section 5.2. For the tracking studies a one-dimensional pursuit situation using a unity-gain plant was employed. The target was a moving light spot which the subject tracked with a pole suspended as shown in Fig. 5-2. Figure D-1 shows the equipment used to generate the moving target and to measure several of the subject's reactions to it. Also shown is the instrumentation used to determine latency between EMG and resulting force.

D.2 Description of the Instrumentation

All of the extended tracking tests reported in Section 5.2 were performed using the input program given in Table D.1. The target moved in a series of 48 discrete steps among 7 different positions. The program was arranged so that two steps of $\pm$ 2, $\pm$ 4, $\pm$ 6, and $\pm$ 8 inches occurred after preparation times of 0.6, 1.0 and 1.4 seconds. The preparation time for a given step is the time the target remained stationary prior to that jump.

The input program was recorded on a seven-track punched-paper tape to insure that identical target motion was presented to all subjects. The output of the punched-paper tape reader was converted into the appropriate analog voltage by a simple digital-to-analog converter. Because a separate channel was devoted to each target position it was possible to compensate for nonlinearities in the geometry (caused by projecting onto a plane rather than circular screen) and nonlinearities in the galvanometer movement. This was accomplished by adjusting the output voltage for each channel to produce exactly the desired target

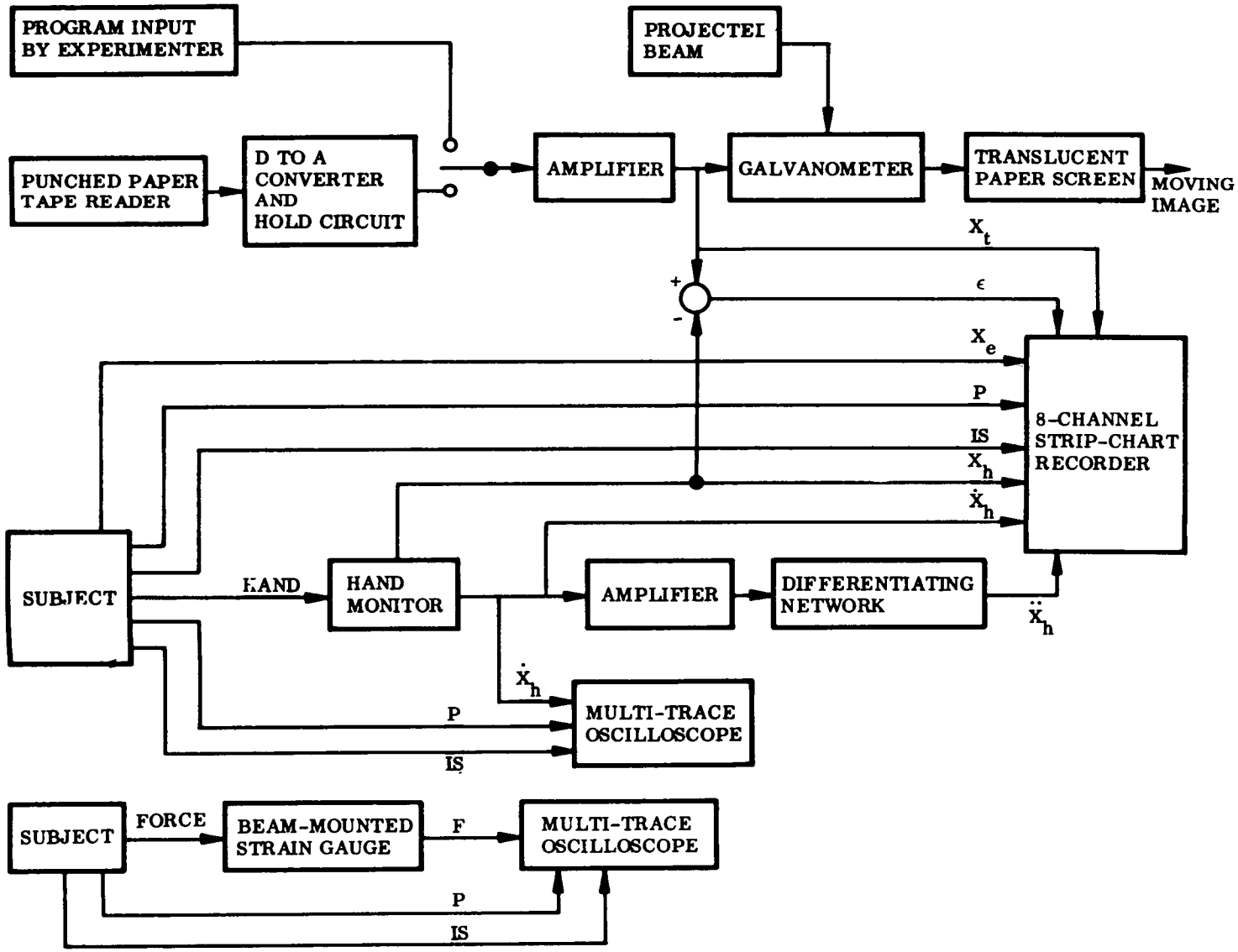

Fig. D-1 Equipment Used for Measurements Reported in Section 5.2

position. The positions designated by Table D.1 were 2 in. apart with position No. 4 located at the neutral (i.e., vertical) position of the Hand Monitor.

Table D.1

Input Program Used for Tracking Studies

Step Number	Preparation Time(sec)	Step Size(in)	Position Initial	Position Final	Step Number	Preparation Time(sec)	Step Size(in)	Position Initial	Position Final
1 & 25	0.6	-4	4	2	13 & 37	0.6	+4	4	6
2 & 26	1.4	+6	2	5	14 & 38	1.4	-6	6	3
3 & 27	0.6	-8	5	1	15 & 39	0.6	+8	3	7
4 & 28	1.4	+4	1	3	16 & 40	1.4	-4	7	5
5 & 29	1.0	+2	3	4	17 & 41	1.0	-2	5	4
6 & 30	0.6	-6	4	1	18 & 42	0.6	+6	4	7
7 & 31	1.0	+4	1	3	19 & 43	1.0	-4	7	5
8 & 32	1.4	+8	3	7	20 & 44	1.4	-8	5	1
9 & 33	0.6	-2	7	6	21 & 45	0.6	+2	1	2
10 & 34	1.4	-2	6	5	22 & 46	1.4	+2	2	3
11 & 35	1.0	-8	5	1	23 & 47	1.0	+8	3	7
12 & 36	1.0	+6	1	4	24 & 48	1.0	-6	7	4

The digital-to-analog converter also included a Hold circuit which maintained the desired voltage on the galvanometer while the punched-paper tape was advanced. Without this circuit the light spot would have alternated between the desired position and a position off the screen at a rate of 10 times/sec.

In addition to the 48 second tracking runs, tests were also conducted using single, isolated step inputs of target motion; for example, see Fig. 5-4. These inputs were programmed by the experimenter who could select step displacements of $\pm$ 1.5, $\pm$ 3.0, $\pm$ 4.5 and $\pm$ 6.0 in.

The voltage from one of the two program sources drove the galvanometer through an isolation amplifier. The galvanometer was constructed by mounting a small mirror on a penmotor taken from a strip-chart recorder. Despite the inertia added by the mirror, the frequency response of the penmotor/mirror combination was flat to approximately 20 cycles/sec and the effect of its dynamics on these measurements is considered to be negligible. The projected beam of light deflected by the mirror was sharply focused into an intense, 1/4-in. diameter spot on a translucent screen approximately 18 in. from the subject.

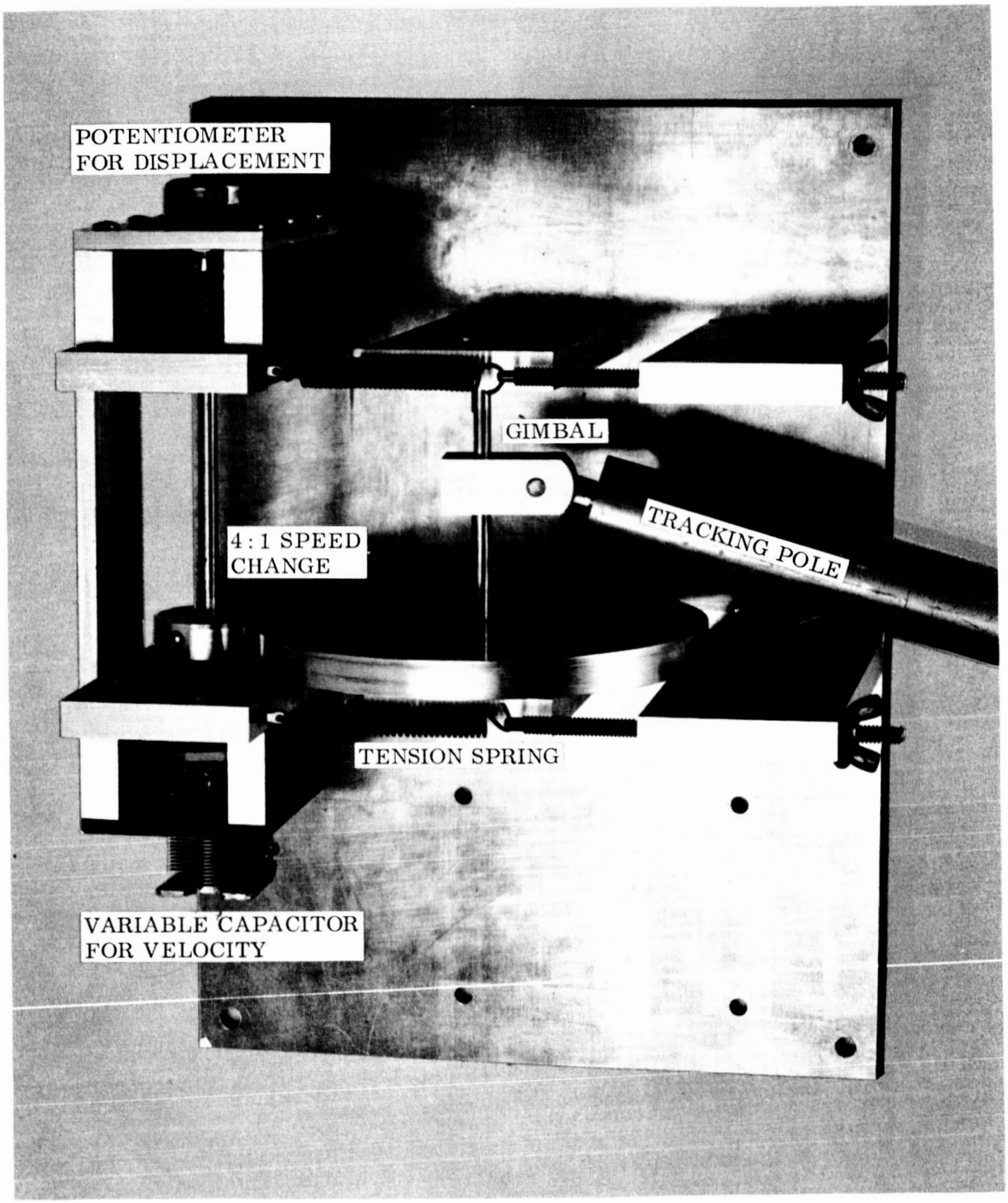

Fig. D-2 Photograph of Hand Monitor

The position and velocity of the subject's hand were measured by the Hand Monitor shown in Fig. D-2. The subject tracked the target by placing the tracking pole over the moving spot of light as shown in Fig. 5-2. The pole was suspended from an axle which turned a potentiometer and a variable capacitor through gear ratio of 4:1.

The potentiometer measured displacement and the variable capacitor measured velocity directly (i.e., without recourse to differentiating the potentiometer voltage) in a way which can be explained by referring to Fig. D-3 and Eq. (D.1).

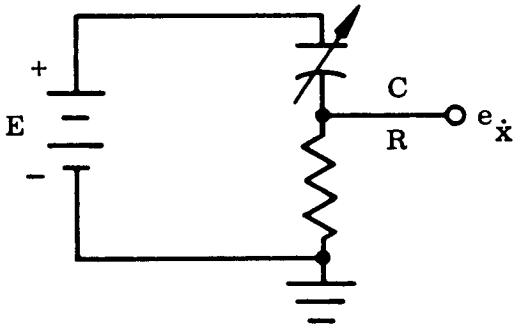

E = 67.5 volts

R = 1×10^{6} ohms

C = 0 to 365×10^{-12} farads

Fig. D-3 Schematic Diagram of Velocity Measuring Circuit

$$e_{\dot{x}} = R \frac{dq}{dt} = R \frac{d}{dt} [C(E - e_{\dot{x}})] \qquad (D.1)$$

In order to obtain an accurate model of the velocity measuring circuit Eq. (D.1) is solved for the conditions given by Eq. (D.2). The exact solution is displayed in Eq. (D.3)

$$C = C_o + \dot{C}t \ , \qquad e_{\dot{x}}(0) = 0 \qquad (D.2)$$

$$e_{\dot{x}}(t) = \frac{ER\dot{C}}{1 + R\dot{C}} \left[1 - \left(1 + \frac{\dot{C}}{C_o} t \right)^{-(1+R\dot{C})/R\dot{C}} \right] \qquad (D.3)$$

This equation can be simplified to Eq. (D.5) by using the relationship

(Ref. 57) given in Eq. (D.4).

$$\lim_{R\dot{C} \to 0} \left\{ \left(1 + \frac{R\dot{C}t}{RC_o} \right)^{-(1+R\dot{C})/R\dot{C}} \right\} = e^{-t/RC_o} \quad \text{for all} \quad R,\ C_o \quad \text{and} \quad t \qquad (D.4)$$

$$\lim_{R\dot{C} \to 0} \quad e_{\dot{x}}(t) = ER\dot{C}\left(1 - e^{-t/RC_o} \right) \qquad (D.5)$$

For the capacitor used here, C was a linear function of rotation so that the value of $\dot{C}$ is related to hand velocity according to Eq. (D.6)

$$\dot{C} \approx 4 \frac{C_{max}}{\pi} \frac{\dot{X}_h}{L} \qquad (D.6)$$

Equations (D.5) and (D.6) show that the operation of the velocity measuring circuit can be described by the equivalent circuit model given in Fig. D-4. For the component values chosen, the velocity-measuring circuit had a time constant of less than 0.4 msec and a sensitivity of 1.4×10^{-3} V-sec/in. Results of tests conducted to calibrate the Hand Monitor sensitivity were in good agreement with the computed value.

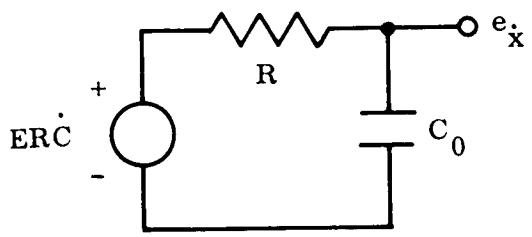

$$RC_o < 0.4 \times 10^{-3} \text{ sec}$$

$$\frac{ER\dot{C}}{\dot{X}_h} \approx 1.4 \times 10^{-3} \frac{\text{volt}}{\text{in./sec}}$$

Fig. D-4 Equivalent Circuit Model for Velocity Measuring Circuit

Several details of the mechanical design should be discussed as they relate to the results reported in Section 5.2. Probably the most troublesome property of the Hand Monitor was the "ringing" in its velocity output voltage caused by bending of the pole during quick tracking move-

ments. This is especially apparent in Figs. 5-11 and 5-12. Figure D-5 shows that applying a force impulse to the pole evokes an extremely lightly damped oscillation having a natural frequency of approximately 50 cycles/sec.

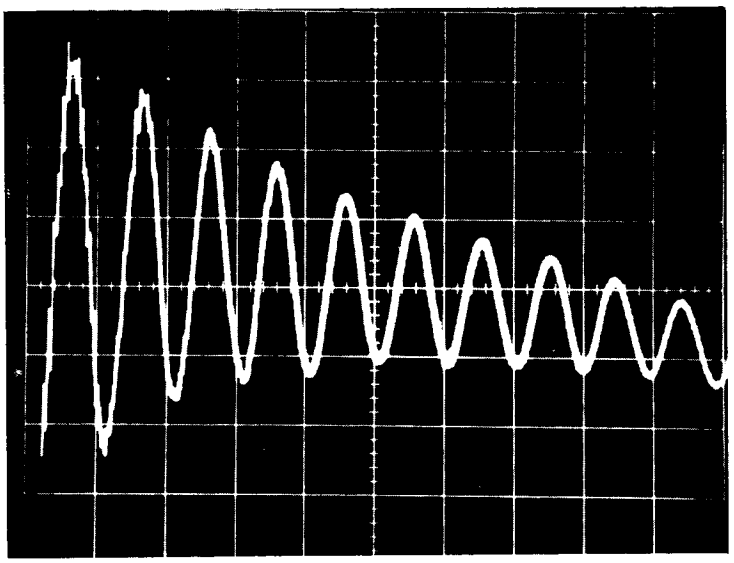

Horizontal: Time 20 msec/cm

Vertical: Velocity Signal $\frac{2 \text{ in./sec}}{\text{cm}}$ (Typical)

Fig. D-5 Ringing in Velocity Output-Voltage Caused by Bending of the Tracking Pole

The moment of inertia of the pole about its axle was approximately 0.04 slug-ft^2. This inertial load is equivalent to attaching a 5 oz weight to the subject's wrist and its effect on the tracking studies is considered to be negligible.

Figure D-2 shows that the tracking pole was connected to its axle through a gimbal which permitted motion out of the plane normal to that axle. This gimbal was necessary because the subjects could not track freely when constrained to move their hand exactly in a plane.

It can be seen from Fig. D-2 that the axle rotation is transmitted (with a 4:1 multiplication) to the potentiometer and variable capacitor by friction between two aluminum disks. Two springs hold the disks together with a force of approximately 20 lb. This arrangement, similar to the capstan/pinch-roller arrangement used in magnetic tape recorders, is preferable to conventional gears because it eliminates backlash.

Figure D-1 shows that acceleration of the hand was derived by amplifying and differentiating the velocity signal; this processing is defined by Eq. (D.7).

$$\ddot{X}_h(s) = \frac{K_a Ts}{Ts + 1} \dot{X}_h(s) \qquad \text{where} \quad \begin{cases} K_a = 100 \\ T = 1 \times 10^{-3} \text{ sec} \end{cases} \tag{D.7}$$

The 1 msec time constant is considered to have negligible effect on the measurements reported in Section 5.2.

Several tests were conducted to determine the relationship between muscle action potential and the force it produces; see Figs. 5-8 and 5-9 for example. In these tests (and the force tracking runs reported in Section 5.3) the force was measured using a pair of strain gauges mounted on a cantilevered aluminum rod. The dimensions chosen (7 in. × 5/16 in. × 5/16 in.) gave an effective spring constant of 70 lb/in. With 45V applied to the strain gauges (Baldwin-Lima-Hamilton, Type C-10) the sensitivity of the overall transducer was 8×10^{-3}V/lb.

Figure D-1 shows that signals representing all of the mechanical and physiological variables were recorded using either an 8-channel strip-chart recorder (Offner, Model TC Electroencephalograph) or a multitrace oscilloscope (Tektronix, Model 564). The strip-chart recorder was used for extended tracking tests and the oscilloscope for single voluntary moves or force applications. The oscilloscope had a storage capability which made it possible to observe transients without photographing them.

Appendix E

MEASUREMENT METHOD—SECTION 5.3

E.1 Objective

The purpose of this appendix is to describe the instrumentation and data reduction procedures used to measure the closed-loop response of a human operator tracking a random continuous input signal.

E.2 Description of the Instrumentation

A one-dimensional pursuit tracking task with unity (or constant) gain plant was employed. The input was displayed as the horizontal displacement of a 1/4-in. diameter circle on an oscilloscope screen; the operator's response was displayed separately as the horizontal displacement of a 1/4-in. vertical line. The line bisected the circle when the operator succeeded in matching his output to the input signal. Figure E-1 shows the instrumentation necessary to generate, display, and record the input signal and the operator's response to it.

The input signal, I(t) formed by filtering the output of a wideband random noise generator, is (after the addition of a phase-shifted sine wave) applied to one horizontal channel of a dual beam oscilloscope. The operator's response, O(t) (one of the three different operator outputs selected for the Control Action Display), is applied to the second horizontal channel of the oscilloscope. The 1000-cps sinusoidal signal applied to the two vertical axes of the oscilloscope forms two different Lissajous patterns (a circle and a vertical line) which enable the operator to distinguish between the two traces. The input signal and the operator's response are recorded on a four-track magnetic tape recorder for subsequent data processing.

The random noise generator used for these experiments was an Electronic Associates Model 201A. It generates an output voltage having a very nearly Gaussian distribution with zero mean and a well regulated

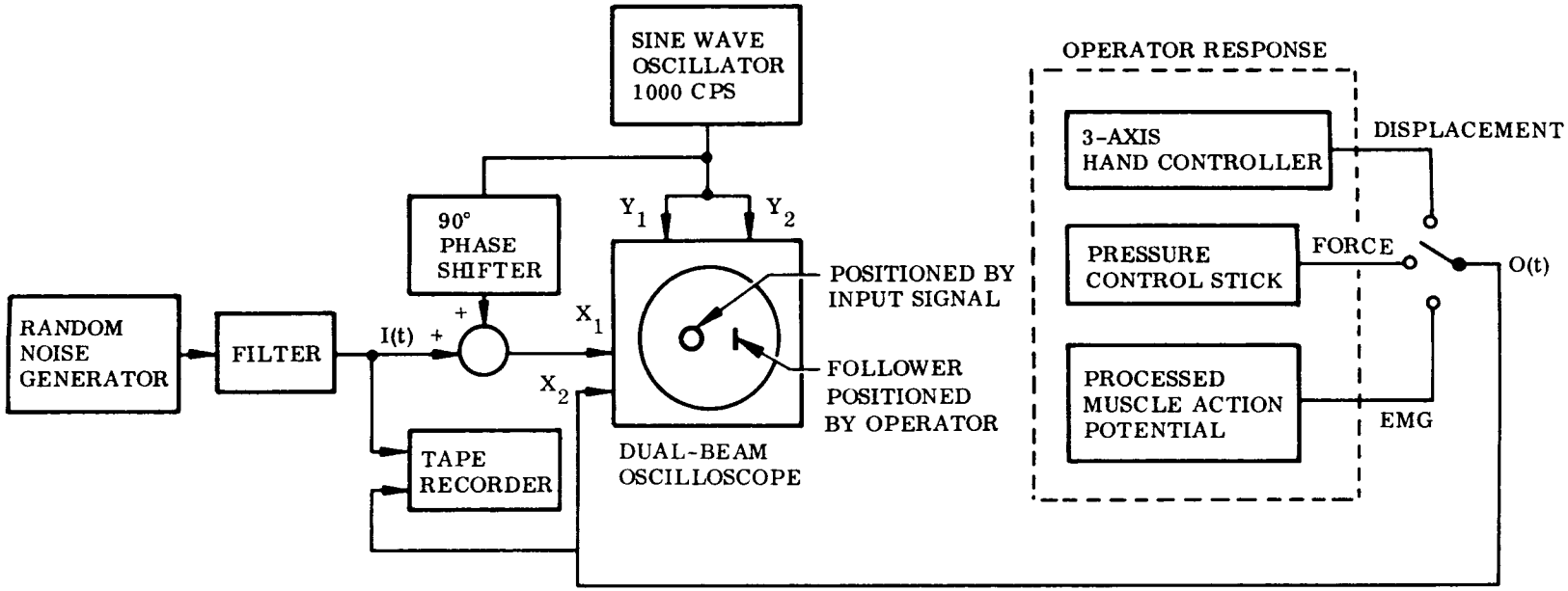

Fig. E-1 Instrumentation Used to Measure Closed-Loop Response for Random Continuous Input Signal

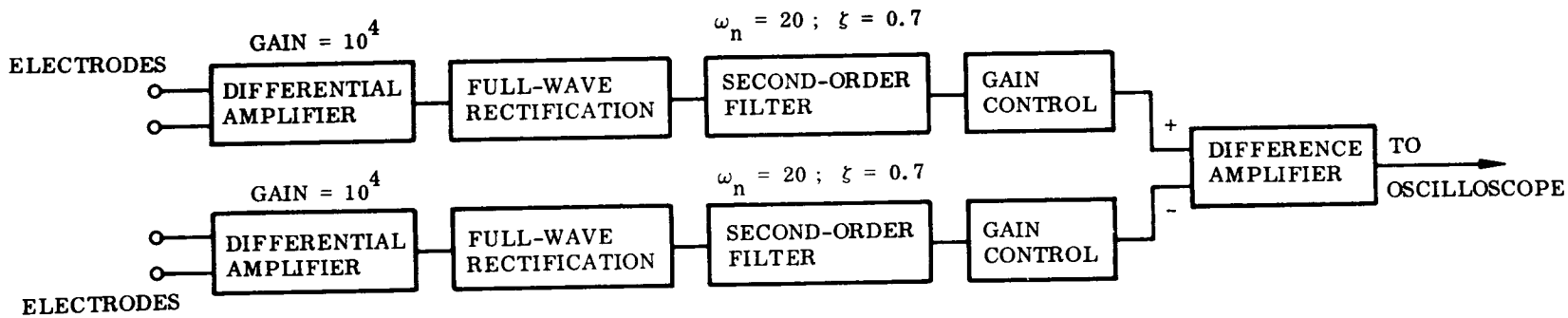

Fig. E-2 Instrumentation Used to Provide EMG Control Action Display

RMS value. The power spectral density of the output voltage is constant (within $\pm$ 0.1 db) over the frequency range from 0 to 35 cps (Ref. 58). This signal was filtered using analog computer circuitry to mechanize the transfer function given by Eq. (E.1).

$$\text{Transfer Function of Filter} = \frac{1}{(Ts + 1)^2} \tag{E.1}$$

This resulted in an input signal, I(t), having an autocorrelation function and power spectral density given by Eq. (E.2) and Eq. (E.3) respectively.

$$\varphi_{ii}(\tau) = \varphi_{ii}(0) \left(1 + \frac{|\tau|}{T}\right) e^{-(|\tau|/T)} \tag{E.2}$$

$$\Phi_{ii}(\omega) = \varphi_{ii}(0) \frac{4T}{(T^2\omega^2 + 1)^2} \tag{E.3}$$

A value of T = 0.25 sec was used for all of the results presented in Section 5.3 and the RMS value of the input displacement, equal to $[\varphi_{ii}(0)]^{1/2}$, was adjusted to approximately 0.65 in. referred to the oscilloscope face. The input signal, I(t), has a Gaussian distribution because it is the output of a linear filter driven by a Gaussian random process (Ref. 59).

The operator tracked the input signal using either displacement, force, or EMG outputs. Displacement was measured using a potentiometer mounted on the yaw channel of the 3-axis hand controller shown in Fig. 3-12. This channel had a very light spring restraint and no detent. The operator-controlled display moved 1.6 in. horizontally on the oscilloscope face for 1.0 in. of hand controller displacement. In the force-control mode force was measured using a pair of strain gauges mounted on a short cantilever beam. The operator-controlled display moved 0.64 in. for each pound of force exerted by the operator. Full-scale deflection on the oscilloscope required approximately $\pm$ 3 lb of

force which caused less than $\pm$ 1/16-in. deflection of the pressure stick. Figure E-2 shows the instrumentation used to derive a Control Action Display signal from the operator's muscle action potentials. The electromyographic signals from two opposing groups of muscles (right Pectoralis major and Infraspinatus) were detected using pairs of surface electrodes. These signals were amplified by a gain of 10^4 using low-noise differential amplifiers and applied to full wave rectifiers. The rectified signals were filtered using identical second-order, low-pass filters mechanized using analog computer circuitry. The filters had a natural frequency of 20 rad/sec and a damping ratio of 0.7. The filtered outputs were passed through two different gains and applied in opposite senses to the final amplifier. Unequal gain control settings were usually required because of the difference in intensity of EMG activity in the two opposing muscle groups. The resulting signal caused a displacement of the operator-controlled display which responded to the net EMG activity generated by the operator. Typically, 1 lb of force caused approximately 0.64 in. of horizontal deflection on the oscilloscope face; i.e., approximately the same force was required for tracking in both the Force and the EMG control modes.

The duration of each tracking run was five minutes. During this time the input signal and the operator's response (i.e., whichever signal was being used for Control Action Display) were recorded using a high-quality instrumentation tape recorder. Figure E-3 shows a section from a typical tracking run using displacement feedback.

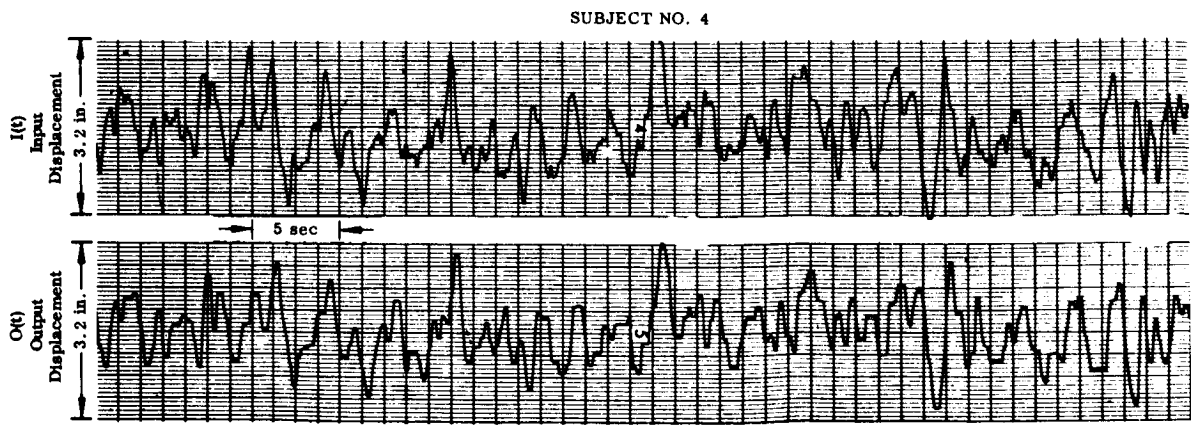

Fig. E-3 Section From a Typical Tracking Run Using Displacement Feedback

E.3 Description of the Data Processing

The data processing required for each tracking run can be divided into two phases:

1. Deriving the various autocorrelation and crosscorrelation functions of analog signals previously recorded on magnetic tape.
2. Transforming these correlation functions into their respective power spectral densities.

These two operations are outlined briefly in the following paragraphs and typical results are presented.

A small, special-purpose, hybrid computer (Computer of Average Transients-Series 400 with Correlation Computer 256 described in Ref. 60) was used to compute the correlation functions. It accepts two analog input voltages and puts out a graph of $\hat{\varphi}_{io}(nT_s)$, given by Eq. (E.4), as a function of n.

$$\hat{\varphi}_{io}(nT_s) = \sum_{k=0}^{T_a/T_s} O(kT_s)\, I(kT_s - nT_s) \qquad n = 0,1,2,\ldots,N \qquad (E.4)$$

For all of the results presented in Section 5.3 the parameters were set as follows: $T_s = 20 \times 10^{-3}$ sec $T_a = 180$ sec and $N = 128$. The crosscorrelation function for negative values of the argument was computed by interchanging the $I(t)$ and $O(t)$ inputs to the computer [see Eq. (E.5)] and playing back the identical section of the run again.

$$\hat{\varphi}_{io}(-nT_s) = \hat{\varphi}_{oi}(nT_s) \qquad (E.5)$$

The autocorrelation function of the input, or output, signal was formed by connecting $I(t)$, or $O(t)$, to both computer inputs and playing back that same section of the run; because they are symmetrical, the autocorrelation functions were computed for only positive values of the argument.

Each of the four correlation functions, plotted on 15 in. × 10 in. graph paper, was translated onto punched cards using a Datareducer/Teleducer reader (Ref. 61). These cards were processed by a large, general-purpose, digital computer. For each correlation curve the data is transformed according to Eq. (E.6) on the first pass.

$$\varphi_{io}(nT_s) = C_2[\hat{\varphi}_{io}(nT_s) - C_1] \qquad n = 0,1,2,\ldots,N \qquad (E.6)$$

The constant C_1 is chosen for each curve so that the correlation function approaches zero for large values of the argument; the constant C_2, common to all correlation functions for a given run, is the value which normalizes $\varphi_{ii}(0)$ for that run. Figure E-4 shows the correlation functions derived from the same tracking test given in Fig. E-3. The theoretical curve for the input signal autocorrelation function [see Eq. (E.2)] is also presented for comparison.

On the second pass the computer determines the magnitude and phase of the power spectral densities according to the equations

$$\mathrm{Re}(m\Delta\omega) = \sum_{n=-N'}^{N'} \varphi_{io}(nT_s') \cos(m\Delta\omega nT_s') \qquad m = 0,1,2,\ldots,M \qquad (E.7)$$

$$\mathrm{Im}(m\Delta\omega) = \sum_{n=-N'}^{N'} \varphi_{io}(nT_s') \sin(m\Delta\omega nT_s') \qquad m = 0,1,2,\ldots,M \qquad (E.8)$$

$$|\Phi_{io}(m\Delta\omega)| = [\mathrm{Re}^2(m\Delta\omega) + \mathrm{Im}^2(m\Delta\omega)]^{1/2} \qquad (E.9)$$

$$\measuredangle \Phi_{io}(m\Delta\omega) = \tan^{-1} \frac{\mathrm{Im}(m\Delta\omega)}{\mathrm{Re}(m\Delta\omega)} \qquad (E.10)$$

For all power spectral densities presented in Section 5.3 the parameters were set as follows:

$\Delta\omega = 0.5$ rad/sec, $N' \approx 35$, $T_s' = 40 \times 10^{-3}$ sec, and $M = 25$.

Figure E-5 shows the power spectral densities for the correlation functions given in Fig. E-4. The theoretical curve for the power spectral density of the input signal [see Eq. (E.3)] is also presented for comparison.

A test was made in which the transfer function of a known plant (second-order filter with $\omega_n = 10$ rad/sec and $\zeta = 0.7$) was derived using

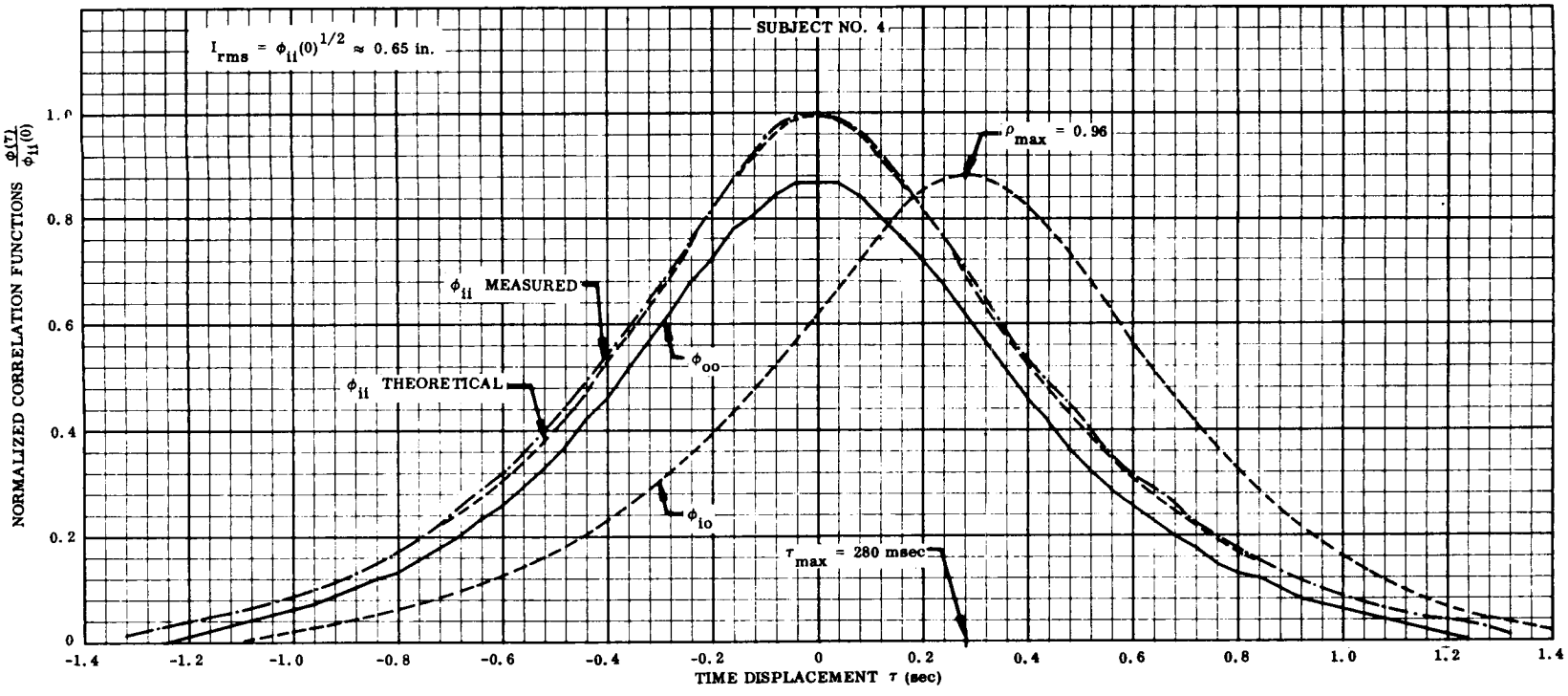

Fig. E-4 Correlation Functions for a Typical Tracking Run Using Displacement Feedback

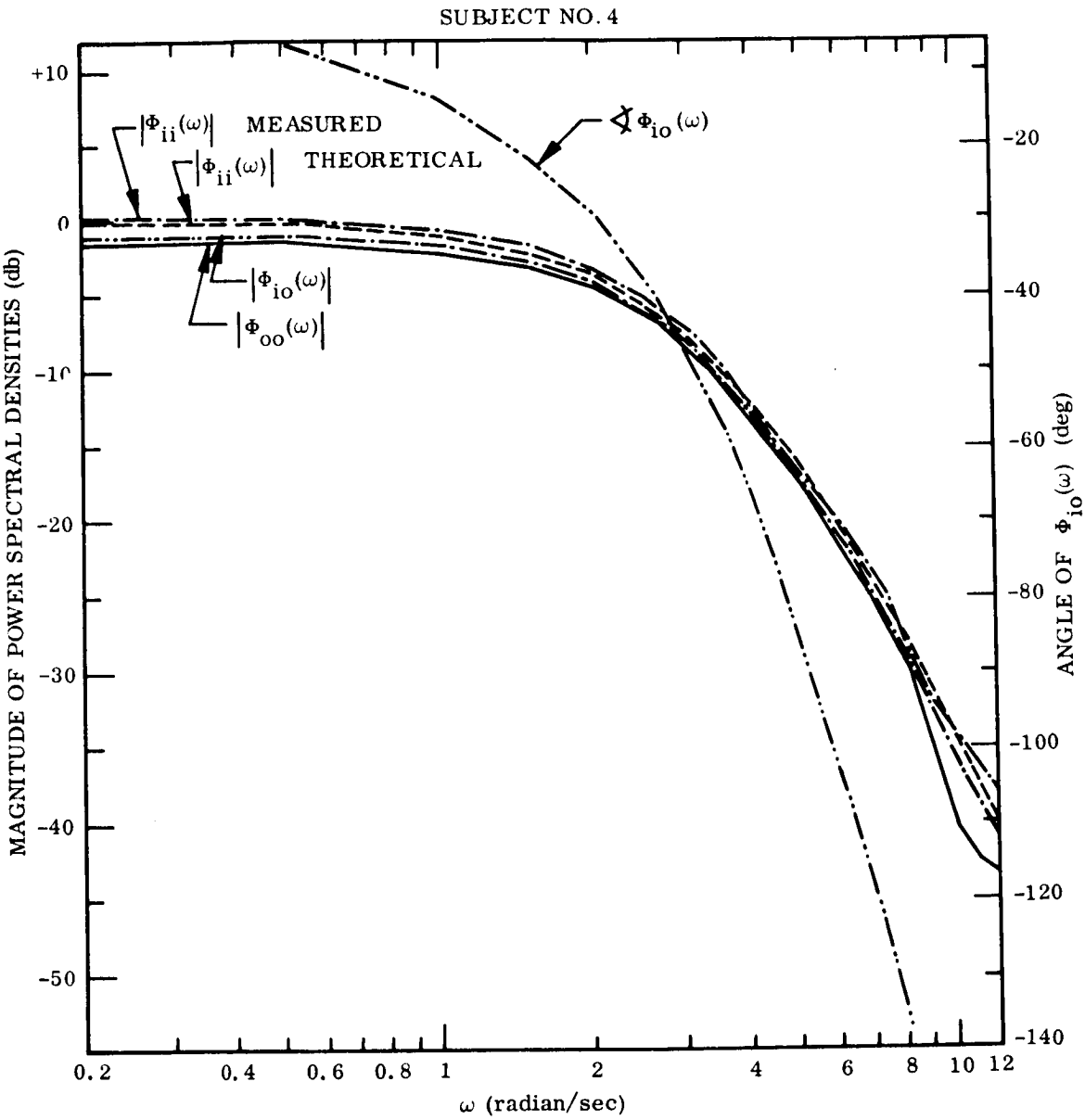

Fig. E-5 Power Spectral Densities for a Typical Tracking Run Using Displacement Feedback

the equipment and procedures described above. The purpose of this test was to estimate the accuracy with which the transfer function of the human operator can be determined. The results, presented in Fig. E-6, show that errors in magnitude and phase determination are less than 1 db and 3 deg, respectively, over the frequency range 0 to 6 rad/sec; this is the range of greatest interest for application of Control Action Display. For frequencies between 0 and 9 rad/sec (a frequency range which contains 97 percent of the power in the input signal) the magnitude and phase errors are less than 2 db and 8 deg, respectively.

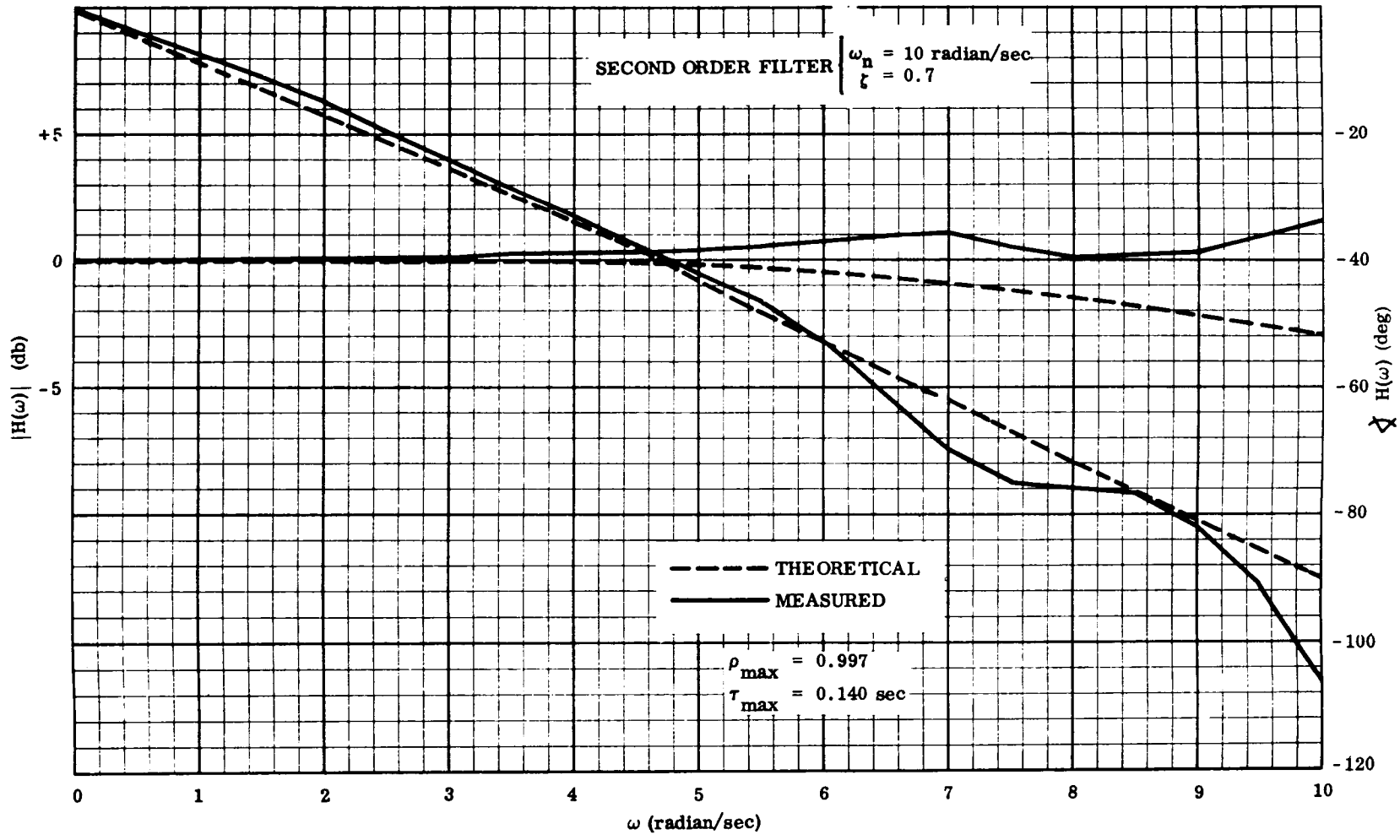

Fig. E-6 Accuracy of Transfer Function Determination

References

1. Walter Eppler and Robert Willstadter, "A Simulation of Map Correlation for Ballistic or Orbital Weapon Terminal Correction", Proceedings of the Seventh Annual Air Force Ballistic Missile Symposium, August 1962.

2. A. A. Dzilvelis, "Celestial Map Matching for Space Navigation", Report SMDO-1-4, Litton Systems, Inc., Guidance and Control Systems Division, pp. 20, 24.

3. S. Seidenstein, and H. P. Birmingham, "The Relation of Electronic and Optical Display Gain to System Performance", IRE Transactions on Human Factors in Electronics, March 1960, pp. 30-32.

4. Jerome I. Elkind, Characteristics of Simple Manual Control Systems, Technical Report No. 111; MIT Lincoln Laboratory, 6 Apr 1956.

5. Duane T. McRuer and Ezra S. Krendel, Dynamic Response of Human Operators, Wright Air Development Center WADC Technical Report 56-524, Wright-Patterson Air Force Base, Ohio, October 1957.

6. Duane McRuer, Dunston Graham, Ezra Krendel, William Reisner, Jr., Human Pilot Dynamics in Compensatory Systems, Air Force Flight Dynamics Laboratory, Research and Technology Division, Air Force Systems Command, Wright-Patterson Air Force Base, Ohio, Report AFFDL-TR-65-15, July 1965.

7. M. E. Campbell, "Tracking Display for Aircraft", U.S. Patent No. 2, 943, 824, July 5, 1960.

8. Harold P. Van Cott, "An Optical System for Manned Vehicle Terminal Guidance", Human Factors, June 1963, pp. 329-333.

9. Hans F. Meissinger, "Lunar Landing by Command Guidance in the Presence of Transmission Time-Delay", AIAA Paper No. 63-346, August 14, 1963.

10. Robert O. Besco, "Handling Qualities Criteria for Manned Spacecraft Attitude Control Systems", Proceedings of Third Manned Space Flight Meeting, November 1964, pp. 271-275.

11. Robert H. Cannon, Jr., and Walter G. Eppler, Jr., "Vector Reticle, Control Action Display in Manual Control of Space Vehicle Attitude", Journal of Spacecraft and Rockets, Vol. 2, No. 2, March-April 1965, pp. 172-182.

12. E. M. Grabbe, S. Ramo, and D. E. Wooldridge, Handbook of Automation, Computation and Control, John Wiley and Sons, Inc., New York, 1958, Vol. 1.

13. John G. Truxal, Automatic Feedback Control System Synthesis, McGraw-Hill Book Company, Inc. New York, 1955.

14. J. W. Iwombly, "The Mercury Capsule Attitude Control System", Proceedings of the National Meeting on Manned Space Flight, Institute of the Aerospace Sciences, New York, 1962, pp. 228-231.

15. F. J. Bailey, Jr., Review of Lessons Learned in the Mercury Program Relative to Spacecraft Design and Operation, AIAA Paper No. 63073-63, 18 Mar 1963.

16. J. W. Senders and M. Cuzen, Tracking Performance on Combined Compensatory and Pursuit Tasks, WADC Tech. Rept., 52-39, 1952.

17. R. S. Gaylord and W. N. Keller, "Attitude Control System Using Logically Controlled Pulses", Guidance and Control, Vol. 8, Academic Press, 1962, pp. 629-648.

18. H. P. Birmingham and F. V. Taylor, A Human Engineering Approach to Man-Operated Continuous Control Systems, U. S. Naval Research Lab Report 4333, Washington, D. C., 1954.

19. H. P. Birmingham and F. V. Taylor, Why Quickening Works, Paper No. 58-AV-9, American Society of Mechanical Engineers.

20. Theodore Gold, "Quickened Manual Flight Control with External Visual Guidance", presented at the IEEE International Convention, New York City, March 1964.

21. R. H. Cannon, Jr., A New Vector Rate Reticle Display for Manual Control of Space Vehicle Attitude and Rendezvous Mancuvers, Lockheed Missiles and Space Company Report A 385590, Palo Alto, Calif., Aug. 1963.

22. R. S. Lincoln and K. V. Smith, "Systematic Analysis of Factors Determining Accuracy in Visual Tracking", Science, Vol. 116, 1952, pp. 183-187.

23. C. R. Kelly, Developing and Testing the Effectiveness of the Predictor Instrument, Dunlap and Associates, Inc., TR 252-60-1, Stamford, Conn., 1960.

24. Charles R. Kelley, Meredith B. Mitchell, Peter H. Strudwick, "Applications of the Predictor Displays to the Control of Space Vehicles", prepared under Contract NASw-619 for NASA, 30 Apr 1964.

25. John W. Sandford, "Design of a One-Man Lunar Transportation Device," Proceedings of the AIAA/NASA Third Manned Space Flight Meeting, Houston, Texas, November 4-6, 1964. AIAA Publication CP-10.

26. Donald T. Higdon, Robert H. Cannon, Jr., "On the Control of Unstable Multiple-Output Mechanical Systems", ASME Pub. 63-WA-148.

27. H. M. Paskin, "Automatic Computation of Root Loci Using a Digital Computer", unpublished thesis. Air Force Institute of Technology, Wright-Patterson A.F. Base, Ohio, March 1962.

28. L. R. Young, A Sampled Data Model for Eye Tracking Movements, Sc.D. Dissertation, Massachusetts Institute of Technology, Cambridge, 1962.

29. L. Stark, G. Vossius, and L. R. Young, "Predictive Control of Eye Tracking Movements," IRE Transactions on Human Factors in Electronics, Vol. HFE-3, Sept. 1962, pp. 52-57.

30. J. Walter Woodbury, Theodore C. Ruch, "Muscle", Chapter 4 of Neurophysiology, by Theordore C. Ruch, Harry D. Patton, J. Walter Woodbury and Arnold L. Towe, W. B. Saunders Company, Philadelphia and London, 1961, pp. 96-127.

31. F. Buchtal, "The Motor Unit and Its Disorders", Chapter 1, Neuromuscular Disorders ARNMD, Vol. 23, The Williams and Wilkins Co., Baltimore, 1960.

32. R. W. Wilde and J. W. Westcott, "The Characteristics of the Human Operator Engaged in a Tracking Task," Automatica, Vol. 1, No. 1, Jan.-Mar. 1963, pp. 5-19.

33. L. P. Lemay and J. H. Westcott, "The Simulation of Human Operator Tracking Using an Intermittent Model," International Congress on Human Factors in Electronics, Long Beach, California, May 1962.

34. O. C. J. Lippold, "The Relation Between Integrated Action Potentials in a Human Muscle and Its Isometric Tension", J. Physiology, Vol. 117, 1952, p. 492.

35. V. T. Inman and others, "Relation of Human Electromyogram to Muscular Tension," Electroencephalography and Clinical Neurophysiology, Vol. 4, 1952, pp. 187-204.

36. P. H. Hammond, "Involuntary Activity in Biceps Following the Sudden Application of Velocity to the Abducted Forearm", J. Physiology, Vol. 127, 1954, pp. 23-25.

37. R. W. Angel, W. Eppler, and A. Iannone, "Silent Period Produced by Unloading of Muscle During Voluntary Contraction," J. Physiology, Vol. 180, No. 4, Oct 1965, pp. 864-870.

38. D. R. Wilkie, "The Relation Between Force and Velocity in Human Muscle", J. Physiology, Vol. 110, No. 4, Dec 1949, pp. 249-280.

39. Morris B. Bender, The Oculomotor System, Hoeber (Medical Division, Harper and Row), 1964, pp. 429-431.

40. Denis Hill and Geoffery Parr, Electroencephalography; A Symposium on its Various Aspects, London, McDonald, 1963, pp. 54-56.

41. John S. Barlow, "Evoked Responses in Relation to Visual Perception and Oculomotor Reaction Times in Man", Annals of the New York Academy of Sciences, Vol. 112, Art. 1, 8 May 1964, Robert Katzman, ed., pp. 432-467.

42. G. A. Bekey, Sampled Data Models of the Human Operator in a Control System, Ph.D. Dissertation, Dept. of Engineering, University of California at Lost Angeles, Jan 1962. Also published by the Aeronautical Systems Division, United States Air Force Systems Command, Wright-Patterson Air Force Base, Dayton, Ohio, Report ASD TDR 62-36, Feb. 1962.

43. J. I. Elkind, J. A. Kelly, R. A. Payne, "Adaptive Characteristics of the Human Controller in Systems Having Complex Dynamics", presented at the Fifth National Symposium on Human Factors in Electronics, San Diego, California, May 1964.

44. B. L. Zuber, J. A. Michael, and L. Stark, "Visual Suppression During Voluntary Saccadic Eye Movements", Quarterly Progress Report No. 74, Research Laboratory of Electronics, M.I.T. 15 Apr 1964, pp. 217-221.

45. Jerome H. Ely, Hugh M. Brown, and Jesse Orlansky, Man-Machine Dynamics, WADC Technical Report 57-582, Wright Air Development Center, 1957, pp. 70-72.

46. Otto J. M. Smith, "Nonlinear Computations in the Human Controller", IRE Transactions on Bio-Medical Electronics, Vol. BME-9, Apr 1962, pp. 125-128.

47. R. S. Brannin, et al., "Myoelectric Control System", U. S. Patent 3, 106, 371, 8 Oct 1963.

48. Myoelectric Servo Control, Bionics Branch, Electronics Technology Division, Air Force Systems Command, Aeronautical Systems Division, Wright-Patterson Air Force Base, Ohio, ASD-TDR-63-70, May 1963.

49. Lee Harrison, "A Study to Investigate the Feasibility of Utilizing Electrical Potentials on the Surface of the Skin for Control Functions", presented at the Space Nuclear Propulsion Office Seminar on Project ROSE, 26 May 1964, Technical Note 64-11, Philco Bio-Technology Laboratory, Blue Bell, Penn.

50. J. V. Basmajian, "Control and Training of Individual Motor Units," Science, Vol. 141, 2 Aug 1963, pp. 440-441.

51. Jerome I. Elkind, Tracking Response Characteristics of the Human Operator, Human Factors Operations Research Laboratory Report HFORL Memo No. 40.

52. Stanley Fifer, Analogue Computation-Theory, Techniques and Applications, Vol. IV, New York, McGraw-Hill, 1961, pp. 1241-1244.

53. James L. Adams, "Remote Control with Long Transmission Delays", Stanford University Ph.D. Dissertation, Mechanical Engineering, 1961.

54. Paul W. Braisted, "Study of a Predictor for Remote Control Systems Operating with Signal Transmission Delays", Stanford University Ph.D. Dissertation, Mechanical Engineering, 1963.

55. Theordore C. Ruch, "Pontobulbar Control of Posture and Orientation in Space", Chapter 8 of Neurophysiology by Theodore C. Ruch, Harry D. Patton, J. Walter Woodbury and Arnold L. Towe, W. B. Saunders Company, Philadelphia and London, 1961, pp. 206-219.

56. George W. Housner, and Donald E. Hudson, Applied Mechanics-Dynamics, D. Van Nostrand Company, Inc., Princeton, New Jersey, 1959, Chapter 6.

57. George B. Thomas, Jr., Calculus and Analytic Geometry, Cambridge, Mass., Addison-Wesley Press, 1951, pp. 625.

58. Low-Frequency Gaussian-Noise Generator-Model 201A. Electronic Associates, Long Branch, New Jersey.

59. W. B. Davenport and W. L. Root, Random Signals and Noise, New York, McGraw-Hill, 1958.

60. Instruction Manuals for Computer of Average Transients-Series 400 and Correlation Computer 256. Mnemotron Division of Technical Measurements Corp., North Haven, Conn.

61. Instruction Manuals for Datareducer-Type 0996, Teleducer-Model 24A, and Program Unit-Type 33J2. Data Instrumentation Company, North Hollywood, Calif.